Modification of Thermally Sprayed Oxide Coatings by Chemical Densification Processing

Yaping Ye

Dissertation zur Erlangung des Doktorgrades

an der Fakultät für Geowissenschaften

der Ludwig-Maximilians-Universität München

vorgelegt von

Yaping Ye

aus Zhejiang, VR China

München, 2016

Erstgutachter: Prof. Dr. Soraya Heuss-Aßbichler

Zweitgutachter: Prof. Dr. Martin Faulstich

Tag der mündlichen Prüfung: 20. Juli 2016

TABLE OF CONTENTS

1 INTRODUCTION

Nowadays, wear and corrosion is still one of the most serious problems in industries. For moulding machines wear and abrasion can not only shorten the maintenance periods of the functional components, but also has a great influence on product accuracy. For instance, high temperature of plasticized material, high abrasion by fillers, and corrosion attacks remain a problem for plastic moulds. Hence, these moulding machines require wear and corrosion protection under these extreme circumstances [1-3].

Yttria stabilized zirconia (YSZ) ceramic coatings have been widely used as wear- and corrosion-resistant coatings and thermal barrier coatings in high temperature applications and aggressive environments for several decades due to their hardness, wear resistance, heat and chemical resistance, and low thermal conductivity [4-7].

For the deposition of ceramic YSZ coatings, thermal spraying technology has been widely applied. Thermal spraying is a very efficient deposition technology for ceramic coatings. However, thermally sprayed coatings are formed by the impact, deformation and solidification of individual liquid droplets so that their structure consists of a series of overlapping lamellae, numerous pores and microcracks because of partially or totally non-molten particles, inadequate flow, and air entrapment [8-11]. These pores, especially inter-lamellar pores which indicate incomplete contact of the lamellae weaken the strength, wear and corrosion resistance of the thermally sprayed ceramic coatings [12, 13]. Although porosity of such a coating could be affected by spray technologies, spray parameters [14, 15], feedback particles [16, 17], and even nano-microstructures [18, 19], the open pores and incomplete inter-lamellar bonding deteriorate the corrosion resistance of the coating-substrate system and also decrease the mechanical properties and wear resistance of the ceramic coatings [20].

Moderate adhesion and a porous structure of the thermally sprayed ceramic coatings are the most often encountered problems for their applications [21]. In order to reduce porosity and improve protection efficiency of thermally sprayed ceramic coatings, post-treatments to close the surface porosity have also been applied. Heat treatments using furnace and laser sintering are usually used. During the furnace heat treatments, new phases of materials are often formed and long annealing time needed. Laser treatment can cause many microcracks owing to the rapid heating and cooling rates [22-27]. The aim of sealing by impregnation for high temperature wear-

and corrosion-resistant ceramic coatings is to close or fill all those open pores and cracks that are connected to the surface at as great a depth as possible, because the high wear and corrosion resistance of a ceramic coating is achieved by a dense structure [28]. Most sealing treatments have been performed by impregnation using polymers, inorganic solutions, or molten metals. During such treatments, the residual air inside the pores can create an opposing force which limits the liquid sealants' penetration and also the densification depth [28-30]. Moreover, these post treatments are essentially unable to improve the adhesion strength of the top ceramic coatings.

The adhesion of thermally sprayed ceramics to metal substrates is relatively poor but can be improved if a sprayed "bond coat" is used between the ceramic coat and metal substrate. The oxidation resistance of the coatings can also be improved if a Ni-based alloy "bond coat" is sprayed. In this study, a two-layer system consisting of YSZ ceramic top coat and Ni-based alloy bond coat will be post-treated by means of a novel solvothermal process. During this processing, reactive species are produced *in-situ* and transported to the two-layer system and diffused along the connected pores in the thermally sprayed ceramic top coat to the topcoat/bondcoat interface. There the solvothermal reactions lead to the densification of the ceramic topcoat. The chemical densification process takes place in the vapour flux, therefore, there is no opposing force of the residual air, and the "sealants" penetration will not be limited.

In order to improve wear resistance of the thermally sprayed YSZ coatings, the addition of a second phase with higher thermal conductivity and a higher level of hardness into the zirconia phase is effective. Alumina is an attractive material for wear resistance application with higher thermal conductivity and hardness. It has been proven that the addition of an alumina phase into the zirconia phase leads to the improved toughness, hardness and wear resistance of the coatings [31, 32]. Composite with 30 wt% alumina in a zirconia matrix as a topcoat will also be investigated during this study.

2 OBJECTIVES OF THESIS

Thermal spraying is a very efficient deposition technology for ceramic coatings. However, moderate bonding strength and high porosity of the thermally sprayed ceramic coatings deteriorate the wear and corrosion resistance of the coating-substrate system, therefore, limiting their industrial applications especially in high temperature wear and corrosion areas.

Therefore, the aim of this thesis is to find an effective way to densify the thermally sprayed ceramic coatings and enhance their bonding strength. In this study, a two-layer system consisting of atmospheric plasma-sprayed 8 wt% yttria-stabilized zirconia (8YSZ) and Ni-based alloy coatings will be used as a model system, post-treated by means of a novel chemical densification process. This densification process will be conducted under atmospheric pressure and at moderate temperatures. Hence, a simple experimental setup for the post-treatments needs to be created in order to study the densification kinetics and determine the optimized conditions for the chemical densification process.

The chemical densification mechanisms need to be investigated and their thermodynamics understood.

Further studies will also be related to the correlation of the microstructures, mechanical properties and tribological behaviours. In order to improve wear resistance of the thermally sprayed YSZ coatings, the addition of a second phase with higher thermal conductivity and higher hardness into the YSZ phase will also be investigated.

Oxidation resistance of the post-treated two-layer system will be evaluated by a defined experimental test, and the spalling failure mechanisms of the examined samples will be proposed.

Finally, new application areas of the optimized two-layer system are to be explored and the corresponding tests carried out.

3 FUNDAMENTALS

3.1 Wear and corrosion

The progressive deterioration of metallic surfaces which encounter physical, chemical, electrical and other forces when they are in use in industries, leads to loss of efficiency of the components, and even to their failure. These degradations are caused by wear and corrosion. In Germany, corrosion, wear or the combined effects of these destructive failures cost industrial economies billions of Euros each year. In order to mitigate these damages due to corrosion and wear, applying a right coating on the component surfaces may be an effective way. A comprehensive understanding of the complex phenomena associated with wear and corrosion to materials is necessary before we are going to find the right coatings for the component surfaces.

Wear

Wear involves the physical removal of material from a solid surface by another surface or material. It has been classified in various ways. In general, wear can be categorized by the surface material, the interacting material, the surface loading and the nature and speed of the relative motion. One of the simplest classifications of wear is based on the presence or absence of effective lubricants, namely lubricated or non-lubricated wear. Another classification, based on the fundamental wear mechanism, has been also developed. This approach is complicated by the fact that more than one mechanism may be operating at the same time and these classifications have developed from different backgrounds and experiences with wear. As a result, different classification schemes have been developed and there is no one scheme which is universally accepted [33]. To understand the wear mechanism, the classification, based on the wear mechanism, will be described in Fig. 3-1. The wear process can be classified into four categories, that is, abrasion, erosion, adhesion, and surface fatigue [34].

Abrasive wear is the removal of material from a surface by harder material, impinging on the surface (i.e., grit blasting), or moving along the surface under load (i.e., grinding). As shown in Fig. 3-1, abrasion is often further categorized as low-stress abrasion, high-stress abrasion, gouging abrasion and polishing [34]. At low-stress abrasion, the forces must be low enough to prevent crushing of the abrasive. Hardness is the most important property in low-stress abrasion. For pure metals, the abrasive wear resistance increases linearly with metal hardness. Wear, under a level

of stress which is high enough to crush the abrasive, is called high-stress abrasion. So plastic deformation of surfaces are occurring and damage is always more severe than low-stress abrasion. Gouge abrasion happens while a relatively large portion of surfaces are moved by impinging with abrasive materials. Strain hardening and plastic deformation are the dominant factors. Polishing abrasion involves extremely-fine-scale abrasion and the polished surfaces are usually smooth and bright.

But how is material removed from a surface during abrasion? Several mechanisms have been proposed to explain that. They include plowing, wedge formation, cutting, microfatigue and microcracking.

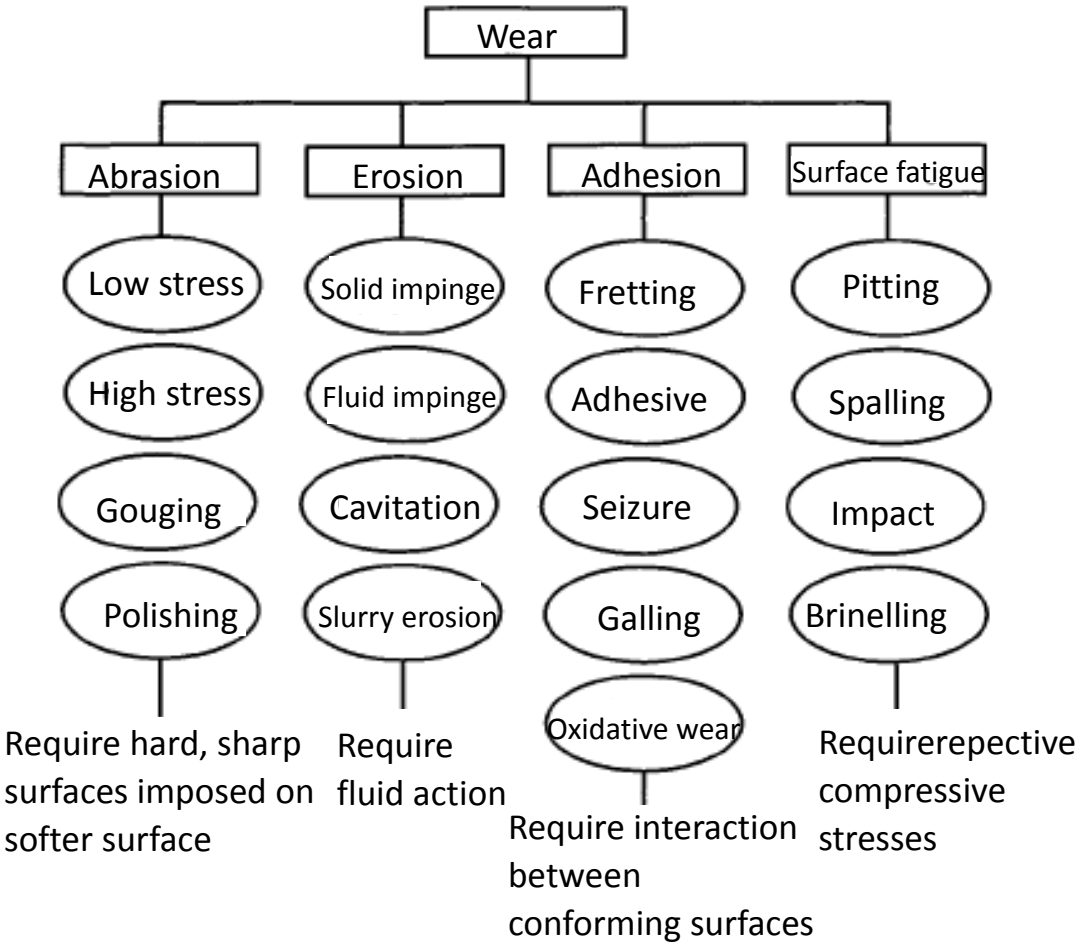

Figure 3-1. *Major categories of wear based on abrasion, erosion, adhesion, and surface fatigue [34].*

In order to prevent a surface from suffering abrasion, proper materials and surface engineering treatments would be applied. Material properties, such as hardness, yield strength, fracture toughness, microstructure and compositions, play an important role in their abrasive behaviours. Surfaces are treated by engineering technologies, such as flame and laser hardening, vapour deposition with hard coatings and thermally-sprayed ceramic coating [35].

Adhesive wear may occur if two surfaces deform and weld together locally during relative motion, under load due to interatomic forces. If the welding bond is stronger than the intrinsic bond of the underlying materials, the material shears or deforms. Adhesive wear can be further divided into mild and severe. All metallic surfaces are normally covered with a layer of adsorbed gases and/or chemical reaction products. When the protective layer regrows faster than it can be removed during relative motion, it is termed mild adhesive. Otherwise, when the oxide layer cannot grow faster enough, the process is termed severe adhesive wear. This wear phenomenon can be described by the following formula (1)

(1) $$V= \frac{kSL}{3H} \text{ or } V= \frac{kSL}{H},$$

where V is the wear scar volume, S is the distance of sliding, L is the load, H is the indentation yield strength of the softer surface, and k is a probability factor that a given area contact will fracture within the weaker material, rather than at the original interface [36].

To prevent adhesive wear, sliding similar materials together, particularly metals should be avoided and high hardness is a desired property of the materials. Lubrication can also reduce wear [33].

Erosion can take place when a surface is impinged or impacted by a liquid or gaseous stream containing particles or by a liquid medium even without solid particles at high speed. The particles or the liquid droplets remove materials through a microcutting action. Cavitation is another special mechanism of liquid erosion, where the formation of bubbles that adhere to the surface and the collapse of these bubbles happen [33]. The surface can be removed or plastic deformed by shock waves with sufficient force which are generated by collapse of the bubbles in contact with the surface.

Reconfiguring the system, surface hardening treatment, applying austenitic steels and ceramic coatings have been developed in order to avoid high erosion rates.

Cracking, then propagating and ultimately spallation may occur when a surface is subjected to cyclic or repetitive loading at levels below the yield strength of the material. Additionally, thermal fatigue can also exhibit when materials encounter the stresses, related to the expansions and contractions associated with thermal cycling.

Corrosion

Corrosion is a chemical or electrochemical process, in which the undesirable interaction of a surface with its environment takes place. Corrosion results normally in the degradation of the surface. In general, corrosion may be classified as oxidation, aqueous corrosion, dry corrosion and stress-enhanced corrosion [33].

Oxidation of metals occurs while a metal losses electrons in the presence of an oxidant, such as oxygen.

Dry corrosion is a chemical process that usually involves the interaction of a surface with a gaseous corrosive phase. This process can become more severe at elevated temperatures. Thermal barrier coatings are usually used in gas turbine or for other high temperature applications, to protect surfaces from exposure to a gaseous corrosive phase at high temperatures [37]. Another example is hot gas corrosion, which is associated with the combustion by-products of sulphur-containing gases [38].

When a surface is exposed to a corrosive environment and stresses are applied to the region, then cracking and failure may occur. This can be explained by stress-enhanced corrosion, where corrosion is enhanced or promoted by stress.

Surface hardening or surface coating with a wear- and corrosion-resistant layer has been usually applied to protect the working surface and extent the service life of machines.

3.2 Thermal spray technology

Principle of thermal spray technology

Thermal spray technology was discovered by Dr. M. U. Schoop and his associates in the early 1900s and has been developed over one hundred years. Thermal spray is a group of coating processes, in which finely-divided metallic or nonmetallic materials in the form of powder, wire, or ceramic rod are heated in the thermal spray gun by energy source in molten or semi-molten state and deposited on a prepared surface to form a coating [39]. The energy source may be flame or electric. According to that, thermal spray processes may be categorized as either combustion or electric processes, with a number of subsets falling under each category. (Cold spray, which uses some modest preheating but a large kinetic energy, is a recent addition to the family of thermal spray processes.)

These energy sources are used to heat the coating materials to a molten or semi-molten state. The heated materials are then accelerated and propelled in the form of particles onto a prepared surface by either process gases or atomization jets. These sprayed particles impinge upon the surface of the prepared substrate, flatten, and form thin platelets (splats) that conform and adhere to the irregularities of the substrate and to each other. As the heated particles strike the substrate, they cool and build up, splat by splat, finally form the thermal spray coating. Therefore, thermal spray coatings usually exhibit a characteristic lamellar structure. Figure 3-2 illustrates a typical structure of cross section of the thermally-sprayed coatings. These coatings normally contain a certain degree of porosity, typically up to 10% due to the unmelted particles or entrapped air. They are also inhomogeneous and contain other inclusions and unexpected oxides. The metal and alloy coatings usually possess oxides because some metals may be partially oxidized by entrained air. In general, the coating becomes harder and denser with the higher particle velocity. The properties of thermally-sprayed coatings are dependent on the feedstock materials, thermal spray processes, spray parameters and post treatments of the applied coatings.

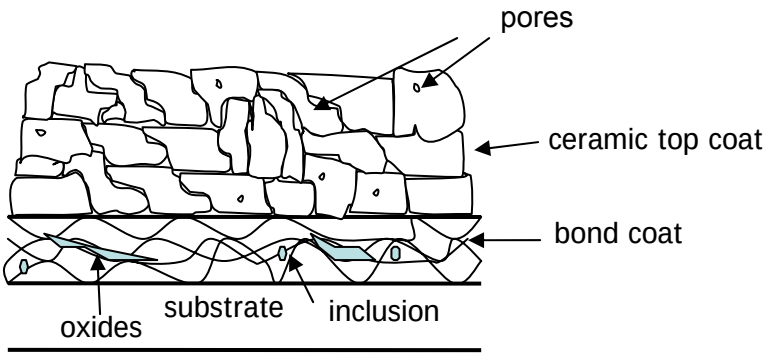

Figure 3-2. *A typical cross-sectional structure of the thermally sprayed coatings.*

Thermal spray processes

Combustion processes include flame spraying, high velocity oxyfuel spraying (HVOF) and the detonation gun (D-gun) spraying. Electric processes include electric arc spraying and plasma spraying.

Flame spraying is the oldest form of thermal spray. A wide variety of feedstock materials, including metal wires, ceramic rods, metallic and non-metallic powders, may be applied for flame spraying processes. In flame spraying, the feedstock material is fed continuously to the tip of the spray gun, where it is melted in a fuel gas flame and propelled to substrate in a stream of aspirating gas (Figure 3-3). The particle speed is relatively low (<100 m/s) and the bond strength and the cohesion of the deposits are generally lower than that of high velocity processes. Substrate temperatures can run quite high, because of flame impingement at flame powder process and excess energy input at wire flame process. Common fuel gases are acetylene, propane and methyl acetylene-propadiene. As the aspirating gas, air is usually applied [39]. The basic components of a flame spray system include the flame spray gun, feedstock material, feeding mechanism, oxygen and fuel gases with flow meters and pressure regulators, and an air compressor and regulator.

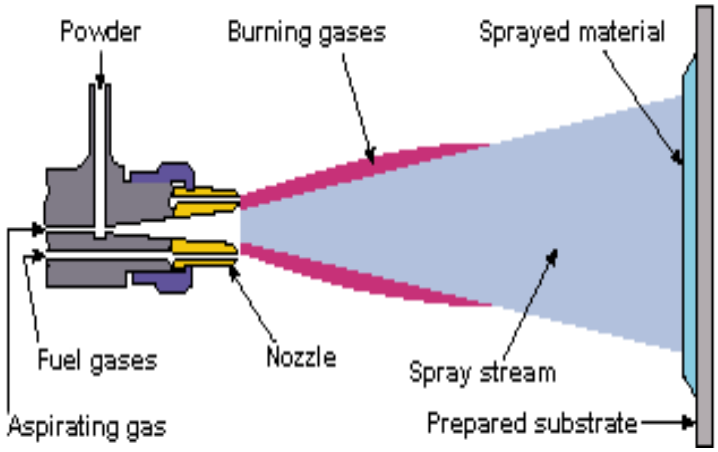

Figure 3-3. *Schematic illustration of typical flame spray process (powder Flame)* [39].

HVOF is one of the newest methods of thermal spray. A fuel gas (hydrogen, propane, or propylene) and oxygen are utilized to create a combustion jet at temperature of 2500 to 3100 °C. The combustion takes place internally at very high chamber pressures and the burning gas mixture goes through a small diameter (8-9 mm) barrel to generate a supersonic gas jet with very high particle speeds (Figure 3-4). This particle kinetic energy minimizes the thermal input. HVOF process can produce a very dense, well-bonded coating; making it attractive for many applications [40].

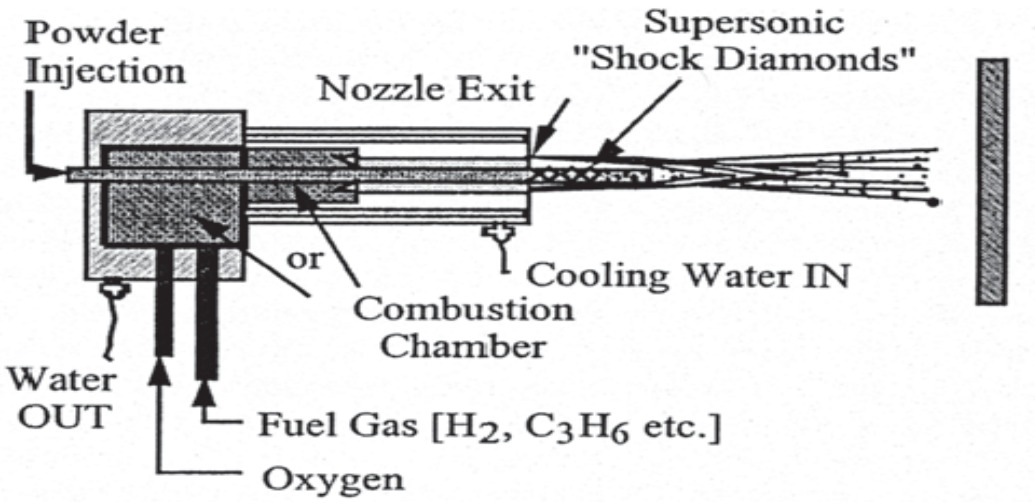

Figure 3-4. *Schematic illustration of HVOF combustion spray process* [40].

In the detonation gun process, a mixture of oxygen, acetylene and powdered feedstock materials are detonated by sparking several times per second in a gun chamber. The high temperatures and pressures blast the particles out of the end of the barrel toward the substrate (Figure 3-5). Very high bond strength and densities, as well as low oxide contents, can be achieved using this process [40].

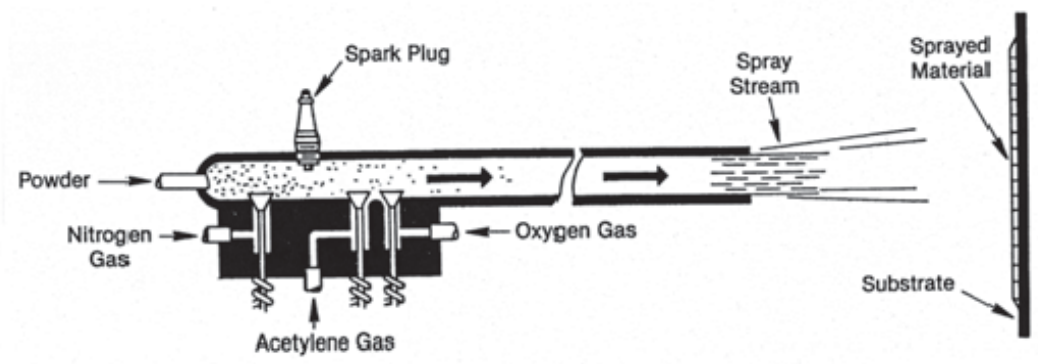

Figure 3-5. *Schematic illustration of a detonation gun process [40].*

Electric arc spraying is generally the most economical thermal spray method for depositing corrosion-resistant metal coatings, including zinc, aluminum and their alloys [39]. In the electric arc spray process, two wire electrodes, connected to a high-current -direct-current (dc) power source-, are fed into the gun and meet. An arc between the two wires is established and used to melt the wires (the coating materials). Compressed gas, usually air, is used to atomize and propel the molten material to the substrate. A low voltage (18-40 volts) of direct current power supply is used, with one wire serving as the cathode and the other as anode (Figure 3-6). Coating quality and properties can be controlled by varying the atomization pressure, air nozzle shape, power, wire feed rate, traverse speed and standoff distance. Electric arc sprayed coatings exhibit excellent adhesive and cohesive strength.

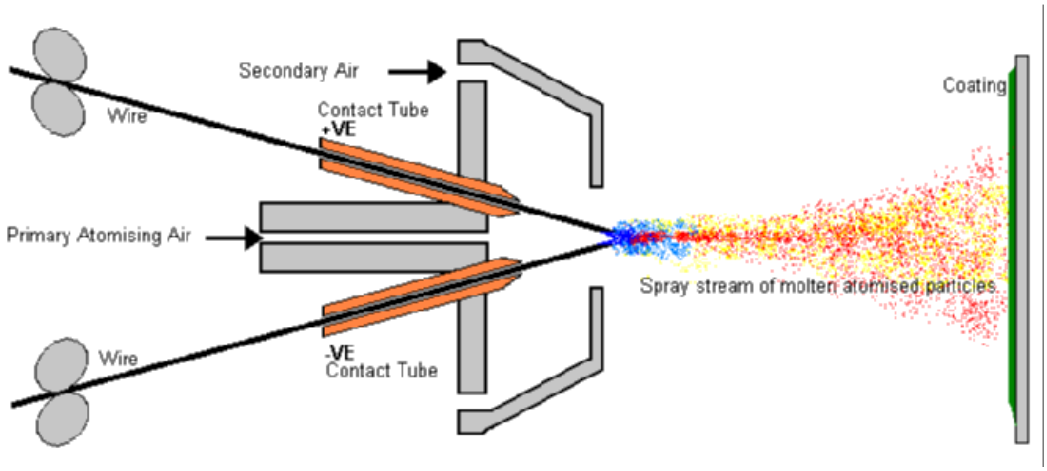

Figure 3-6. *Schematic illustration of typical two-wire arc spray gun [39].*

Plasma arc processes include air (atmospheric) plasma spray (APS) and vacuum plasma spray (VPS). These processes are applied to spray the coating materials that melt at very high temperatures. A plasma arc is established between an electrode and the spray nozzle that acts as the second electrode. Plasma temperatures in the powder heating region range from about 6000 to 15,000 °C [40]. To generate the plasma, an inert gas (argon or an argon-hygrogen mixture) is superheated by a dc arc. Powder feedstock is injected with an inert carrier gas into the heated gas, where it melts and is propelled at a high velocity (240-550 m/s) towards the substrate by the plasma jet (Figure 3-7). This Process may be applied to deposit thermal barrier coatings, such as zirconia and alumina, and wear resistant coatings, such as chromium oxide.

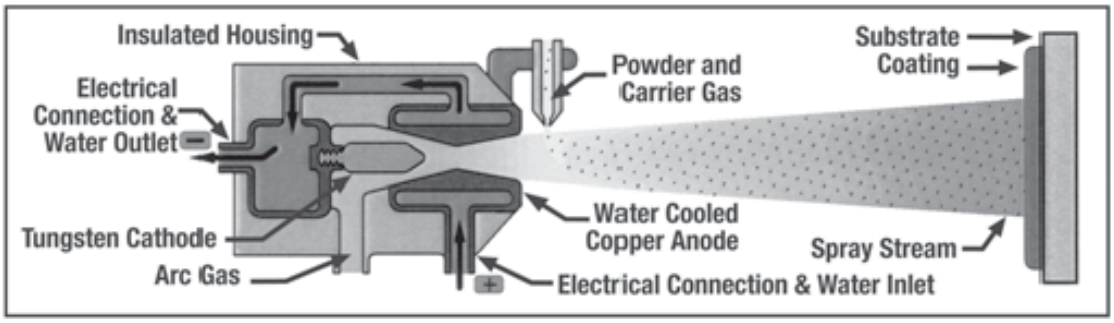

Figure 3-7. *Schematic illustration of plasma spray process [40].*

A wide variety of materials such as metals, oxides, cements, glasses, polymers and so on can be used as feedstock for thermal spraying to produce coatings. Most thermal spray processes can be carried out without significant heat input and with a high deposition rate. Therefore, thermal spray processes have been further developed and widely applied in laboratorial and industrial fields. However, Thermal spraying has the line-of-sight nature, that means, only the surfaces which the torch or gun “sees” can be coated. Of course, there are also size limitations. It is impossible to coat small and deep cavities, where a torch or gun does not fit.

3.3 The ceramic/alloy two-layer system

Yttria stabilized zirconia is one of the most relevant structural ceramic materials for high-temperature applications. Especially, partially stabilized zirconia with yttria contents in the zirconia-rich region of the phase diagram has been intensively studied for more than a century. In order to summarize the aspect of ZrO_2-Y_2O_3 phase diagram, a schematic drawing of the Zr-rich region (Y_2O_3 content <10 mol%) of ZrO_2-Y_2O_3 phase diagram is given in Fig. 3-8. According to the phase diagram, pure zirconia exhibits three stable crystal structures depending on temperature: cubic at high temperatures, tetragonal at intermediate temperatures while at low temperatures zirconia transforms into the monoclinic phase [41]. A miscibility gap exists in the zirconia-rich region of the ZrO_2-Y_2O_3 system and the temperature of c->c+t transformation decreases with increasing Y content as depicted in Fig. 3-8. If a sufficient amount of Y_2O_3 is added, the cubic phase (c-YDZ) may be stabilized at room temperature, as indicated on the right-hand side of Fig. 3-8. After rapid cooling, the crystal structural phases t'-YDZ and t''-YDZ can be formed, independent on the Y-content (3-7 mol% and 7-8 mol%, respectively) as shown in Fig. 3-8.

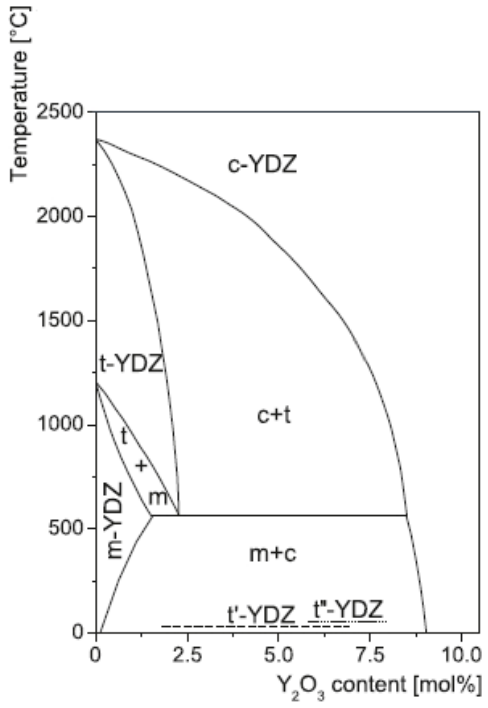

Figure 3-8. *Schematic drawing of the Y_2O_3-ZrO_2 phase diagram in the zirconia-rich region, after Scott [41]. (m, c, t and t´ stand for monoclinic, cubic tetragonal and metastable phase, respectively; YDZ stands for yttria stabilized zirconia.)*

Yttria stabilized zirconia (ZrO_2-8 mol% Y_2O_3), as an excellent solid oxygen ion conducting electrolyte, is widely used in the fields of oxygen sensor, oxygen pump and solid oxide fuel cell (SOFC) [42, 43]. SOFCs with an electrolyte support usually work at high temperatures ranging from 800 °C to 1000 °C [44, 45]. Fig. 3-9 shows a fuel-cell arrangement in which the chemical formation energy of water is directly converted into electrical energy.

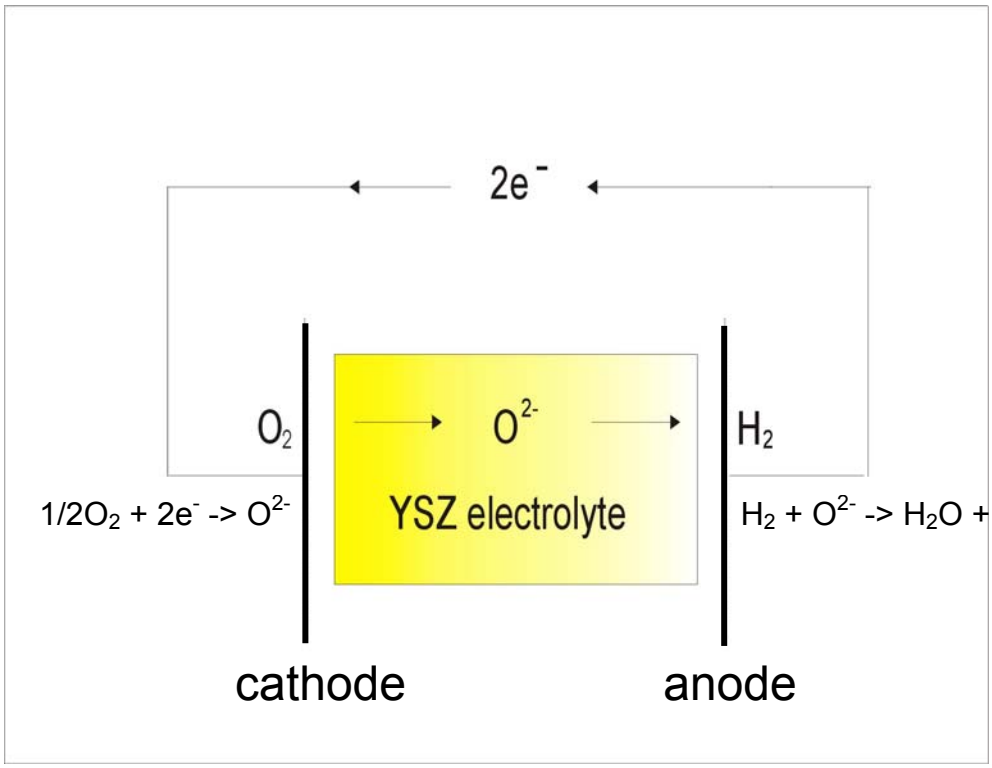

Figure 3-9. *A typical solid oxide fuel-cell arrangement [42, 46].*

Yttria stabilized zirconia (YSZ) ceramic coatings have also been widely applied as wear- and corrosion-resistant coatings and thermal barrier coatings in high temperature applications and aggressive environments due to their high hardness, wear resistance, heat and chemical resistance, and low thermal conductivity [4-6]. Due to a large difference in thermal expansion coefficients between metal substrate and ceramic coating, a bond coat from alloys, such as MCrAlY (M: Ni, Co or NiCo), is usually deposited by vacuum plasma spraying (VPS) and high velocity oxy-fuel (HVOF) in order to enhance the adhesion of thermally-sprayed ceramic topcoat to the substrate during the high temperature applications [47].

Plasma-sprayed YSZ ceramic coatings usually possess many open pores and cracks. Aggressive gaseous species can diffuse through the open structural volume defects

of the ceramic topcoat and corrode the metal substrate, which deteriorates the corrosion-resistance of the coating-substrate system and results in spalling. Ni-based alloys are applied as a bond coat against oxidation and corrosion during this study.

Due to the low thermal conductivity of zirconia, frictional heat can cause high temperatures, hence inducing stress in the coatings during the anti-wear applications. In order to improve its thermal stability and wear resistance, an addition of a second phase with high thermal conductivity and a higher level of hardness to the zirconia phase is effective. Alumina is considered to be an attractive material for wear resistance application with higher thermal conductivity and hardness [31, 32]. Composite with 30 wt% alumina in a zirconia matrix as a topcoat will be applied for this study.

3.4 Solvothermal processes as sealing post treatment

A porous structure of the thermally-sprayed ceramic coatings is always a problem in their applications involving corrosive wear. It not only deteriorates the corrosion-resistance of the coating-substrate system, but also decreases the mechanical properties and consequently the wear-resistance of the coatings. Although porosity of such a coating could be affected by spray technologies, spray parameters [14] and feedback particles [16], the transport of corrosive species to the substrate can still only be prevented by post treatments of the coatings.

The aim of sealing post treatment by impregnation is to fill or close all the open structural volume defects that are connected to the surface. These volume defects can be distinguished by their shape and means of formation as pores and cracks. The penetration depth and velocity are determined largely by interfacial surface tension and viscosity of a sealant [28].

The materials for sealing by impregnation are usually organic sealants, inorganic sealants and metals.

Typical organic sealants are one- or two-component unfilled resin systems, formulated for suitable viscosity and surface tension. Formulation is usually done by using solvents, reactive diluents or surfactants. In one component, system curing is catalyzed by heat, ultraviolet light or high-energy radiation, such as electron beam (EB) or laser radiation. In two-component systems, the cross linking is activated by curing catalysts. The often-used organic sealants are based on epoxies, phenolics, furans, polymethacrylates, silicones, polyesters, polyurethanes and polyvinylesters. Waxes can be used also [48].

Inorganic sealants are usually aimed for high-temperature applications. Typically, they also reacted to solid material at elevated temperatures. Besides aluminum phosphates and sodium and ethyl silicates, various sol-gel type solutions and chromic acid have been used for sealing purposes. Inorganic sealants are normally used for preventing corrosion by molten salts, metals and even aggressive gaseous species, but earlier studies also have shown that a high level of strengthening and improvement in wear resistance can be achieved using aluminum phosphate- based sealants [29].

Molten metals also have been used for sealing and strengthening purposes. Copper infiltration has increased coating adhesion, wear resistance of a plasma-sprayed Ti-30Mo coating and corrosion resistance against HCl and H_2SO_4 solutions [49]. For

another example, molten manganese has been infiltrated in a vacuum furnace into plasma-sprayed alumina and zirconia-8 wt% yttria coatings, which increased the coating hardness [50].

During these treatments, the residual air inside the pores can create an opposing force which limits the liquid sealants' penetration and also the densification depth [28]. Moreover, these post treatments could not essentially improve the adhesion strength of the top ceramic coatings.

Solvothermal reaction can usually be described as a chemical reaction involving a solvent either in subcritical or supercritical conditions [51]. Such a solvent can act as a chemical component or a fluid phase to modify the reaction mechanisms. Solvothermal reactions are mainly characterized by different chemical parameters (nature of the reagents or precursors and of the solvent) and thermodynamical parameters (in particular temperature, pressure and the reaction time). The chemical composition of the precursors must be appropriated to that of the target-materials, and the concentration also seems to play a role on the control of nanocrystallites during a solvothermal process. In addition, the selection of the solvent plays a key-role through the control of the chemical mechanisms, leading to the target-material. The increase of the thermodynamical parameters enhances the solubility of precursors in the solvent and induces the crystallite growing process.

Solvothermal reactions take place also in nature. Baddeleyite (ZrO_2) has recently become a mineral of interest in geochronology and petrology. It is known to occur as an accessory phase in many different terrestrial rocks and also in carbonatites, the most important zirconium-bearing phase of which is Baddeleyite, not zircon, because of the lower silica activity in carbonatite melts [52]. At high pressures and high temperatures baddeleyite crystallizes from silicate or carbonate liquids.

Solvothermal reactions involve "*in situ*" different reaction-types in non-aqueous solvents, such as oxidation-reduction, hydrolysis, thermolysis and metathesis reactions. Solvothermal reactions have been developed not only for synthesis of novel materials and crystal growth, but also for low temperature sintering and for thin film depositions [53].

4 CHARACTERIZATION METHODS

4.1 Micrometry

The microstructures and elemental distributions along a cross section of the as-sprayed and post-treated coatings were characterized by EPMA (electron probe micro-analyzer, SX100, CAMECA, SMPG-DGU, LMU) with a back-scattered electron imaging mode. Before the measurements were conducted, the specimens were cut using SiC precision saw then embedded in epoxy. After hardening, they were ground on the 500-grid and further polished on 5000-grid SiC papers.

4.2 Solubility

In order to determine the composition of the solvothermal solvent and the conditions for the following post-treatments, the solubility of zirconia in the molten salts has to be investigated. During the solubility experiments, excessive zirconia powders (GTV, Germany) were mixed in solvent salts in ratio 1:10 and put in a quartz crucible as a salt container. After being heated, the molten salt solution was sucked through an alumina tube, taken out of the oven for use as a sample, and then dissolved in the deionized water. A schematic illustration of the experimental apparatus for solubility investigations is shown in Fig. 4-1. The concentrations of Zr and the other cations in the deionized water were measured by an ICP mass spectrometry spectrometry (PE Sciex Elan 6100. Perkin Elmer) at the Institute of Hydrochemistry of TUM in Munich. The measured data were used for the calculation of the concentration of zirconia in the molten salts.

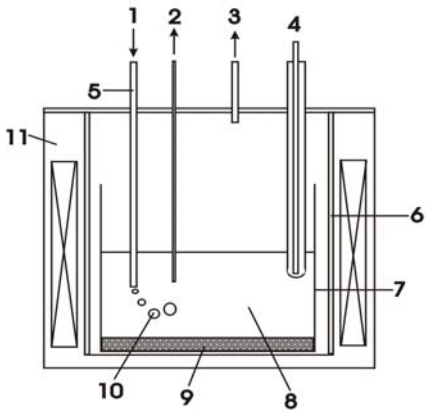

1. Gas inlet
2. Sampling tube
3. Gas outlet
4. Thermocouple
5. Alumina tube
6. Alumina tube
7. Quartz crucible
8. Molten salt
9. Oxide
10. Gas
11. Furnace

Figure 4-1. *A schematic illustration of the experimental apparatus for solubility determination.*

4.3 Porosity

The porosity of the YSZ top coat in 2-dimension was determined with the help of image analysis (dhs Image Data Base, V14, Fraunhofer UMSICHT, Sulzbach-Rosenberg), where a binary image that gives an indication of the porosity of the chosen region can be obtained through thresholding the image. For image analysis, an optical microscope (Nikon, eclipse LV150, Fraunhofer UMSICHT, Sulzbach-Rosenberg) was applied to obtain 500 magnification images. 3 fields were analysed at the same cross section for each coating and an average porosity of each coating can be determined. Before the measurements were carried out, the specimens were ground on the 500-grid and further polished on 5000-grid SiC papers.

4.4 Hardness

A Vickers diamond indenter (Micromet1, Micro Hardness tester, Buehler, Fraunhofer UMSICHT, Sulzbach-Rosenberg) was used for hardness evaluation on the polished cross section of the coatings. A 300 g load was applied. 5 measurements were carried out on the cross section from the interface to the surface for each coating. Before the measurements were conducted, the specimens were ground on the 500-grid and further polished on 5000-grid SiC papers.

4.5 X-ray-diffractometry

X-Ray-Diffractometer (Siemens, Fraunhofer UMSICHT, Sulzbach-Rosenberg) with a CuKα radiation was applied in order to analyze and control the crystalline structure of post-treated YSZ-coatings. The measurements were carried out by step method (0.02°) ranged from 10° to 90° in 2θ.

4.6 Adhesion

The adhesive strength of the plasma-sprayed and post-treated YSZ coatings was evaluated by shear tests (Typ STM 20-A, w+b walter & bay ag, Germany) according to the guideline DIN EN 15340. This measurement was performed by Mr. Wolf at Fraunhofer UMSICHT, Sulzbach-Rosenberg. The shear testing device is shown in Figure 4-2.

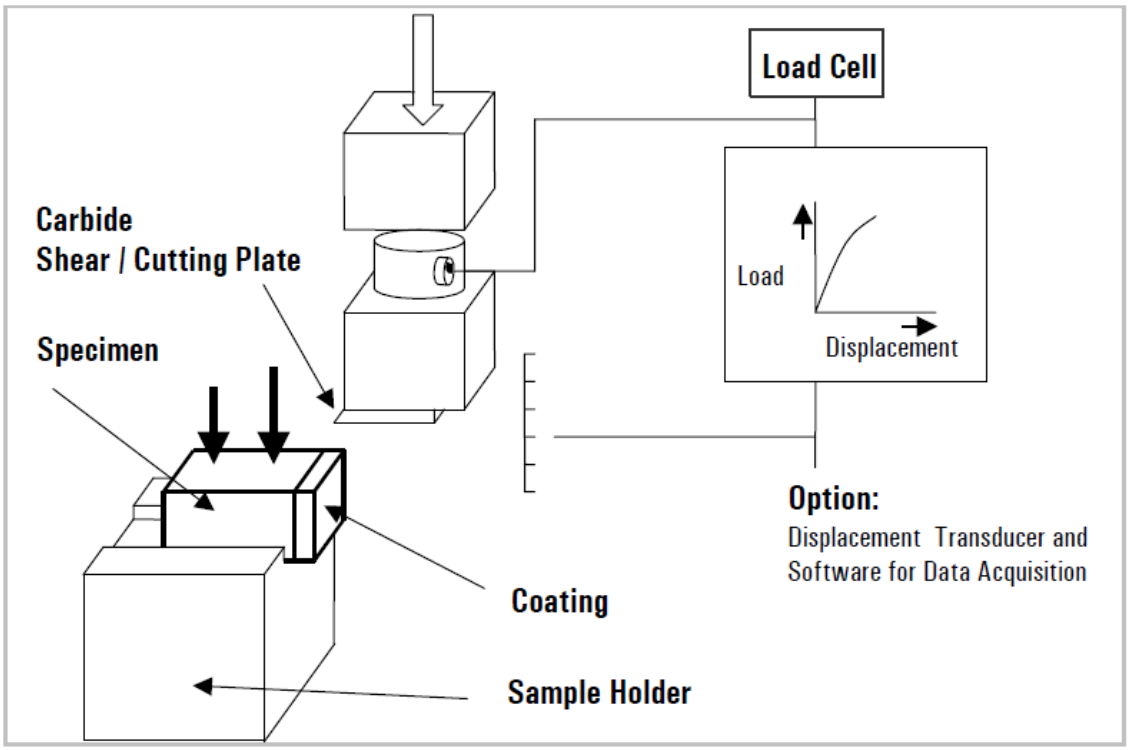

Figure 4-2. *Shear testing device for the determination of shear load resistance of thermally sprayed coatings (see the guideline DIN EN 15340).*

4.7 Rockwell test

Rockwell tests are usually used to determine the hardness of thin coatings. In this study, Rockwell tests were conducted for evaluation of the cohesive strength of plasma-sprayed ceramic coatings. The plasma-sprayed coatings were polished using 2400-grit SiC papers, resulting in an arithmetic mean surface roughness of 0.45+/-0.09 µm. The reduction of surface roughness is necessary for accurate measurements. Rockwell tests were carried out according to the guideline VDI 3824 by Mr. Schrader at Lehrstuhl für Fertigungstechnologie (LFT) of Friedrich-Alexander-University Erlangen-Nürnberg.

4.8 Scratch test

Scratch tests were carried out according to the guideline DIN EN 1071-3 by Mr. Schrader at LFT of Friedrich-Alexander-University Erlangen-Nürnberg. During the scratch tests, scratch traces of 10 mm length were generated using a sliding rate of 10 mm/min and a load rising from 0 to 100 N. An arithmetic mean surface roughness of the specimens for the scratch tests was 0.45+/-0.09 µm.

4.9 Friction and wear tests

In order to investigate the tribological behaviours of the as-sprayed and post-treated YSZ coatings, tribological tests were performed in form of the three-ball-on-disc test that is a modified version of the well known pin-on-disc test [54]. The three-ball-on-disc test was chosen in order to avoid tipping of the pin on the coated specimen. The tests were performed on a WAZAU tribometer TRM 1000 by Mr. Schrader at LFT of Friedrich-Alexander-University Erlangen-Nürnberg. In the setup of the test, three balls of the bearing steel 1.3505 (100Cr6) rotated on a planar coated specimen with an oscillation of 90°, meaning a rotation of the specimen of 90° and a rotation backwards to its initial position (Figure 4-3). The diameter of the balls was 4.78 mm. A load of 60 N and a sliding speed of 25 mm/s were applied. With a rotation diameter of 25 mm, the sliding path for one trace and one cycle added up to 39.27 mm. The tests were carried out at room temperature, and under dry conditions. The wear traces were investigated by confocal microscopy, measuring also the profile depths of the wear traces. The coefficients of friction against sliding were calculated by the relation of the friction torque to the applied load. In addition to confocal microscopy, the worn surfaces were analysed using scanning electron microscopy (Zeiss LEO, 1450VP, Fraunhofer UMSICHT, Sulzbach-Rosenberg) for the investigations of wear mechanisms. Another sliding wear tests - using a 10.8 diameter WCCo ball and 200g load, with a sliding rate of 60 cycles per minute and for 40h - were conducted on a ball-on-disc arrangement of a simple tribometer by Mr. Wolf at Fraunhofer UMSICHT, Sulzbach-Rosenberg, to determine the wear rates. The specimens for the tests were polished using 2400-grit SiC papers, resulting in an arithmetic mean surface roughness of 0.45+/-0.09 µm.

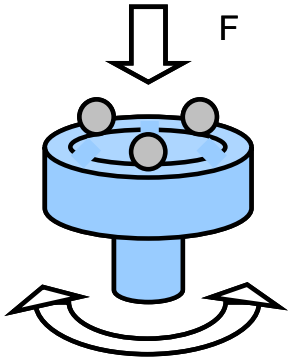

Figure 4-3. *Schematic drawing of the three-ball-on-disc test [54].*

4.10 Thermal shock cycling tests

The thermal shock cycling tests of the “as-sprayed” and post-treated thermal barrier coatings (TBCs) were conducted in an electric furnace with an air atmosphere (chemistry lab, SMPG-DGU, LMU). A thermal cycle consisted of directly inserting samples to the temperature 1100 °C, holding for 30 min, and quenching to ambient temperature. The spalled ceramic top coat was investigated by a scanning electron microscopy (Zeiss LEO, 1450VP, Fraunhofer UMSICHT, Sulzbach-Rosenberg), equipped with energy dispersive spectrometer (EDS). The microstructures and elemental distributions of cross section of the thermal shock examined specimens were characterized by EPMA (electron probe micro-analyzer, SX100, CAMECA, SMPG-DGU, LMU) with a back-scattered electron imaging mode.

5 EXPERIMENTAL RESULTS

5.1 Materials and plasma spraying process

Plasma spraying for the sample preparation was carried out by technicians at Fraunhofer UMSICHT, Sulzbach-Rosenberg. A steel cylinder from steel 1.3343 with a radius and height of 1 cm, respectively was grit blasted with aluminium oxide (F24) to activate the surface. Commercial Ni-based superalloy 625 (Sulzer Metco, Switzerland), 8wt% Y_2O_3 stabilized ZrO_2 (GTV, Germany) and YSZ/Al_2O_3 (70/30) (GTV, Germany) were used as feedstock powders for the atmospheric plasma spraying. A plasma torch F4 of Sulzer Metco was used. The Ni-based superalloy 625 was deposited as a bond coat for the ceramic top coat on the surface of the pre-treated steel cylinder. Later on a 200 µm YSZ coating was sprayed on the bond coat. The chemical composition of the superalloy 625 is shown in Table 5-1.

Table 5-1: *Chemical composition of superalloy 625 in weight percent*

Elements	Ni	Cr	Mo	Fe	Nb+Ta	Si	Ti	Al	Mn
Weight (%)	62.5	21.3	8.3	3.7	3.36	0.3	0.2	0.1	0.1

Table 5-2: *Plasma spraying parameters for the superalloy 625 and 8YSZ coatings*

Powder type	ZrO_2/Y_2O_3 92/8	YSZ/Al_2O_3 70/30	Superalloy 625
Particle size (µm)	20-45	11-45	11-45
Power input (kW)	41.6	49	35
Primary gas Ar (slpm)	40	40	43
Secondary gas H2 (slpm)	12	13	9.5
Carrier gas Ar (slpm)	2.8	3.0	3.2
Powder feed rate (g/min)	30	30	60
Stand-off distance (mm)	120	120	120

For further study, composite with 30 wt% alumina in a zirconia matrix was applied as the top coat of the two-layer system. The specimens were well coated and no cracks

were seen. The applied parameters of the plasma spraying process are summarized in Table 5-2.

5.2 Experimental apparatus for solvothermal processings

In order to conduct the solvothermal processings for the chemical densification post-treatment on the two-layer system - consisting of the atmospheric plasma-sprayed 8 wt% yttria-stabilized zirconia (8YSZ) as a top coat and Ni-based alloy as a bond coat- at atmospheric pressure, a simple experimental apparatus was created. It contains an oven and a gas system including off-gas cleaning up as shown in Figure 5-1. The temperature in the oven (aluminium oxide tube) may go up to 1100 °C and the concentration of HCl in nitrogen gas can be computer-regulated and -controlled. This apparatus can realize the purge of oxygen from the oven with nitrogen gas before carrying out the post-treatment, and also can clean up the off-gas using the desiccant and caustic solution.

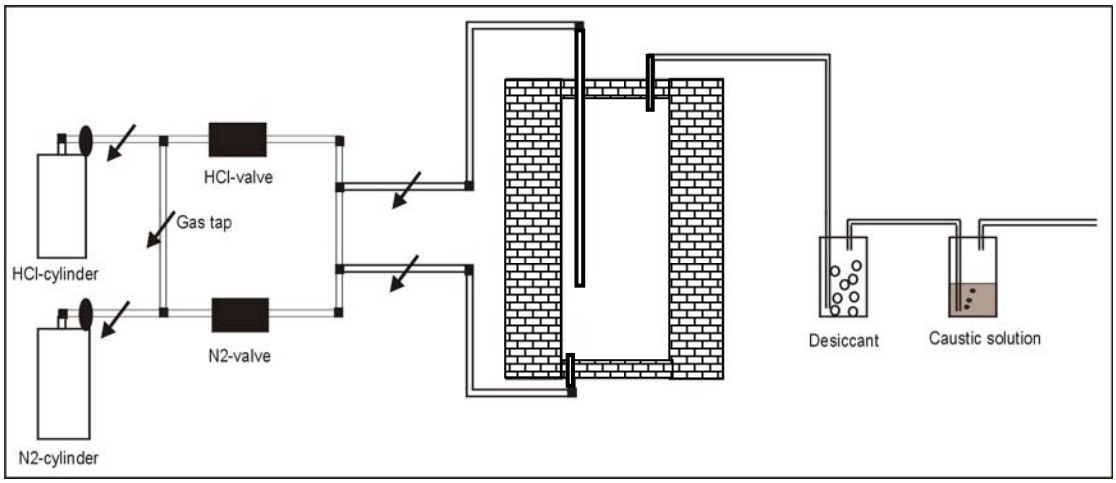

Figure 5-1. *Experimental apparatus for the determination of solvothermal solvent and the chemical densification post-treatment.*

5.3 Solvothermal solvent determination

Before the chemical densification post-treatments on the plasma sprayed coatings were conducted, compositions of the solvothermal solvents and conditions for the following post-treatments were investigated. A quartz crucible was applied as a

solvent container, which was located in the oven of the experimental apparatus (Figure 5-1). Excessive commercial 8 wt% Y_2O_3 stabilized ZrO_2 powders (GTV, Germany) were added to the mixture of equimolar salts of KCl and $ZnCl_2$ or KCl, $ZnCl_2$, K_2SO_4 and $ZnSO_4$ in ratio 1:10 and then heated at the temperatures ranging from 600 °C to 800 °C in the presence of a N_2 atmosphere with or without HCl partial pressure. The total flow rate is 100 sccm. It is assumed that after 12 hours no more zirconia is dissolved in the molten salts. After being heated for 12 hours at the prescribed temperatures, the molten salts were sucked through an alumina tube, taken out of the oven for use as a sample and then dissolved in the deionized water. The experimental principle was according to the literature [55]. The concentrations of the Zr, K and Zn ions in the deionized water were determined by an ICP mass spectrometry. The concentrations of zirconia in the molten chlorides of equimolar KCl and $ZnCl_2$ and in the mixture of equimolar molten salts of KCl, $ZnCl_2$, K_2SO_4 and $ZnSO_4$ were calculated from concentrations of the Zr, K and Zn ions which were measured by an ICP mass spectrometry. The results are listed in Table 5-3.

Table 5-3: *The solubility of zirconia in molten salts in different atmosphere at temperatures ranging from 600 °C-800 °C*

Sample	S1	S2	S3	S4	S5
Temperature (°C)	600	700	700	700	800
Molten salts	chlorides, sulfates	chlorides, sulfates	chlorides	chlorides, sulfates	chlorides, sulfates
HCl in N2 atmophere (%)	2	2	2	0	2
Solubility of zirconia (%)	6.1E-02	1.8E-01	1.1E-04	1.2E-03	1.2E-01

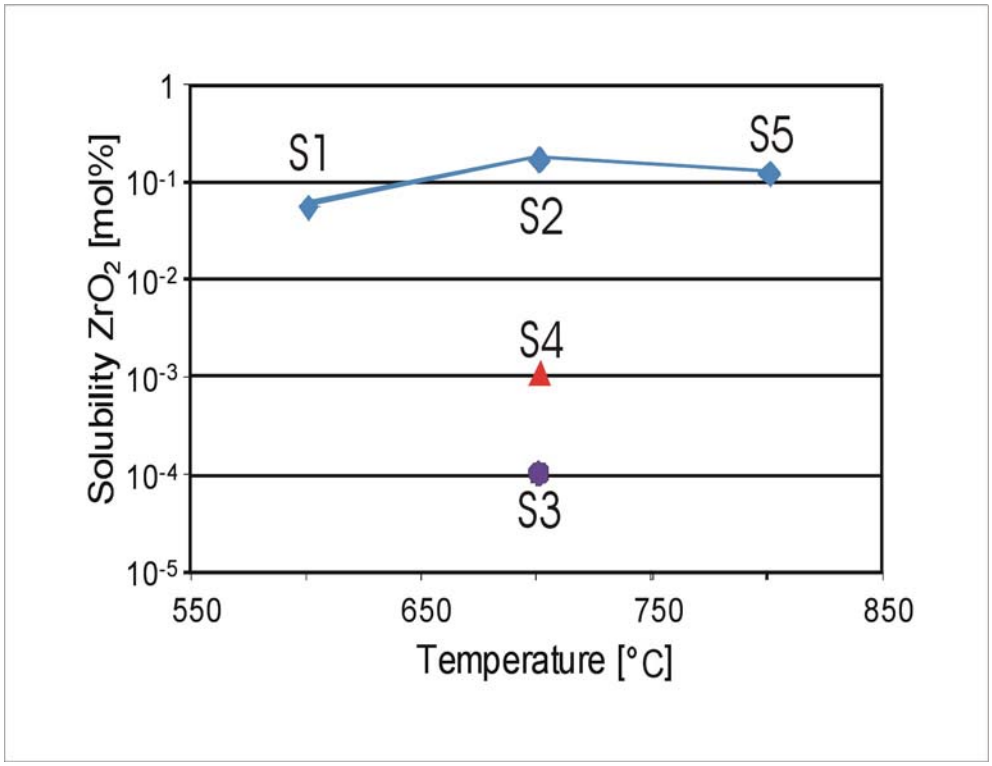

Figure 5-2. *The solubility of zirconia in molten salts in different atmosphere at temperatures ranging from 600 °C-800 °C.*

Figure 5-2 shows the solubility of zirconia (the concentration of zirconia in the molten salts after dissolution for 12 hours) in the two above mentioned molten salts under the different conditions. It is clearly seen that at temperatures between 600 °C and 800 °C the solubilities of zirconia of samples S1, S2 and S5 in the mixture of equimolar molten salts of KCl, $ZnCl_2$, K_2SO_4 and $ZnSO_4$ in a N_2 atmosphere containing 2% HCl is many orders of magnitude that of sample S3 in the molten chlorides. It is therefore deduced that sulfates are one necessary component of the solvothermal solvents. According to the solubility of zirconia of sample S4, HCl-content in a N_2 atmosphere enhances the dissolution of zirconia in the molten salts. A maximum solubility of zirconia of 0.18% was achieved at 700 °C in a N_2 atmosphere containing 2% HCl in the mixture of equimolar molten salts of KCl, $ZnCl_2$, K_2SO_4 and $ZnSO_4$. Therefore, this reaction condition at temperatures ranging from 600 °C to 800 °C was used for the solvothermal processings on the plasma sprayed coatings.

5.4 Solvothermal treatment on the two-layer systems

Steel cylinders, coated with Ni-based superalloy 625 as a bond coat and ceramics (yttria stabilized zirconia (YSZ) or YSZ/alumina 70/30) as a top coat by the plasma spray process, were post-treated by means of a solvothermal process [56]. For the post-treatment, commercial 8 wt% Y_2O_3 stabilized ZrO_2 powders (GTV, Germany) were added to the mixture of equimolar KCl, $ZnCl_2$, K_2SO_4 and $ZnSO_4$, then heated at the temperatures ranging from 600 °C to 800 °C in the presence of a N_2 atmosphere containing 2% HCl partial pressure since the maximum solubility of zirconia was achieved in these conditions. The coated specimens were located upon the molten inorganic solvents as shown in Fig. 5-3. The total flow rate was 100 sccm. The solvothermal gas phase transported to the two-layer system which was also heated at the same temperatures. The off-gas was cleaned up with a basic solution. The heat rate is 3 K/min and the cooling rate is lower than 3 K/min. Specimens, coated with Ni-based superalloy 625 as a bond coat and 8 wt% yttria stabilized zirconia (8YSZ) as a top coat, were solvothermal post-treated at different temperatures for the further microstructure investigations. Parameters of the solvothermal post treatment are summarized in Table 5-4.

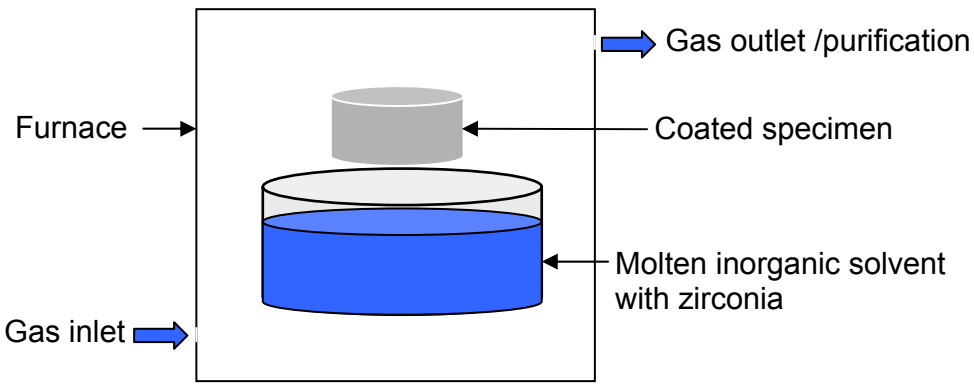

Figure 5-3. *Coated specimens in the oven for solvothermal post treatment.*

Table 5-4: *Specimens post treated for microstructural investigations*

Specimen	C1	C2	C3	C4
Temperature (°C)	600	700	800	800
Molten salts	chlorides, sulfates	chlorides, sulfates	chlorides, sulfates	chlorides, sulfates
HCl in N2 atmosphere (%)	2	2	2	2
Treatment duration (h)	72	72	72	24

In order to investigate the microstructure of post-treated YSZ top-coats, the microstructure and elemental distributions of the cross-sectional as-sprayed and post-treated coatings were studied by EPMA. Figure 5-4 shows a typical microstructure of the “as-sprayed” plasma sprayed ceramic coatings, which demonstrates a number of pores and microcracks in the YSZ coating. The lamellar structure with numerous globular pores, interlamellar pores and microcracks can be clearly recognized in the magnified image. The magnified region was characterized by element mapping of oxygen, zirconia and yttrium. The pores were also indicated by the corresponding elemental distributions in this region.

Figure 5-5 demonstrates the microstructure and elemental distributions of the cross-sectional specimen C2 which was treated at 700 °C under the determined solvothermal conditions. The densification phenomena were observed in the ceramic scale, but there was still a region near the ceramic topcoat surface, which was not modified yet. From the EPMA mapping analysis, it can be obviously seen that the elements oxygen and zirconium were almost homogeneously distributed in the measured region, compared with Fig. 5-4. However, there still remained pores in the densified region.

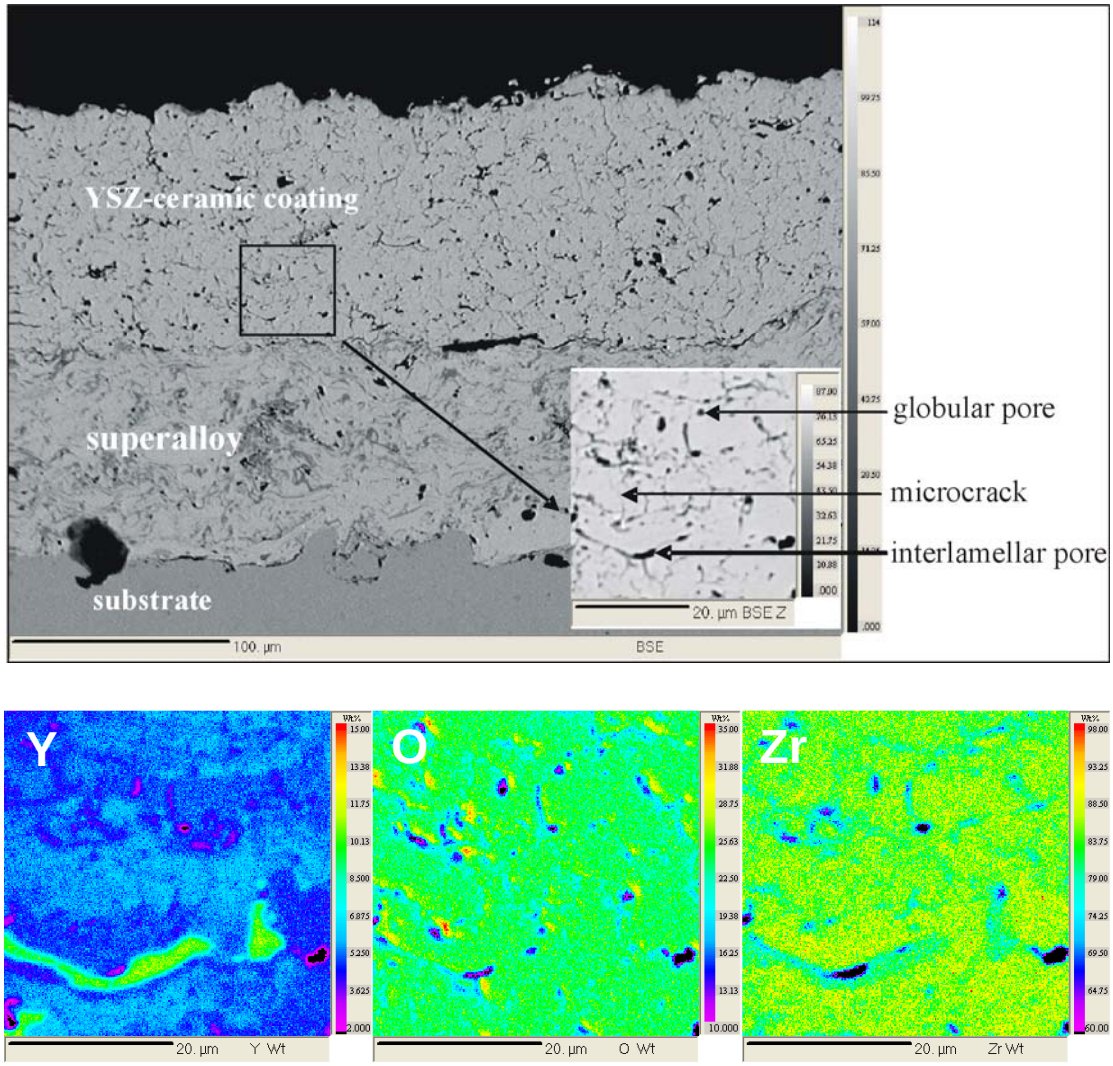

Figure 5-4. *BSE image and element distribution images for Y, O and Zr of cross section of the "as-sprayed" YSZ coating.*

The solvothermal post-treatments were carried out on the plasma-sprayed two-layer system at a temperature of 600 °C (specimen C1), 700 °C (specimen C2) and 800 °C (specimen C3) for 72 hours in order to investigate the influence of temperatures on the microstructure of the YSZ coatings. Only 100 µm (in the direction from the interface to the surface) of the YSZ coat of specimen C1 could be densified after the treatment at 600 °C for 72 hours while the densified region of the YSZ topcoat of specimen C2 was thicker and denser after being post-treated at 700 °C as shown in Figure 5-6(a) and Figure 5-6(b). At 800 °C, the top coat of specimen C3 was much better densified. However, new microcracks were formed in the ceramic coat of specimen C3, which can be observed in Figure 5-6(c). Therefore, just shorter processing time is required at 800 °C until the whole ceramic coating is to be

densified. Figure 5-6(d) demonstrates the microstructure of the ceramic coat of specimen C4 that was post-treated at 800 °C for 24 h. It is seen that the densification processing was already finished from the interface to the ceramic surface and no microcracks were formed.

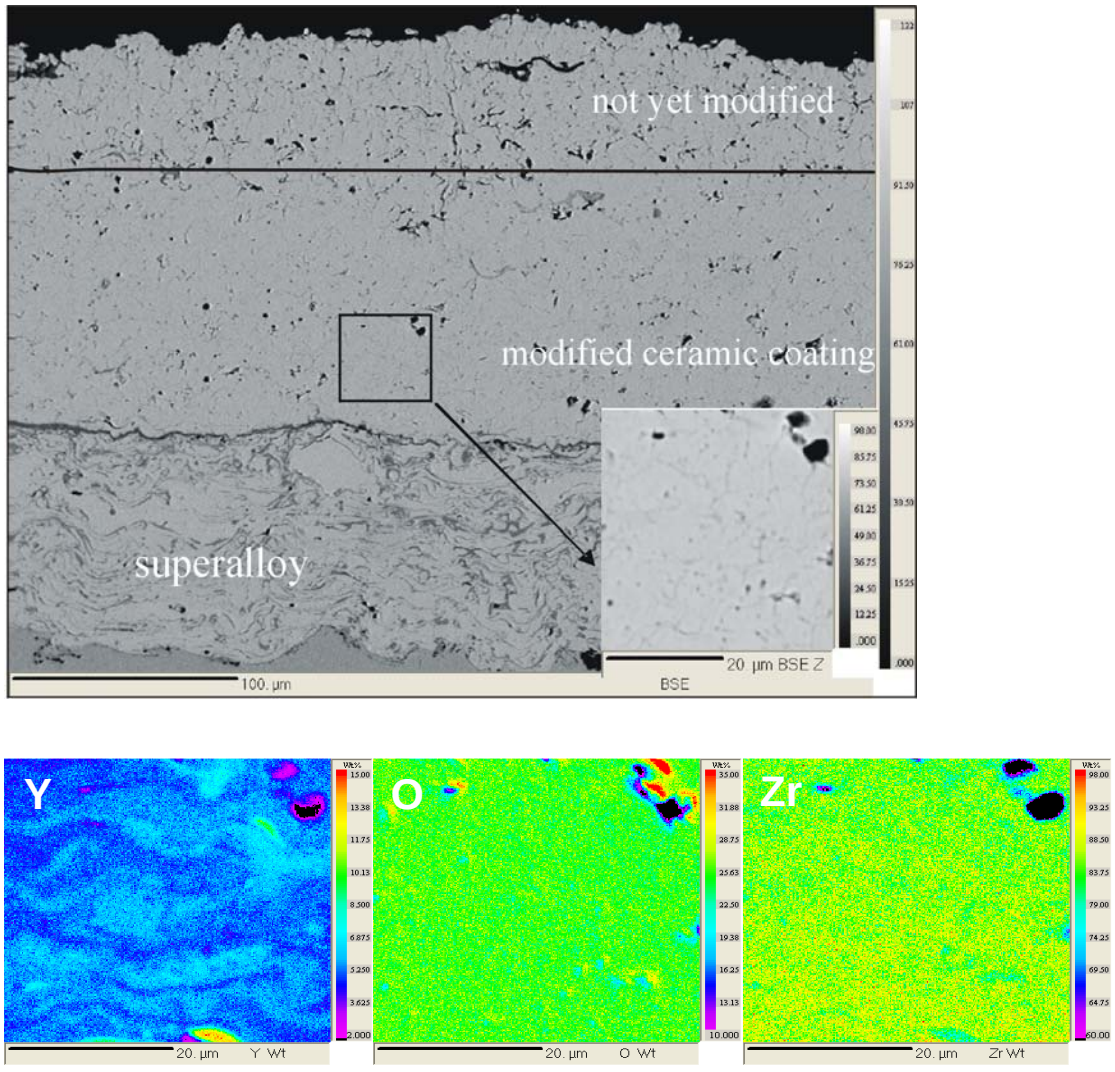

Figure 5-5. *BSE image and element distribution images for Y, O and Zr of cross section of Specimen C2.*

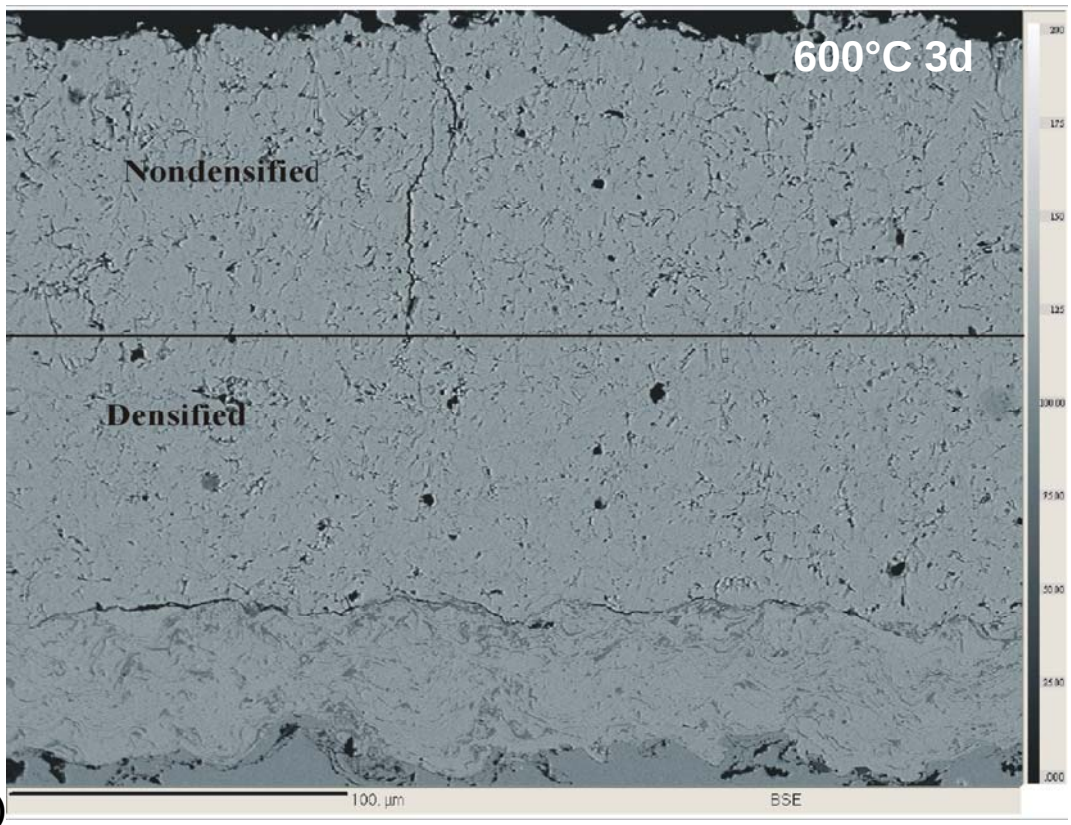

(a)

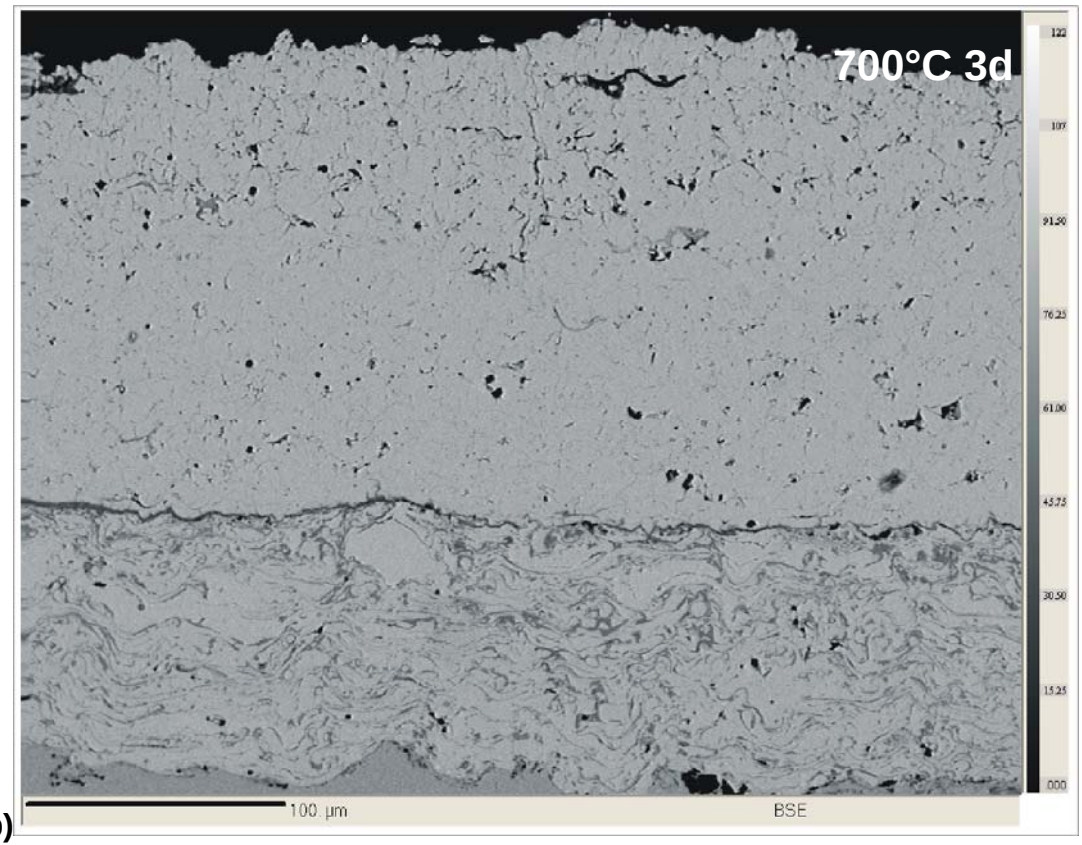

(b)

Figure 5-6. *BSE images of the cross-sectional specimens* ***(a)*** *C1,* ***(b)*** *C2.*

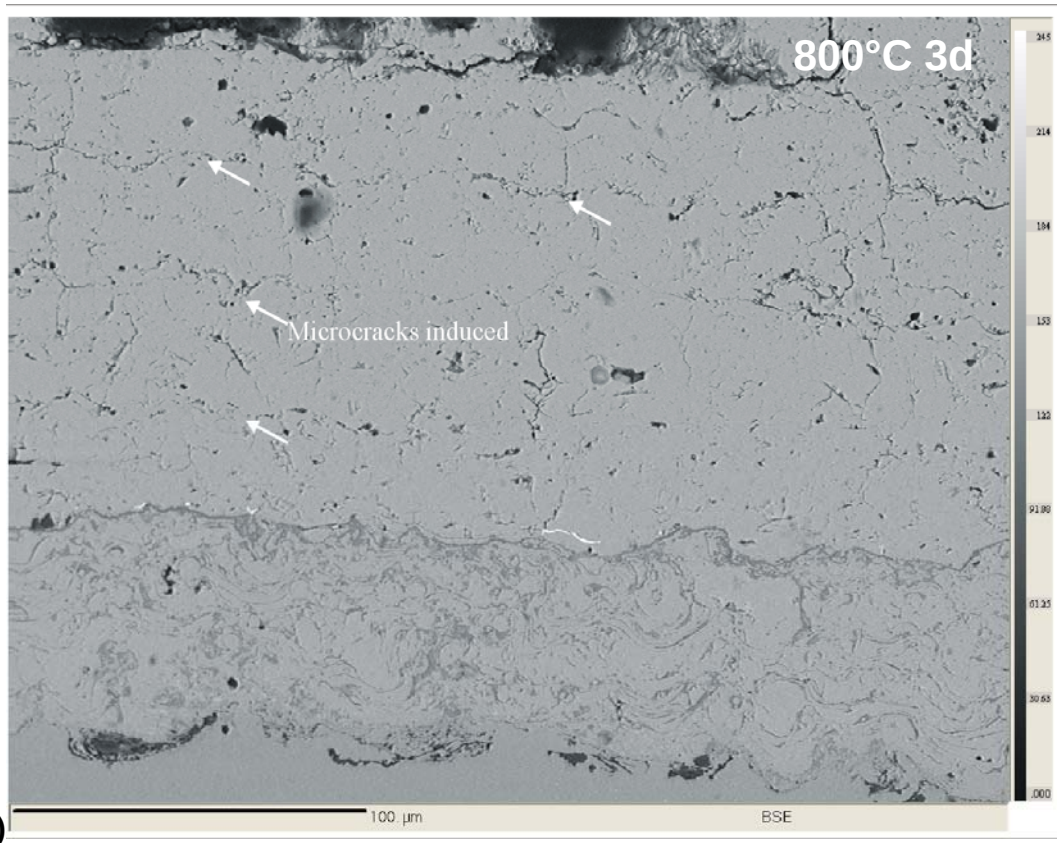

(c)

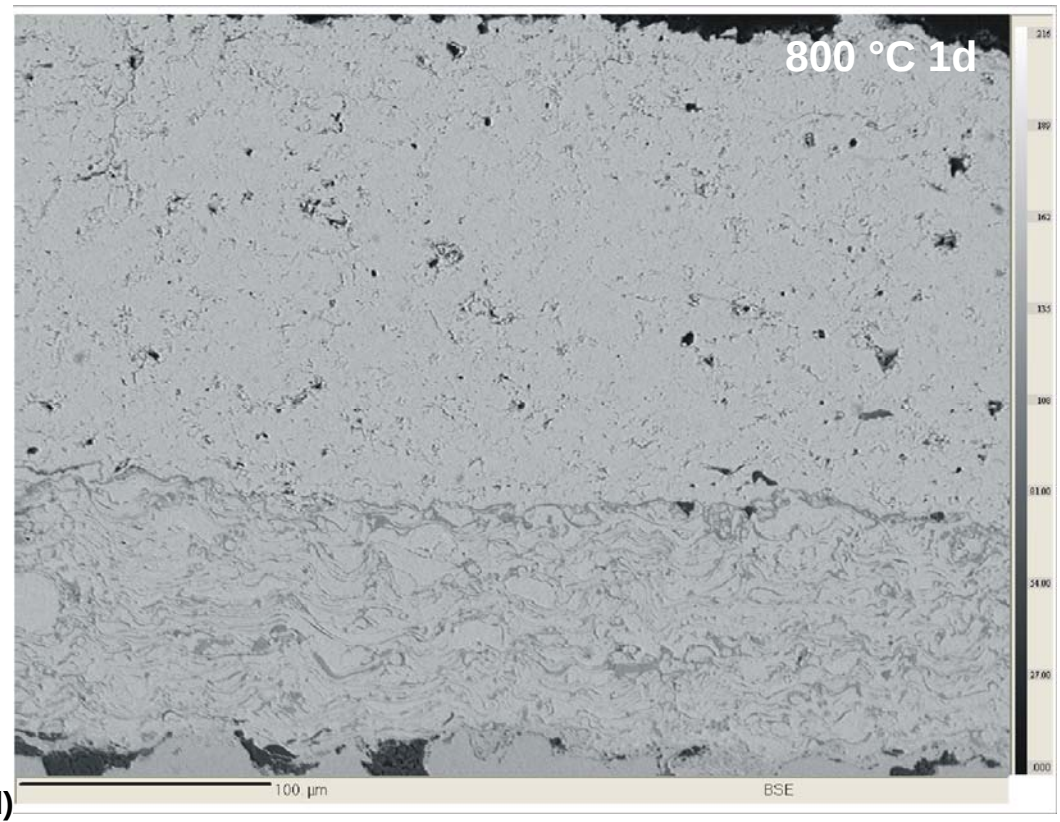

(d)

Figure 5-6. *(continued) BSE images of the cross-sectional specimens* ***(c)*** *C3, and* ***(d)*** *C4.*

According to the phase diagram (Figure 3-8), pure zirconia exhibits three stable crystal structures depending on temperature and zirconia is monoclinic at low temperatures. Tetragonal zirconia can be stabilized by addition of Yttria at low temperatures. However there is still a question: Is the tetragonal phase of YSZ still stable during the solvothermal processings? Three cylinders from steel 1.3343 with a radius of 2.5 cm and height of 0.5 cm were coated with Ni-based alloy as a bond coat and 8YSZ as a top coat for x-ray diffraction measurements. One was applied as “as-sprayed” and the others were post treated at 700 °C and 800 °C for 72 hours as demonstrated in Table 5-5. During the x-ray diffraction measurements, specimens were located on the sample holder. Figure 5-7 shows XRD patterns of as-sprayed and post-treated YSZ coatings of specimens X2 and X3. Both of the as-prayed and post-treated coatings consist of the tetragonal zirconia and no new phases were formed after the chemical densification process.

Table 5-5: *Specimens post treated for x-ray diffraction measurements*

Specimen	X1	X2	X3
Temperature (°C)	as-sprayed	700	800
Molten salts		chlorides,sulfates	chlorides,sulfates
HCl in N2 atmosphere (%)		2	2
Treat time (h)		72	72

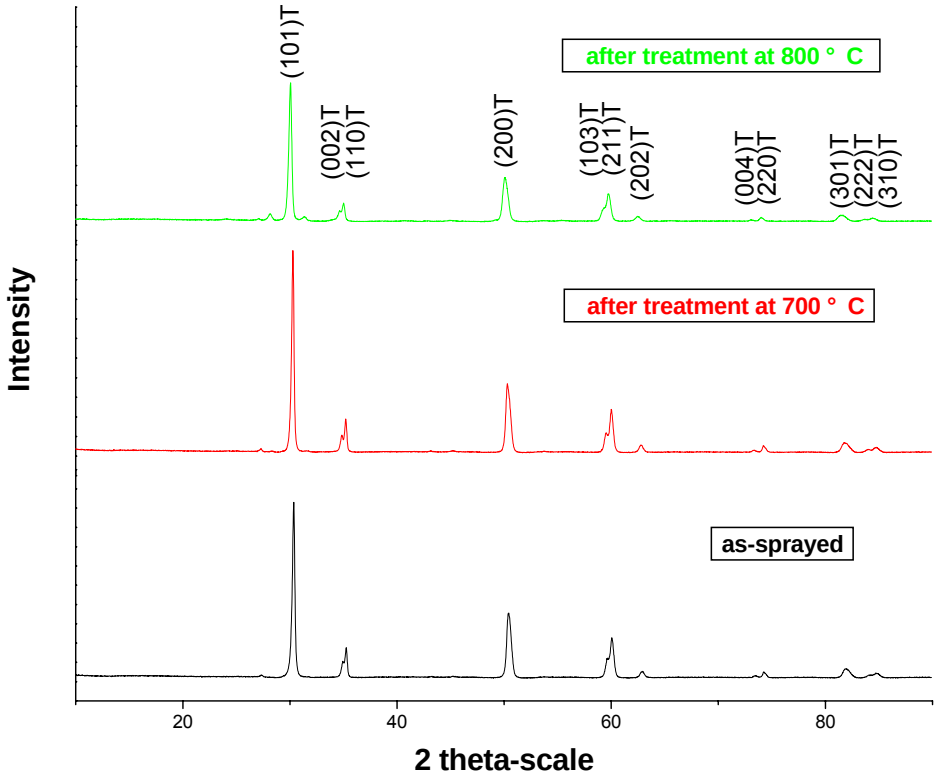

Figure 5-7. *XRD patterns of as-sprayed and post-treated YSZ coatings.*

In order to investigate the influence of the post-treatments on the superalloy bond coat and the bond-coat/top-coat interface, the microstructures of the cross sections and elemental compositions of the bond coat were also analyzed by EPMA mapping. Figure 5-8(a) shows the mapping results of the as-sprayed bond coat. It is seen that the elements were randomly distributed in the bond coat and an oxygen content of up to 15% was detected. Pores arising from the incomplete contact could be observed at the top-coat/bond-coat interface as shown in the BSE image.

Figure 5-8(b) shows the results of the EPMA mapping analysis on the cross-section of specimen C2 that was solvothermal post treated at 700°C for 72 hours. In the BSE image, a ca. 1 µm new layer was observed at the top-coat/bond-coat interface. According to the corresponding mapping analysis, it is deduced that this layer consists mainly of chromia that was formed during the post-treatments and arises from the oxidation of chromium from the bond coat. Aluminium from the bond coat was also oxidized, however, the alumina, detected by the mapping analysis, can be also from the grit blasting before the plasma spraying. In this new formed layer no pores or cracks could be observed.

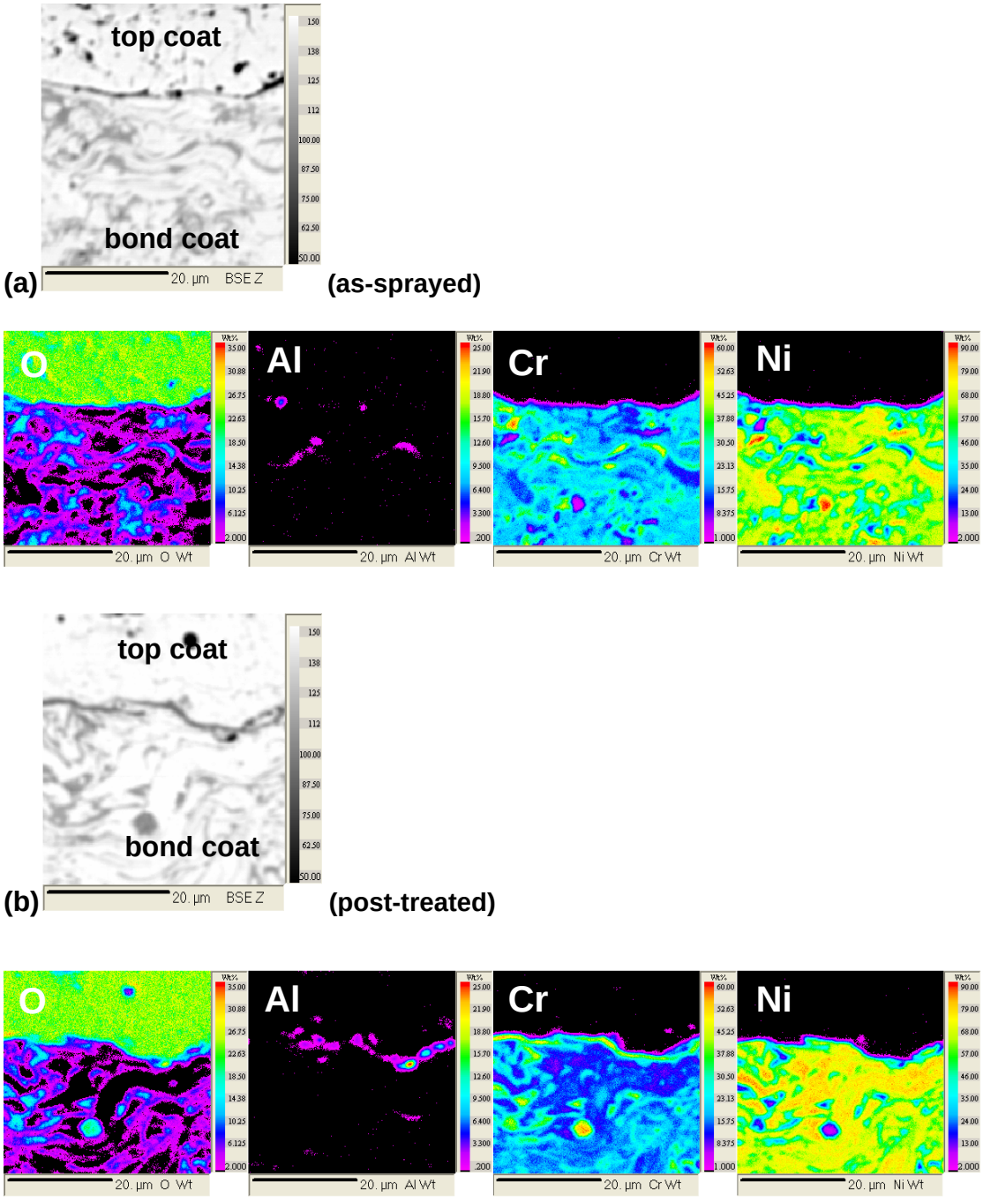

***Figure 5-8**. BSE images and element distributions of cross section of the "as-sprayed" **(a)** and post-treated specimen C2 **(b)** bond coats and the topcoat/bondcoat interface.*

5.5 Porosity and microhardness of the YSZ top coats

The porosity of the YSZ top coat in 2-dimension was determined with the help of image analysis, where a binary image of the chosen region can be obtained through thresholding the image and an indication of the porosity of this region is given as shown in Fig. 5-9. For image analysis, an optical microscope was applied to obtain 500 magnification images. 3 fields were analysed at the same cross section for the porosity determination of each coating (as-sprayed and specimens C1-C3). The results of the porosity measurements on the as-sprayed and post treated ceramic coats are shown in Table 5-6.

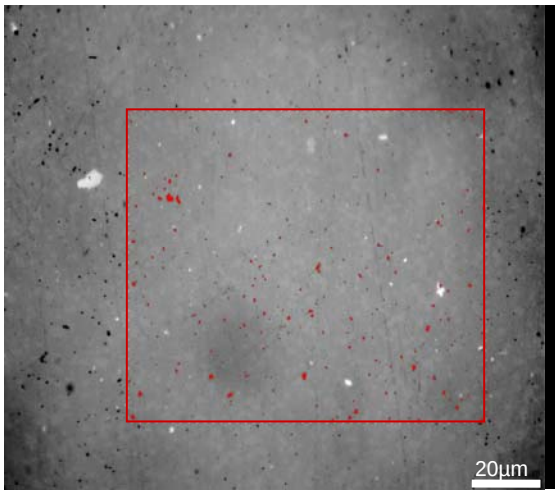

Figure 5-9. *Optical microscopic images for porosity determination with the help of image analysis, where a binary image gives an indication of the porosity of the chosen region (pores are in red).*

The plasma-sprayed ceramic coatings normally contain many pores. Applying the parameters for the plasma spray process, the as-sprayed YSZ coat has a relatively high average porosity of 7.9% due to a low velocity of the spray particles during spraying. The porosity of the plasma-sprayed YSZ coatings was obviously reduced by the solvothermal post-treatments. The porosity of the post-treated ceramic coats decreased with a higher treatment temperature. The top coat of specimen C3 with a porosity of 4.3%, post-treated at 800 °C for 72 hours, was denser than that of specimen C2 with 5.0% porosity, treated at 700 °C and also specimen C1 with 7.2% porosity, treated at 600 °C. At 600 °C, only half of the coat was densified after 72

hours treatment. The average porosity of the undensified ceramic region was 10.9% while the densified region had a porosity of 7.2%. All the measured porosities of top coats are displayed in Fig. 5-10. During the solvothermal processes, the connected pores were sealed by the crystallized zirconia, which was indicated from the results of EPMA mapping analysis (see Fig. 5-5).

Table 5-6: *Porosities of the as-sprayed and post-treated YSZ top-coats at different treatment temperatures, measured by image analysis*

Specimen	as-sprayed	C1 (undensified)	C1 (densified)	C2 (densified)	C3 (densified)
Temperature (°C)	as-sprayed	600	600	700	800
Average porosity (%)	7.9	7.2	10.9	5.0	4.3
Error (%)	0.41	0.19	0.84	0.22	0.36

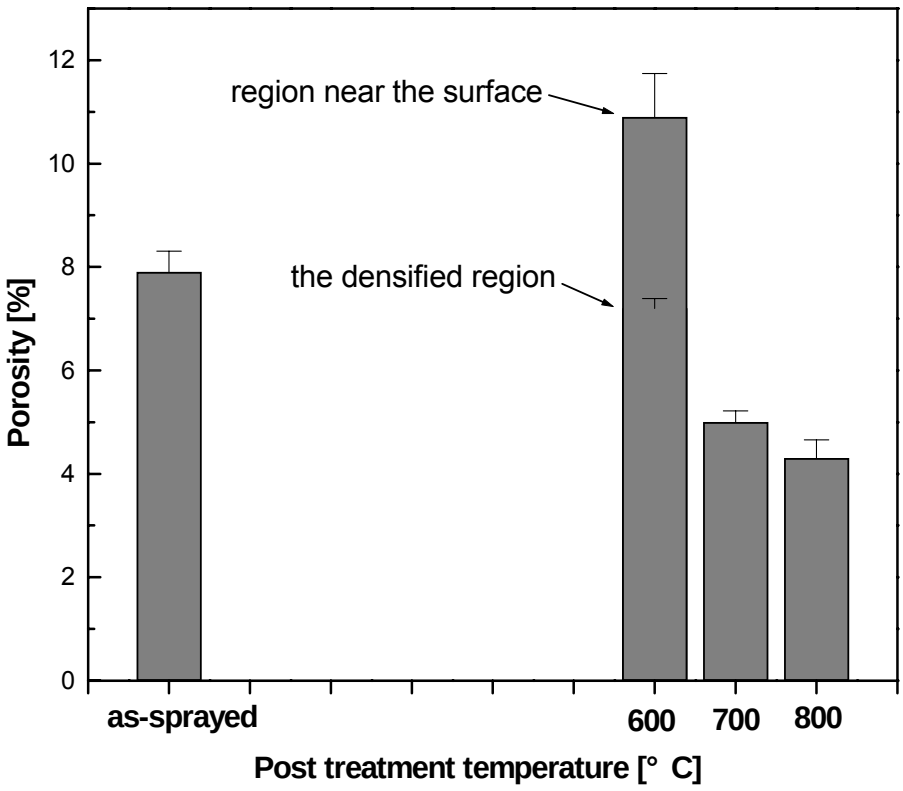

Figure 5-10. *The porosities of the as-sprayed and post-treated YSZ coatings at different treatment temperatures, measured by image analysis.*

Table 5-7: *Microhardness of the as-sprayed and post-treated YSZ top-coats at different treatment temperatures, measured by a Vickers diamond indenter*

Specimen	as-sprayed	C1 (undensified)	C1 (densified)	C2 (densified)	C3 (densified)
Temperature (°C)	as-sprayed	600	600	700	800
Average hardness (Hv)	706.6	553.0	829.4	954.2	1033.0
Error (Hv)	70	87	47	43	69

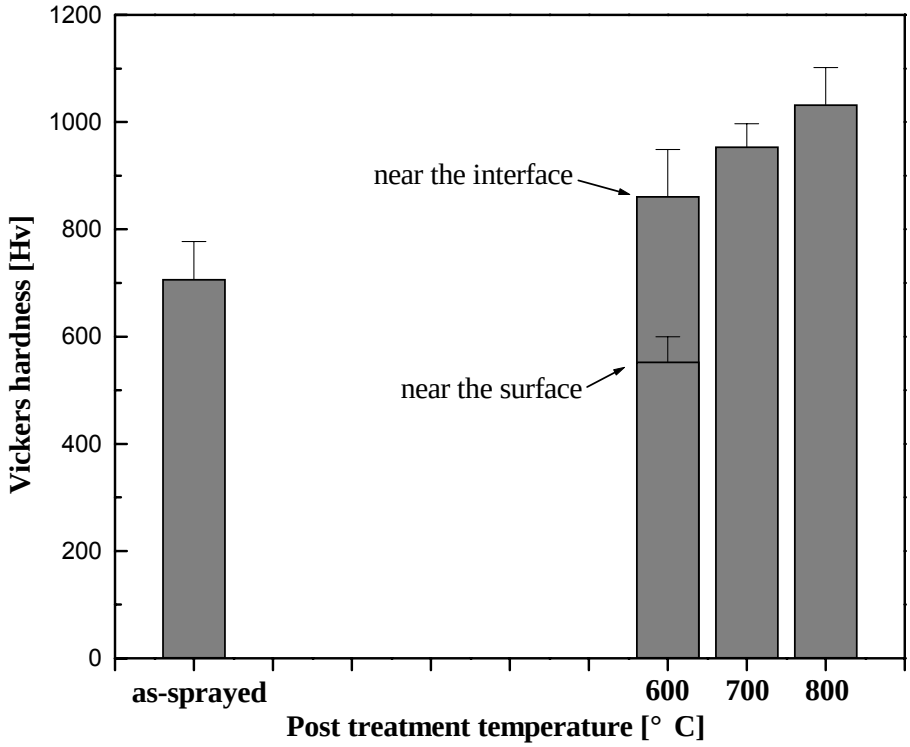

Figure 5-11. *Vickers hardness of the as-sprayed and post-treated YSZ coatings at different temperatures.*

For the microhardness evaluation, a Vickers diamond indenter was used and pressed on the polished cross-section of the ceramic top coats. 5 measurements were conducted on the same cross-section for each coating. Generally, denser ceramic coatings have a higher level of microhardness [26], which was also reflected on our post-treated YSZ coatings, as shown in Table 5-6 and Table 5-7. The

microhardness of the plasma-sprayed YSZ top coat could be also improved by the densification post-treatments. The as-sprayed YSZ coat for our experiments has an average hardness of Hv = 706, whereas a higher hardness of Hv = 1033 of specimen C3 could be achieved by the post-treatments at 800 °C for 72 hours. The results of the measured hardness are shown in Figure 5-11. The YSZ coatings with lower porosity had a higher level of microhardness.

5.6 Adhesive strength of the plasma-sprayed YSZ top coat

It is known that the key to the durability improvement of the plasma-sprayed coatings is retention of strong bonding between the ceramic top coat and the bond coat [57]. Two types of specimens with a size of 30*10*5 mm were applied for evaluating the adhesive strength of the ceramic top coat. Only one side of 10*5 mm was coated with 100 µm Ni-based alloy as a bond coat and 300 µm YSZ as a top coat by the plasma spraying processes. For each type, five specimens were used. One type was as-sprayed and the other was post-treated at 700 °C for 72 hours. The adhesive strength of the ceramic top coats was evaluated by shear tests according to the guideline DIN EN 15340. The experimental results are listed in Table 5-8. The shear force of the as-sprayed ceramic top coat was around 300 N except specimen 5 with 792 N while the shear force of the post-treated top coat reached about 600 N except specimen 9 with 1462 N. This might be ascribed to the stability of the plasma spraying process or a big error, occurring during the shear testing.

Table 5-8: *Adhesive strength of the as-sprayed and post-treated YSZ top coat at 700°C for 72 hours evaluated by shear tests*

Type	As-sprayed					Post-treated				
Specimen No.	1	2	3	4	5	6	7	8	9	10
Shear force (N)	196	273	268	399	792	586	633	420	1462	897
Average shear force (N)	385.6					799.6				
Average adhesive strength (MPa)	7.7					16.0				

Figure 5-12 shows the shear strength at the rupture between the ceramic coat and the bond coat of the as-sprayed and post-treated specimens. It is obviously seen that the average adhesive strength of the post-treated top coat was double that of the as-sprayed.

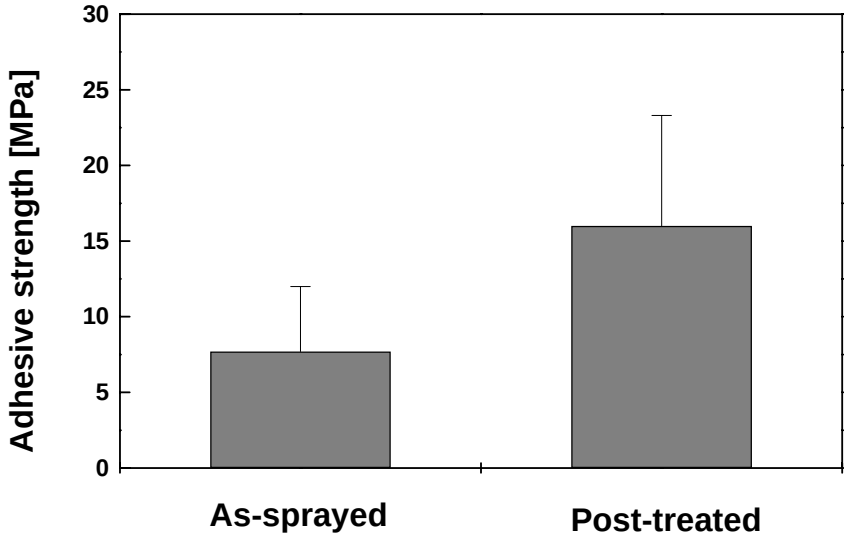

Figure 5-12. *Adhesive strength of the plasma as-sprayed and post-treated YSZ top coat evaluated by shear tests.*

5.7 Mechanical properties

Two cylinders from steel 1.3343 with a radius of 2.5 cm and height of 0.5 cm were coated with Ni-based alloy as a bond coat and 8YSZ as a top coat. The specimens were further polished until an arithmetic mean surface roughness reached 0.45+/-0.09 µm. For further mechanical property investigations, such as scratch tests, Rockwell tests and tribological investigations, the plasma sprayed coatings of cylinder M1 was applied as “as-sprayed” and the other of cylinder M2 was solvothermal post-treated at 700 °C for 72 hours

(a)

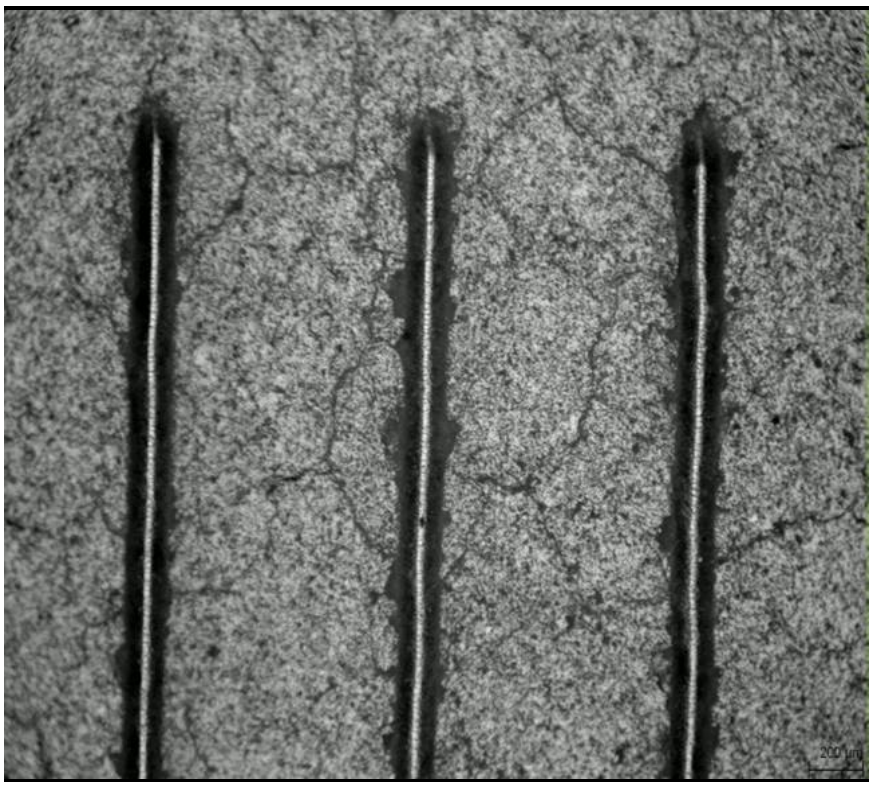

(b)

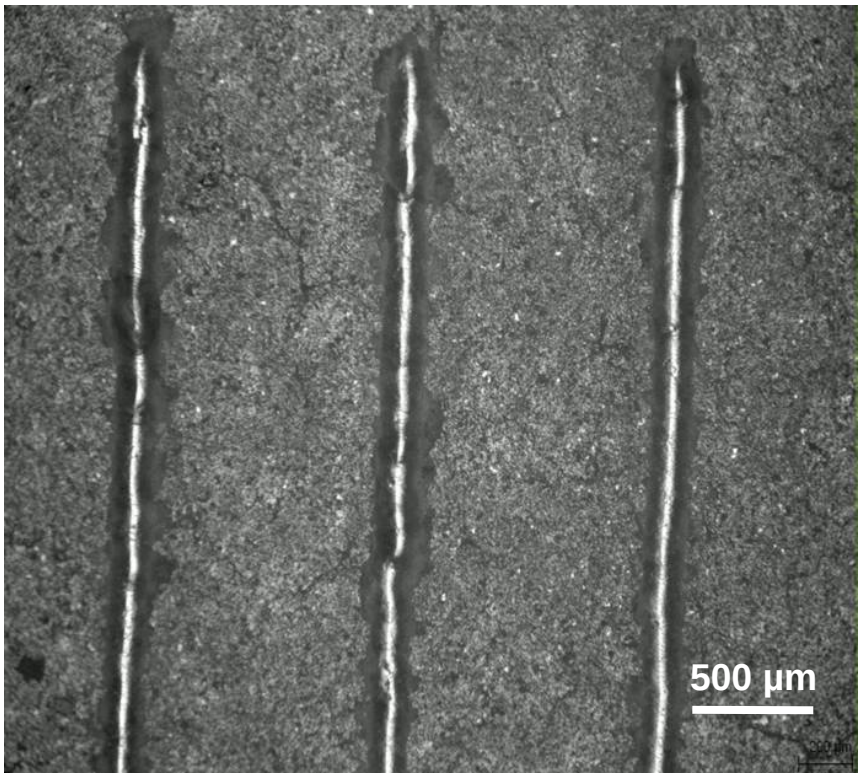

Figure 5-13. *The scratch test trace on (a) the as-sprayed YSZ top coat of M1 and (b) the post-treated of M2.*

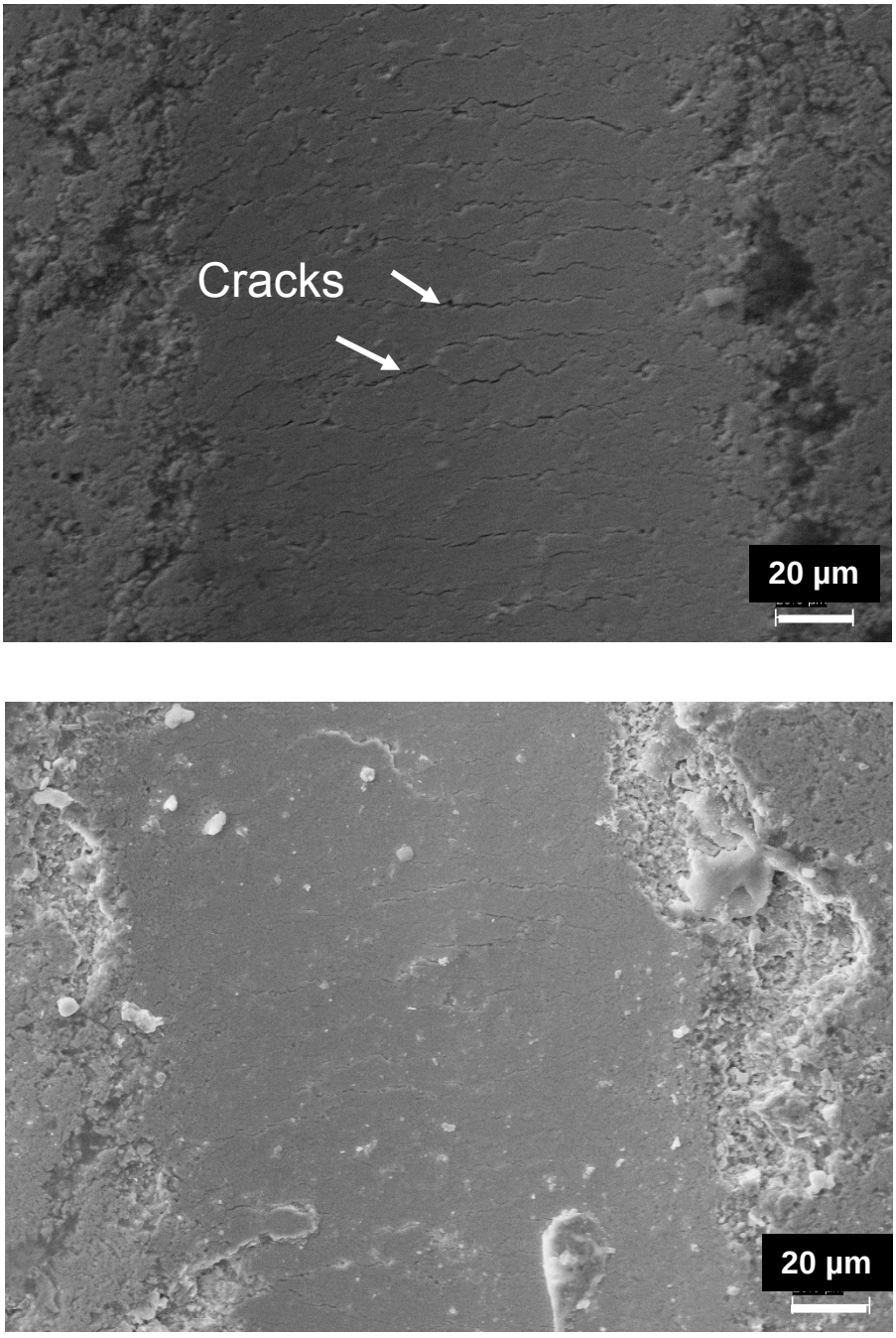

Figure 5-14. *The morphology of the scratch test trace on* ***(a)*** *the as-sprayed YSZ top coat of M1 and* ***(b)*** *the post-treated YSZ of M2.*

Scratch tests were carried out according to the guideline DIN EN 1071-3. During the scratch test, scratch traces of 10 mm length were generated on the YSZ top coats using a sliding rate of 10 mm/min and a load, rising from 0 to 100 N. The results are shown in Figure 5-13. The interfacial strength of the ceramic top coats could be evaluated by the scratch tests. According to the morphology of the scratch test traces

(Figure 5-14), periodic patterns of large cracks which are perpendicular to the scratch direction were obviously observed on the as-sprayed YSZ top coat of the cylinder M1 due to the weak interfacial strength of the splats, whereas the results for the post-treated coating of the cylinder M2 revealed the much less degree of microcracks and fractures.

The interfacial strength of the ceramic top coat is also presented here as the fracture toughness, which could be evaluated by Rockwell test. Rockwell test is normally applied to evaluate the adhesive strength of thin coatings, but for the relatively thick plasma-sprayed coatings, the fracture toughness was tested. Figure 5-15 shows the results of the Rockwell tests. Fractures were generated in the as-sprayed YSZ top coat of M1 after testing while no fracture was presented in the post-treated top coat of M2, which indicates that the fracture toughness of the plasma-sprayed YSZ coating was enhanced by the chemical densification process and this could result in the improved wear resistance.

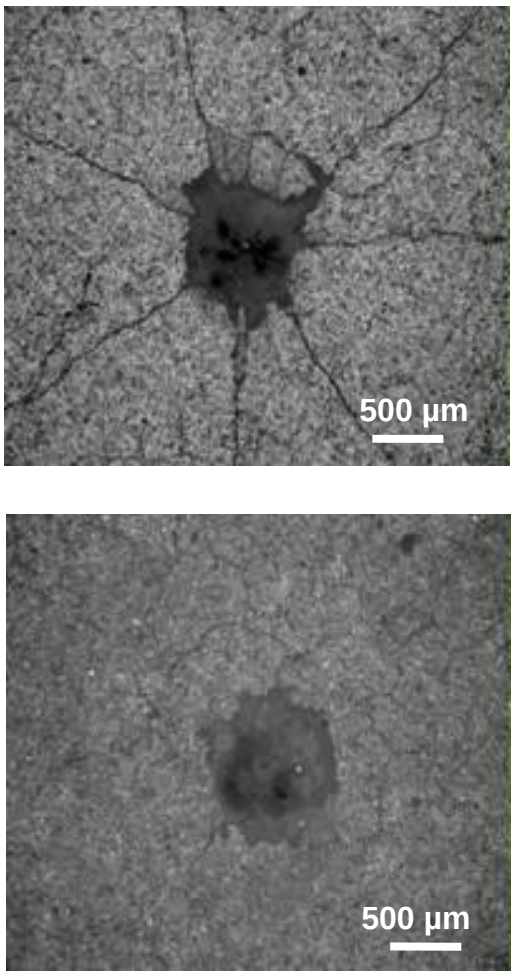

Figure 5-15. *Optical micrographs of the results of Rockwell tests for* ***(a)*** *as-sprayed YSZ top coat of M1 and* ***(b)*** *the post-treated YSZ coating of M2.*

5.8 Tribological behaviours

Friction force is an important parameter of the wear behaviour. Normally, the higher the friction force generated, the lower the wear resistance. The coated and polished specimens were tested, regarding their tribological behaviour in the three-ball-on-disc test. Figure 5-16 shows the evolution of the friction coefficients as a function of sliding cycles at a sliding rate of 25 mm/s, using an applied load of 60 N against 100Cr6 steel balls for the as-sprayed YSZ top coat of the cylinder M1 and post-treated YSZ top coat of M2. At the beginning of the sliding process, both of the coatings had a friction coefficient of nearly 0.13. With increasing sliding cycles, the friction coefficient of the as-sprayed coating of M1 however increased rapidly to 0.5. In contrast, the friction coefficient of the post-treated YSZ-coating of M2 remained nearly constant within the range of 0.13 to 0.18. At the end of the test, a friction coefficient of 0.16 for the post-treated YSZ-coating was recorded as shown in Figure 5-16.

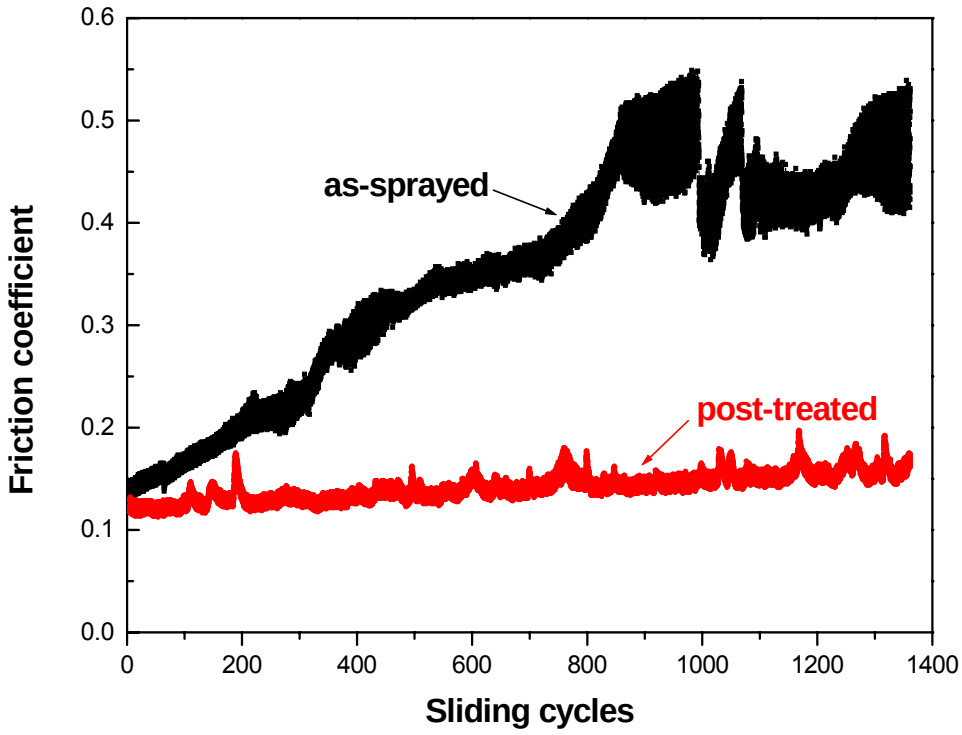

Figure 5-16. *Friction coefficient evolutions on the as-sprayed YSZ top coat of M1 and the post-treated YSZ coating of M2 against 100Cr6 steel balls.*

The depth profiles of the sliding traces on the examined YSZ top coats of M1 and M2 after 1350 sliding cycles are shown in Figure 5-17. The corresponding optical images of the sliding traces were recorded by confocal microscope with white light. The sliding trace image of M1 presented a worn surface with ca. 3 µm wear depth. It can be deduced that the as-sprayed ceramic coatings has a weak cohesion and strength, resulting in the rising friction coefficient. Compared with this, the sliding trace surface of the post-treated coating of M2 was still smooth and the wear depth was negligible.

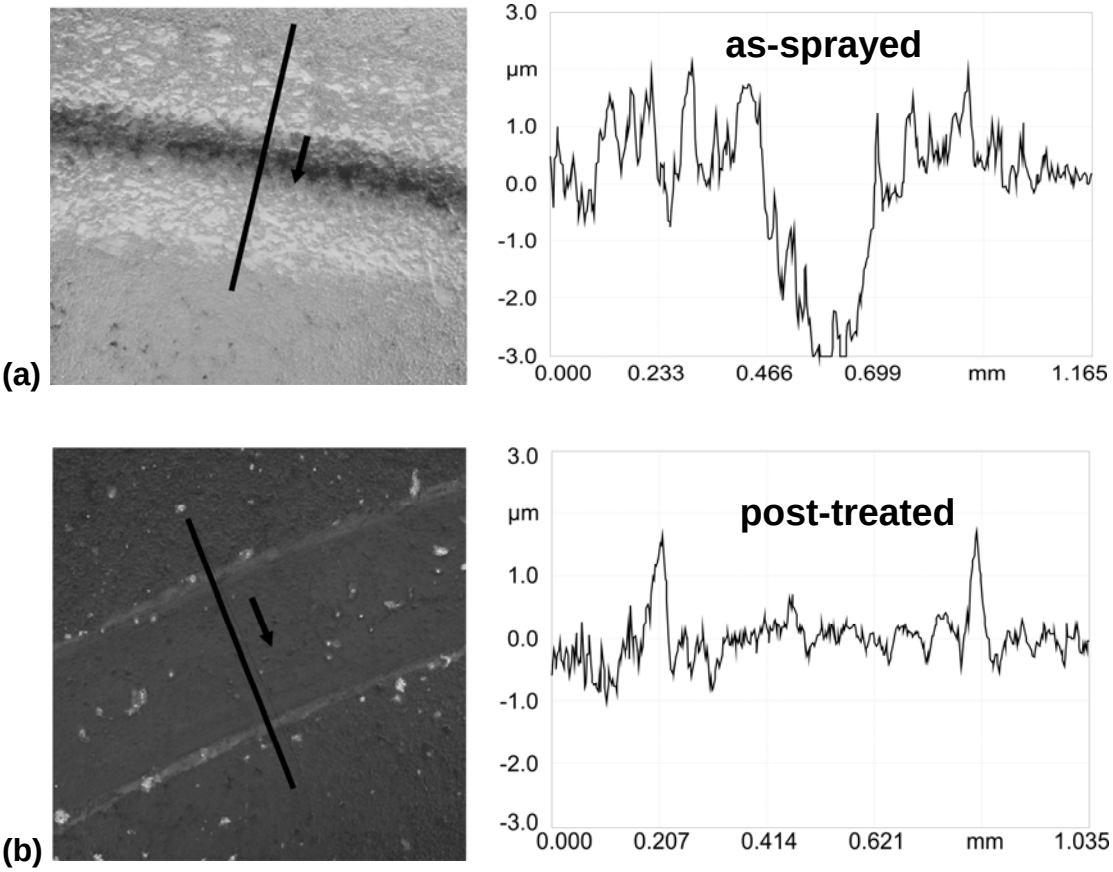

Figure 5-17. *The depth profiles of the sliding traces on* ***(a)*** *the as-sprayed YSZ top coat of M1 and* ***(b)*** *the post-treated YSZ coating of M2 after 1350 sliding cycles.*

Two specimens were prepared for the other sliding tests against WCCo balls using a 200g load with a sliding rate of 60 cycles per minute for 40 hours. They were coated with Ni-based alloy as a bond coat and YSZ as a top coat, applying the plasma spray processes. One was used as the as-sprayed and the other was post-treated by the solvothermal processing at 700 °C for 72 hours. After testing, the weight degradation of the as-sprayed YSZ coating was 15.79 mg while the post-treated coating

presented a wear resistance with a weight reduction of 0.81 mg. The wear rates are shown in Figure 5-18. Under the same wear conditions, the post-treated YSZ-coatings had higher wear resistance than the as-sprayed by a factor of 20.

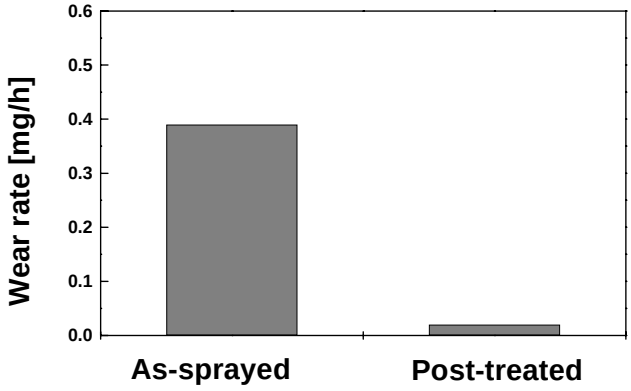

Figure 5-18. *Wear rates of the as-sprayed and post-treated YSZ top coat.*

Figure 5-19(a) shows the worn surface of the wear track of the as-sprayed YSZ top coat of M1. The microstructure of the worn surface revealed the plastic deformation of the remaining splats and the hollows with a several microns size due to the removal of material by grain pull-out. The surface of the wear track on the post-treated YSZ coating of M2 seems to be much smoother than the as-sprayed as shown in Figure 5-19(b). Compared with the original polished surface in Figure 5-19(c), there was no microcracking along the splats but a fatigue surface of the post-treated coating after the abrasive wear.

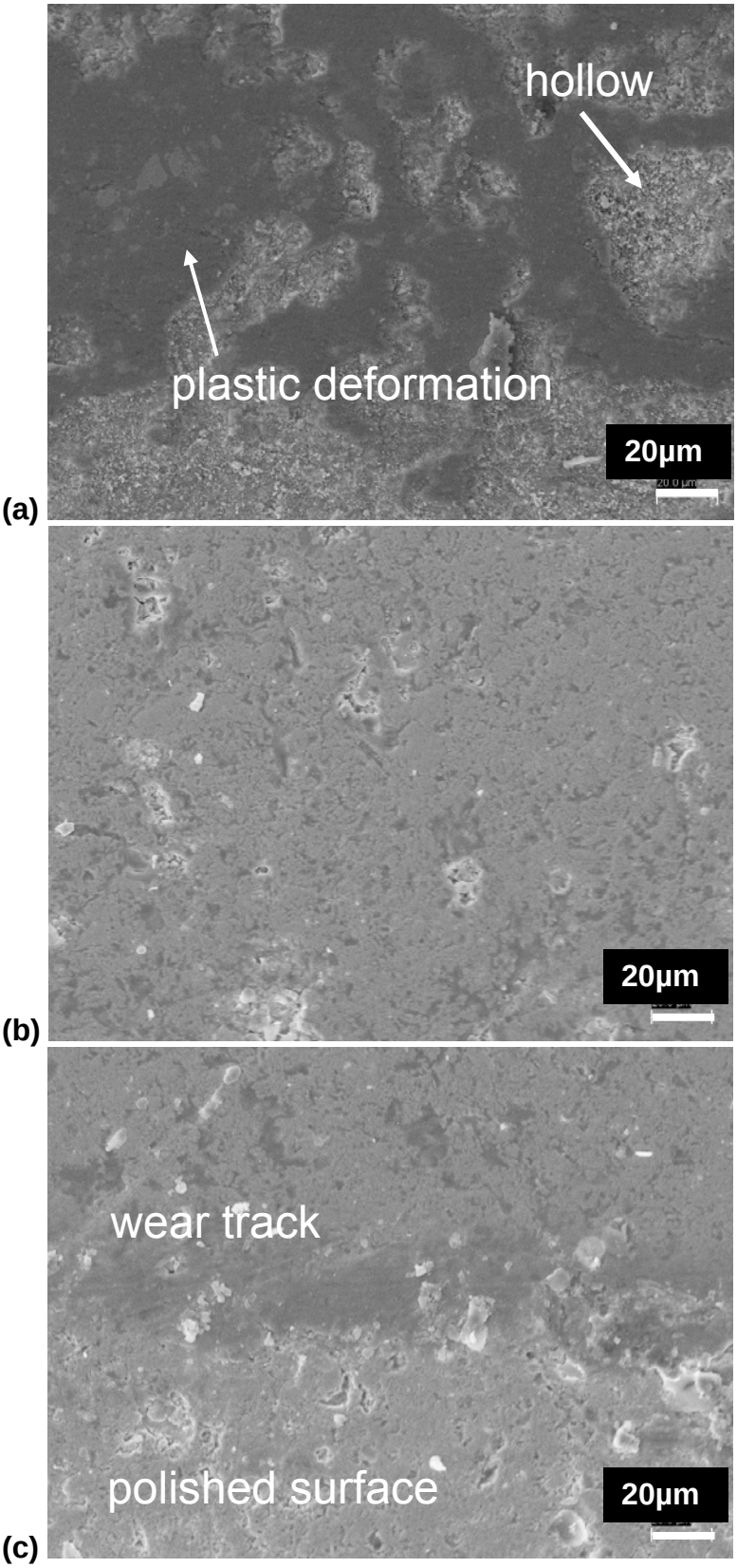

Figure 5-19. *Scanning electron microscopy of the wear track of* ***(a)*** *as-sprayed YSZ of M1 and* ***(b)*** *post-treated YSZ coating of M2 and of* ***(c)*** *polished surface of M2 before sliding tests (the lower half part in light grey).*

5.9 Chemical densification on YSZ/Al_2O_3 ceramic/alloy two-layer system

In this part of the present study, composite with 30 wt% alumina in a zirconia matrix as a topcoat was deposited by the atmospheric plasma spray processes for the chemical densification post-treatments. The modified microstructure of post-treated ceramic top coats was characterized and their mechanical and tribological properties were investigated.

Figure 5-20(a) shows a cross section review of the two-layer system of specimen ZA1, consisting of zirconia-alumina as a top coat and Ni-based alloy as a bond coat. This is a typical microstructure of the “as-sprayed” plasma-sprayed ceramic coatings, which demonstrates a lamellar structure and many pores in the ceramic top coat. These pores, especially inter-lamellar pores, arising from incomplete contact of the lamellae, determine the fracture strength and the wear resistance of the plasma-sprayed ceramic coatings. The lamellar structure with numerous globular pores and inter-lamellar pores could be clearly recognized in the BSE image as shown in Figure 5-20(a). The epoxy between the top coat and bond coat of the specimen ZA1 -which was embedded during the sample preparation-, indicated the weak adhesive strength of the as-sprayed ceramic top coat.

Figure 5-20(b) demonstrates the microstructure of the densified ceramic top coat of the specimen ZA2 which was post-treated under the solvothermal conditions at 700 °C for 72 hours. This chemical densification process is considered to be a progressive densification from the top-coat/bond-coat interface towards the ceramic top-coat surface. Hence, the modified zirconia-alumina top-coat was densified and the ceramic top coat did not peel off during the sample preparation.

Based on the results of the post treatment on the YSZ system, the ceramic top coat was densified much more rapidly at higher temperatures during the post-treatment. Figure 5-21 shows the cross-sectional microstructures of the system of specimens ZA3 and ZA4 that were post-treated at 800 °C for 24 hours and 48 hours, respectively. After being post-treated for 48 hours, the whole ceramic region of specimen ZA4 was densified with a reduced porosity of 3.4% while a porosity of 3.8% for the ceramic top coat of specimen ZA3 was reached after 24 hours. It is deduced that the treatment duration had an effect on the porosity of the ceramic top coats. The porosities of the examined specimens are shown in Table 5-9.

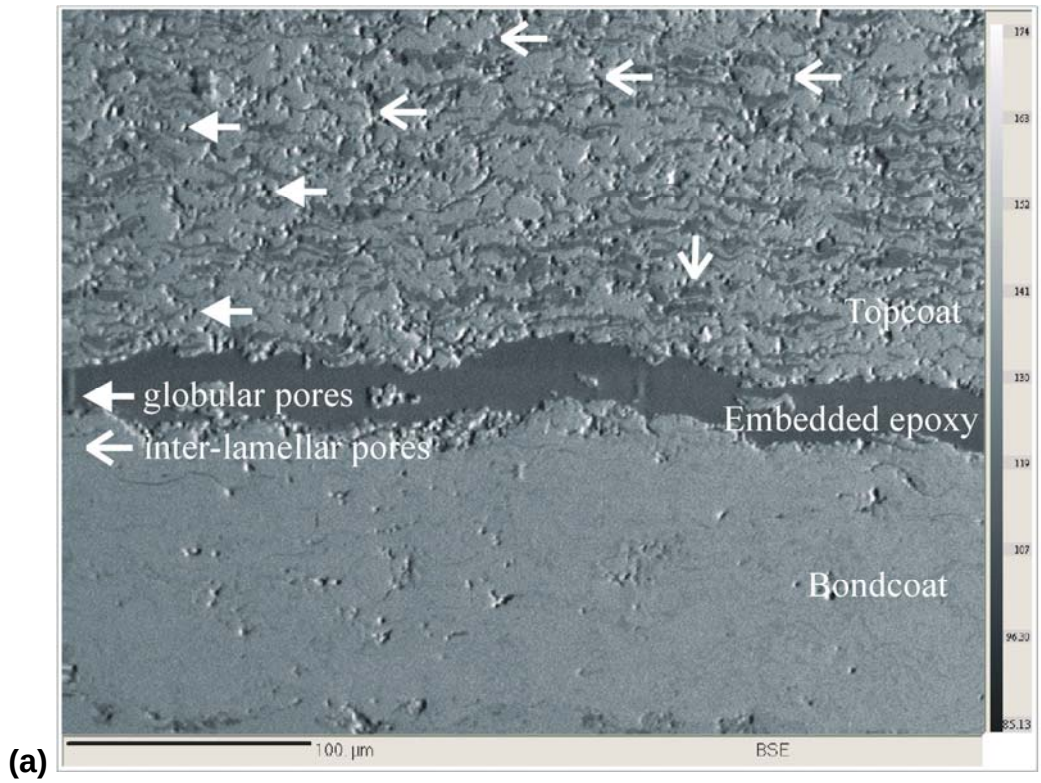

(a)

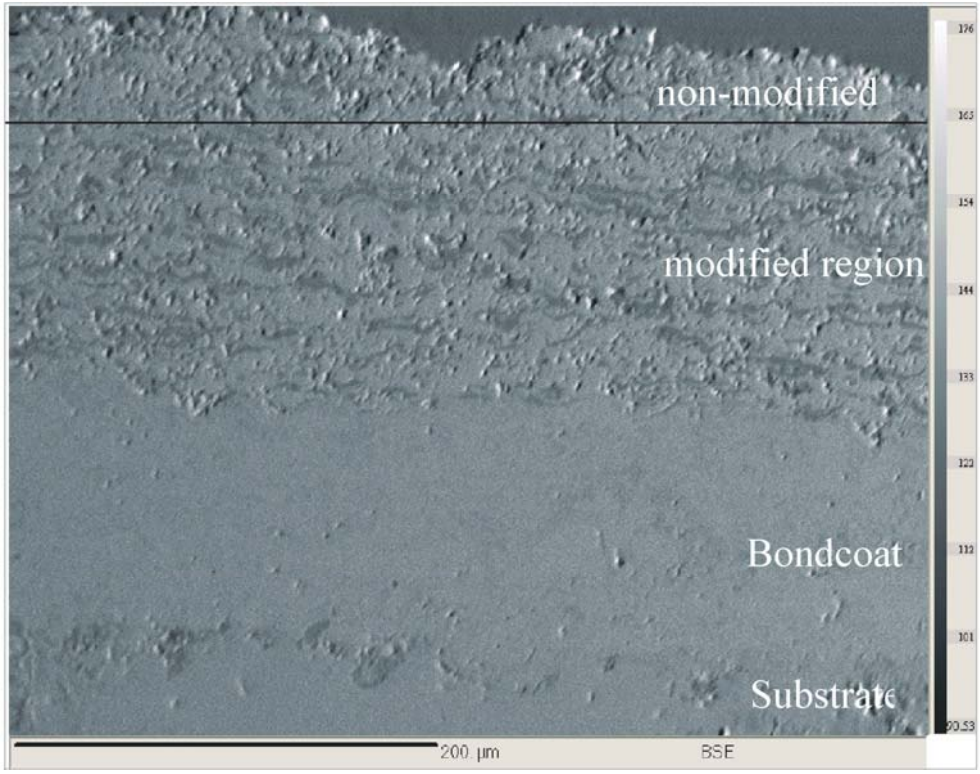

(b)

Figure 5-20. *BSE images of as-sprayed* ***(a)*** *and post-treated* ***(b)*** *zirconia-alumina/Ni-based alloy two-layer system, in top coat zirconia (light gray), alumina (dark gray).*

(a)

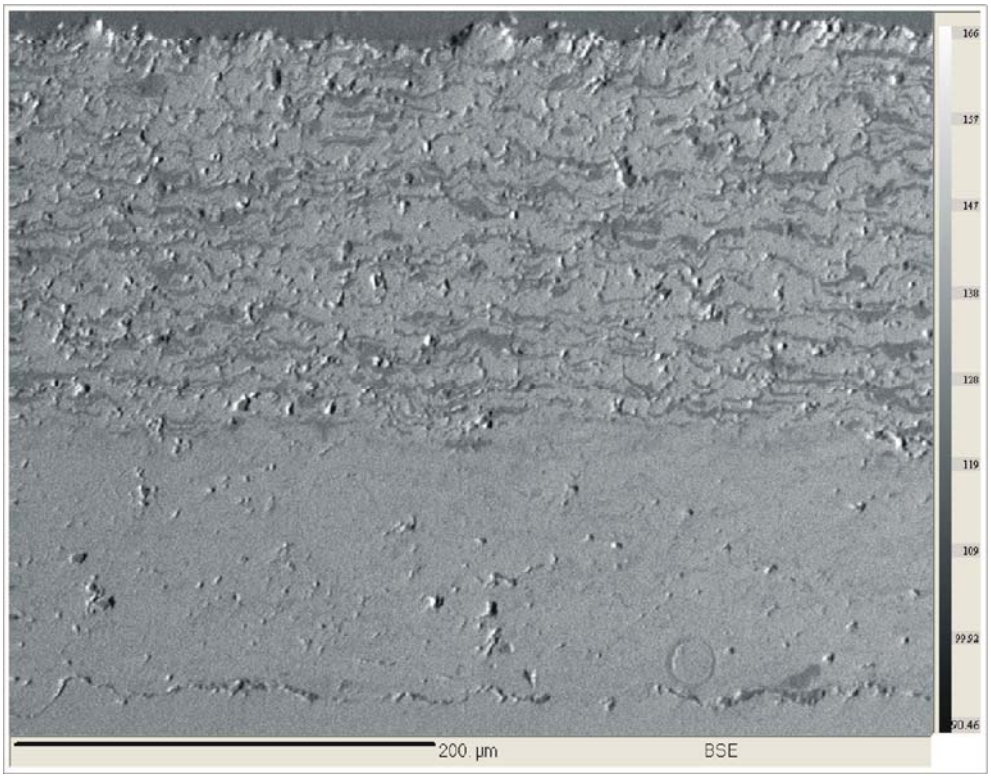

(b)

Figure 5-21. *Microstructures of zirconia-alumina/Ni-based alloy two-layer systems, post-treated at 800 °C for 24 h* ***(a)*** *and 48h* ***(b).***

Table 5-9: *The porosities of the as-sprayed and post-treated zirconia-alumina top coat at different treatment temperatures and duration, measured by image analysis*

Specimen	ZA1	ZA2	ZA3	ZA4
Temperature (°C)	0 (as-sprayed)	700	800	800
Treatment duration (h)	0	72	24	48
Average porosity (%)	8.8	5.6	3.8	3.4
Error (%)	0.75	0.24	0.83	0.31

The microstructure of the plasma-sprayed ceramic coatings is normally porous. The as-sprayed YSZ-alumina (70/30) coat of the specimen ZA1 had a relatively high average porosity of 8.8%, using the plasma spray processes. The porosity of the plasma sprayed YSZ-alumina coatings could be obviously reduced by the chemical densification post-treatments. The porosity of post-treated ceramic top coats was decreased with higher treatment temperatures. The top coat of the specimen ZA3 -that was post treated at 800 °C for 24 hours- with a reduced porosity of 3.8% was denser than the one of the specimen ZA2 -that was treated at 700 °C for 72 hours- with 5.6% porosity. All the measured porosities of the top coats are displayed in Figure 5-22.

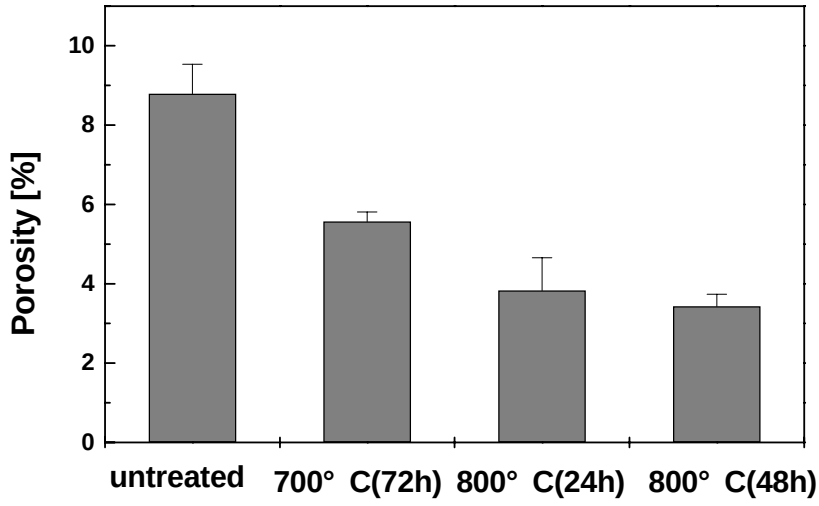

Figure 5-22. *The porosities of the as-sprayed and post-treated zirconia-alumina top coat at different treatment temperatures and duration, measured by image analysis.*

Table 5-10: *Comparison of hardness of YSZ and YSZ/Al_2O_3 (70/30) topcoats versus the treatment duration and temperature (ZA stands for YSZ-Al_2O_3)*

Temperature (°C)	0 (asprayed)		700		800		800	
Treat duration (h)	0		72		24		48	
Specimen	C0	ZA1	C2	ZA2	C4	ZA3	C5	ZA4
Microhardness (Hv)	706.6	724.4	954.2	1058.6	814	833.6	1269.3	1105.4
Deviation (Hv)	70.0	41.2	43	51.1	62.6	24.3	167.5	84.0

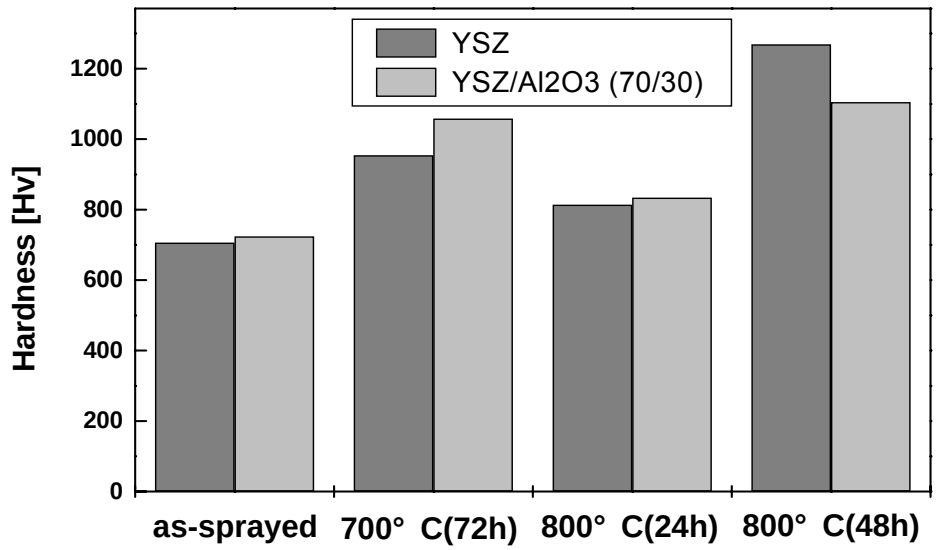

Figure 5-23. *Comparison of hardness of YSZ (dark gray) and YSZ/Al_2O_3 70/30 (light gray) topcoats versus the treatment duration and temperature.*

As a result of the densification of the oxide layer, the micro hardness of the ceramic top coat was found to be increased by a factor of 50% in the YSZ-alumina system, which can be explained by a better cohesion at the local scale. The hardness of the examined specimens is listed in Table 5-10, compared with that of YSZ top coat. The results show that a higher hardness of plasma-sprayed ceramic top-coat was achieved by an addition of 30 wt% alumina as a second phase in a zirconia matrix, except that of the specimen ZA4 which was post-treated at 800 °C for 48 hours,

which might be attributed to a huge margin error of 167.5 for the hardness of YSZ top coat of specimen C5. Comparison of the hardness of YSZ with that of YSZ/Al_2O_3 70/30 topcoats versus the treatment duration and temperature is demonstrated in Fig. 5-23. The hardness of YSZ of specimen C5 or YSZ/Al_2O_3 (70/30) top coat of specimen ZA4 -which was post-treated at 800 °C for 48 hours-, was higher than that of specimens C4 and ZA3, post-treated at 800 °C for 24 hours. It is deduced that the micro hardness of the post-treated ceramic top coats was increased with the treatment duration.

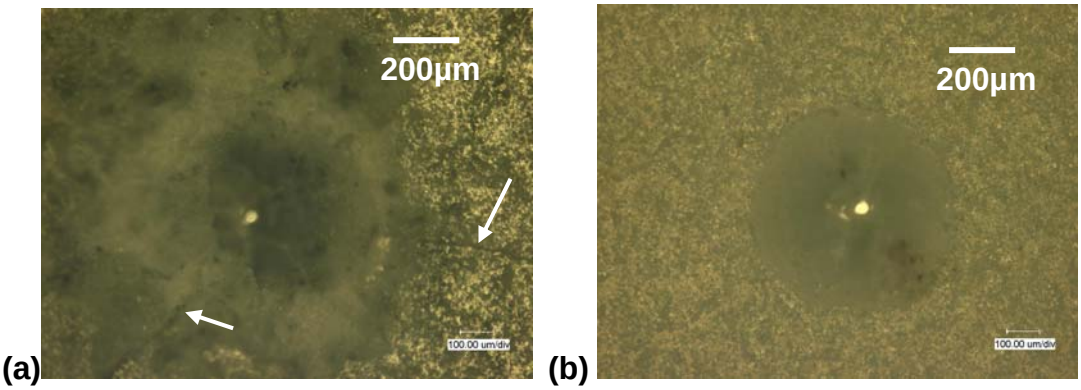

Figure 5-24. *Optical micrographs of the results of Rockwell tests for* ***(a)*** *as-sprayed (→cracks) and* ***(b)*** *post-treated YSZ/Al_2O_3 (70/30) top-coats at 700 °C for 40h.*

Two cylinders from steel 1.3343 with a radius of 2.5 cm and height of 0.5 cm were coated with Ni-based alloy as a bond coat and YSZ/Al_2O_3 (70/30) as a top coat. The specimens were further polished until an arithmetic mean surface roughness reached 0.45+/-0.09 µm. One was applied as “as-sprayed”, and the other was solvothermal post treated at 700 °C for 40 hours for Rockwell tests and tribological investigations.

The interfacial strength of the YSZ/Al_2O_3 top coats was also evaluated by Rockwell test. Rockwell test is normally applied to evaluate the adhesive strength and micro hardness of thin coatings. For the relatively thick plasma-sprayed coatings, the fracture toughness was tested by Rockwell test. Figure 5-24 shows the results of the Rockwell tests on the YSZ/Al_2O_3 system. Fractures were generated in the as-sprayed coating while no fractures were observed in the post-treated. It indicates that the fracture toughness of the plasma-sprayed YSZ/Al_2O_3 coatings was increased by the chemical densification process and could result in the improved wear resistance.

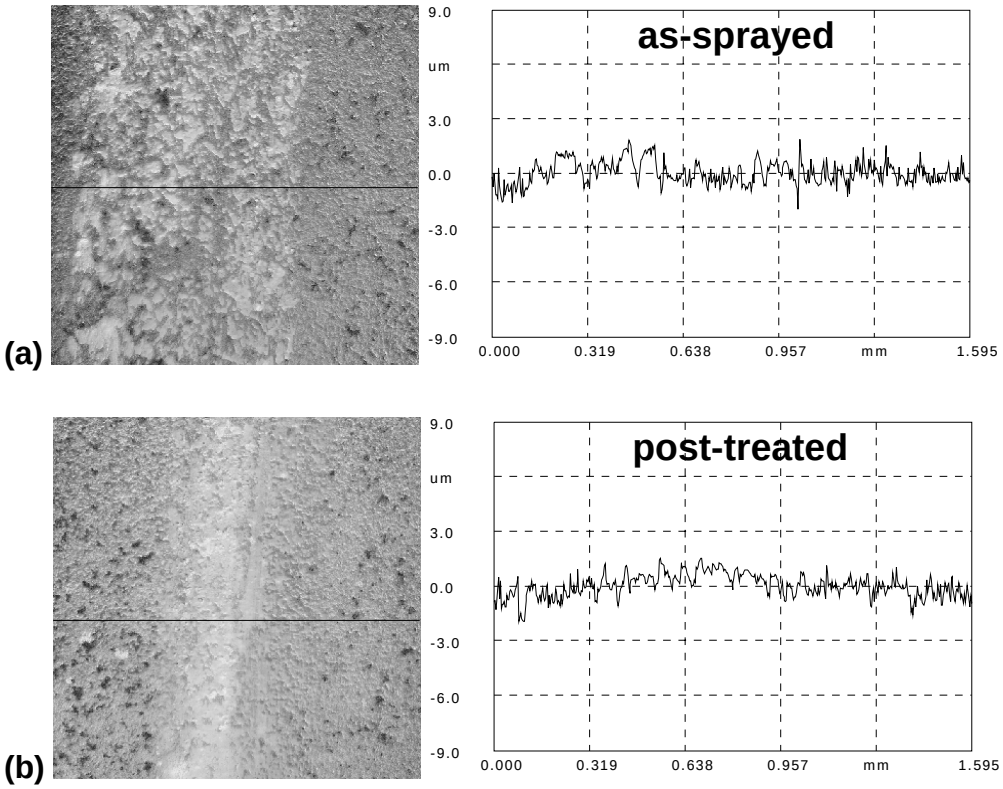

Figure 5-25. *The depth profiles of the sliding traces on* ***(a)*** *the as-sprayed and* ***(b)*** *the post-treated YSZ/Al_2O_3 (70/30) top-coats at 700 °C for 40 hours after 1000 sliding cycles.*

The depth profiles of the sliding traces on the YSZ/Al_2O_3 top-coats after 1000 sliding cycles are shown in Figure 5-25. The corresponding optical image of the sliding trace on the as-sprayed coating was recorded by confocal microscope with white light and presented a wide worn trace. Nevertheless, the wear depth of the as-sprayed YSZ/Al_2O_3 topcoat was negligible after 1000 sliding cycle. A narrower sliding trace on the post-treated YSZ/Al_2O_3 top coat was observed after 1000 sliding cycles. The depth profile of the sliding trace on the post-treated specimen was recorded as “positive”, which indicates that the wear occurred on the surface of the 100Cr6 test balls.

5.10 Thermal shock resistance

In this part of the study, six cylinders from steel 1.3343 -with a radius of 1 cm and height of 1 cm- were coated with Ni-based alloy as a bond coat and 8YSZ as a top coat. Three specimens of them were post-treated by the solvothermal processes and the others were used as “as-sprayed”. All of them were prepared for the thermal shock cycle testing in order to investigate the stability and durability of plasma-sprayed Ni-based alloy/YSZ systems in the high temperature applications. The average porosities of the four types of ceramic top coats are summarized in Table 5-11, according to the previous investigations.

Table 5-11: *the average porosities of the four types of ceramic top coats.*

Specimen	TS1	TS2	TS3	TS4
Post-treatment	untreated	700 °C for 72 h	800 °C for 72 h	800 °C for 48 h
Porosity (%)	7.9	5.0	4.3	2.2

The adhesive strength of the ceramic top coats was evaluated for the as-sprayed and post-treated specimens by shear tests. The previous study revealed that the average adhesive strength of the post-treated top coat was double that of the as-sprayed.

Four types of the specimens -1) as-sprayed; 2) chemical densification post-treated at 700 °C for 72 h; 3) chemical densification post-treated at 800 °C for 72 h; 4) chemical densification post-treated at 800 °C for 48 h- were exposed to the thermal cycle conditions as listed in Table 5-11. The thermal shock cycling tests of the “as-sprayed” and post-treated specimens were conducted in an electric furnace with an air atmosphere. A thermal cycle consisted of directly inserting samples to the temperature 1100 °C, holding for 30 min and quenching to ambient temperature in air. The results are summarized in Figure 5-26. It should be indicated that the thermal cycle lifetime was defined as the number of thermal cycles, after which the defined area of the top coat had delaminated. All the three as-sprayed YSZ top coats of specimens TS1 were completely spalled after 2 thermal cycles as shown in Fig. 5-27(a). The other examined specimens that were post-treated by the chemical densification processing, had higher thermal shock resistance and high temperature oxidation resistance. The thermal lifetime for the post-treated specimens was

recorded when about two fifths area of the top coat had delaminated. The results are shown in Figure 5-26. The thermal lifetime for specimen TS3 with lower porosity was much shorter than that of TS2 that was post-treated at 700 °C for 72 hours. The tested specimen TS2 after 14 cycles is seen in Fig 5-27b and only two small white top coat remained on the surface. The thermal cycle test for TS4 was stopped after 20 thermal cycles even though most of the top coat remained and no more top coat peeled off. But the explored substrate was badly oxidized, affecting the resistance of the YSZ top coat (Fig. 5-27c).

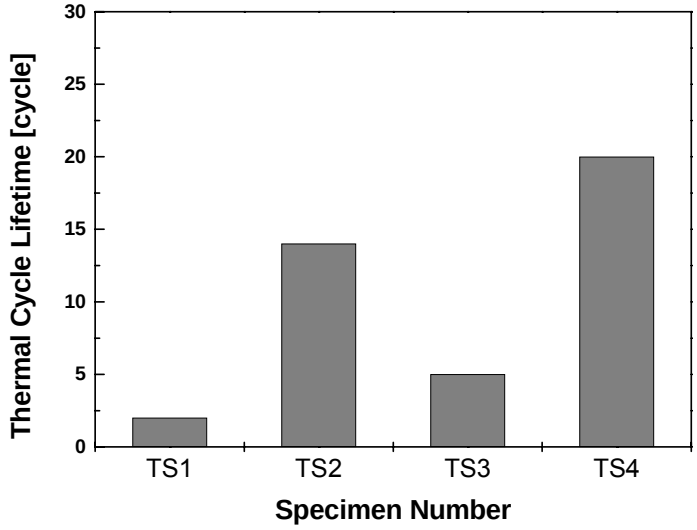

Figure 5-26. *Thermal cycle lifetime of the examined specimens.*

Figure 5-27. *Photos of the examined specimens:* ***(a)*** *TS1 after 2 thermal cycles;* ***(b)*** *TS2 after 14 thermal cycles;* ***(c)*** *TS4 after 20 thermal cycles.*

The YSZ top coats of all the three as-sprayed specimens TS1 were completely spalled after 2 thermal cycles. The backside of the spalled YSZ top coats of as-sprayed specimens was green. The examination of this backside by EDS revealed a high percentage of Cr, Ni, Al and O along with the Zr and Y as shown in Figure 5-28. Thus these oxides, such as Cr_2O_3, Al_2O_3, NiO, or others that were detected at the backside of the spalled YSZ top coats, might be formed during the thermal cycle tests and can be called thermally grown oxides (TGOs).

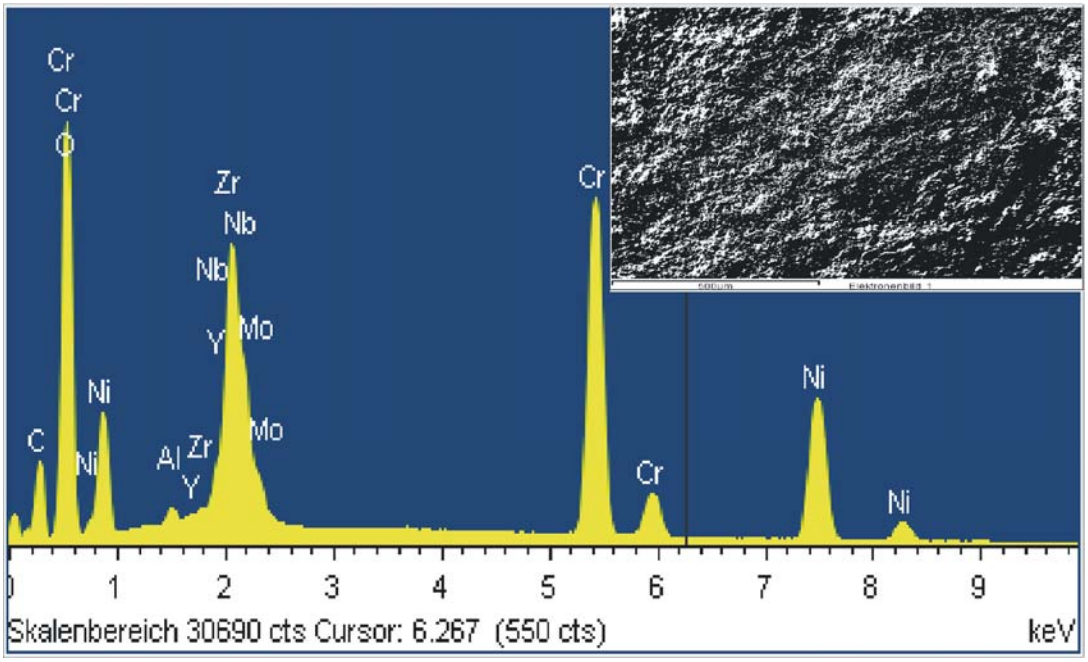

Figure 5-28. *EDS analysis on the backside of the spalled YSZ top coat of the as-sprayed specimen TS1 after thermal cycle tests.*

The specimen TS3 with lower porosity that was post-treated at 800 °C for 72 hours had a relatively shorter thermal cycle lifetime. The cross-sectional microstructure of the non-spalled position of the specimen TS3 after 5 thermal cycle tests is shown in Figure 5-29. The results of the mapping analysis of the TGO layer at the interface indicated that the TGO layer consisted mainly of Cr_2O_3. A slight amount of Al_2O_3 was also detected at the bond-coat/top-coat interface. This cromia-alumina layer is considered to be formed during the post treatment and thermal cycle tests. This homogeneous oxide layer limited the oxygen penetration towards the bond coat and hence retarded the internal oxidation to some extent [57].

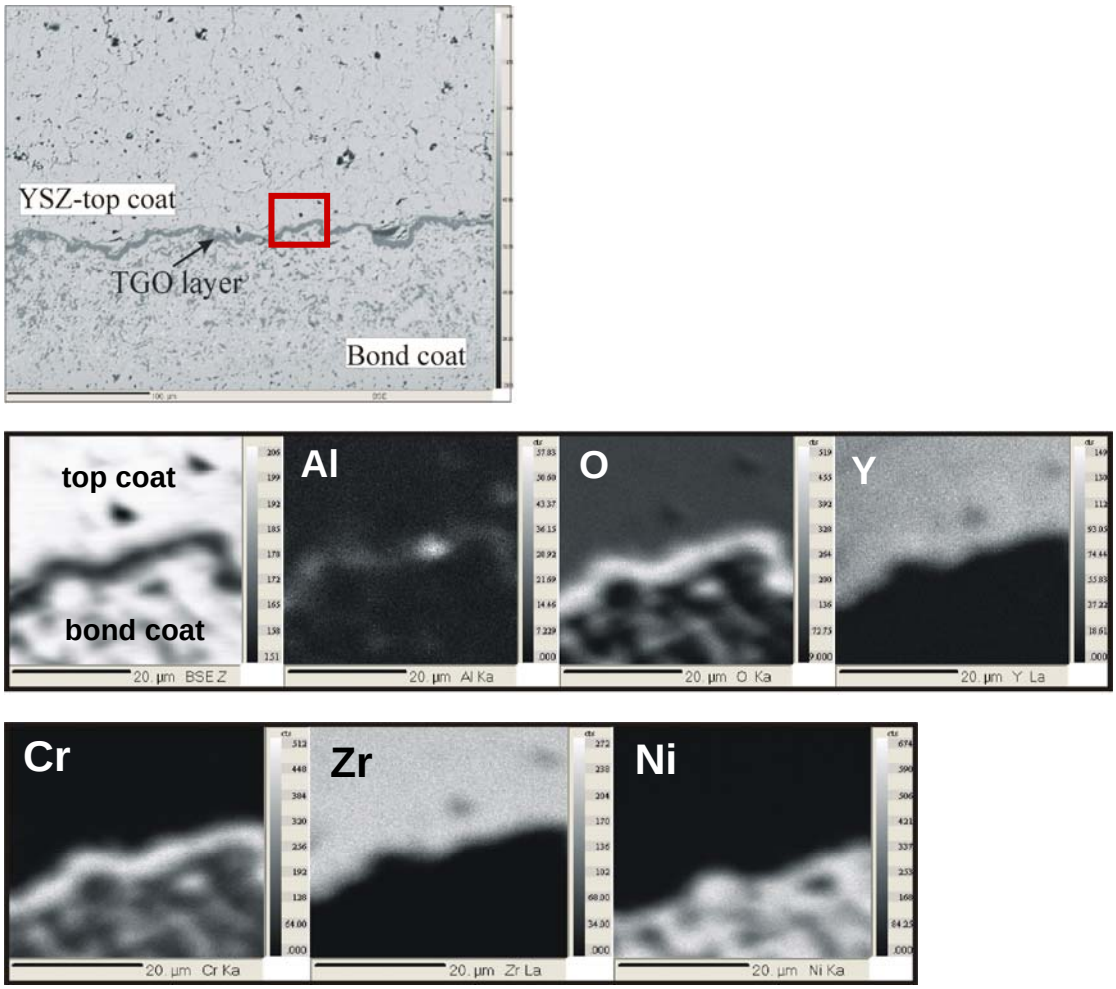

Figure 5-29. *BSE images and the element distributions (of the square) of cross section of non-spalled position of the specimen TS3 after thermal cycle tests.*

Figure 5-30 shows the microstructure of the delamination area of the specimen TS3. It is obviously seen that the spallation did not occur at the top-coat/bond-coat interface, but near the interface and in the ceramic top coat region, which is related to the induced microcracks formed during the post treatment as described in the previous chapter. These induced stresses in the ceramic top region could be prevented by shorter post treatment duration. The specimen TS4 that was post-treated for shorter duration exhibited the highest thermal shock resistance among these specimens as shown in Fig. 5-26.

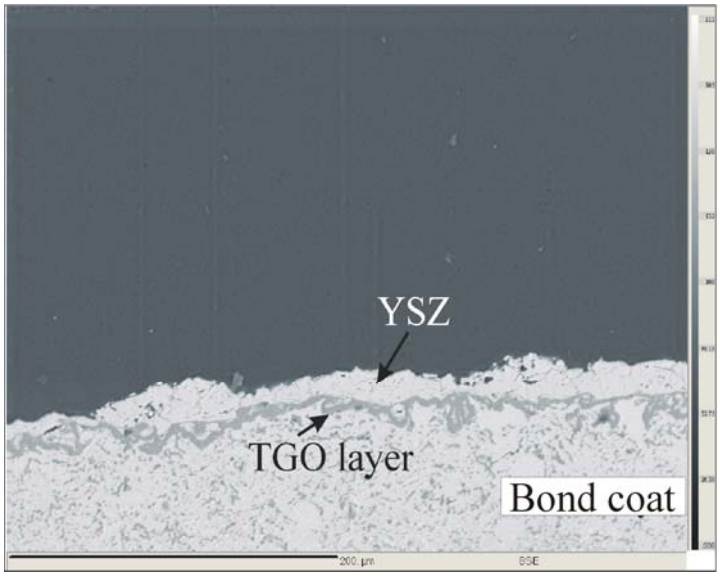

Figure 5-30. *BSE Images of the cross-sectional delamination area of the specimen TS3 after the thermal cycle tests.*

6 DISCUSSION

6.1 Solvothermal solvent determination

In this study, a novel solvothermal process was applied to densify the plasma sprayed oxide layers in order to enhance the wear and corrosion resistance of the plasma-sprayed ceramic coatings. The wear and corrosion resistance of a ceramic coating is achieved by a dense structure [28]. The chemical densification process is different from the impregnation processes [20, 28]. There is no opposing force of the residual air so the solvothermal reactants' penetration is not limited and the chemical densification process can take place at the bondcoat/topcoat interface. During this process, dissolved zirconia in molten salts was applied as an active reactant to densify the plasma sprayed ceramic coatings. Figure 5-2 shows the solubility of zirconia in the chloride or chloride and sulfate molten salts under the different conditions. A maximum solubility of zirconia of 0.18% was achieved at 700 °C in a N_2 atmosphere containing 2% HCl in the mixture of equimolar molten salts of KCl, $ZnCl_2$, K_2SO_4 and $ZnSO_4$. According to the experimental results, sulfates are suggested to be one necessary component of the solvothermal solvent, and the hydrogen chloride content in the atmosphere also enhances the dissolution of the zirconia in the molten salts. Therefore, the mixture of equimolar molten salts of KCl, $ZnCl_2$, K_2SO_4 and $ZnSO_4$ in a N_2 atmosphere containing 2% HCl was applied as a solvothermal solvent during the chemical densification process.

6.2 Microstructure of the as-sprayed and post-treated two layer systems

In this study, the two-layer system -consisting of 8 wt% yttria-stabilized zirconia (8YSZ) as a top coat and Ni-based alloy as a bond coat- was sprayed using an atmospheric plasma spray process under the optimized spray parameters at Fraunhofer UMSICHT. The EPMA mapping analysis revealed a lamellar structure with numerous globular pores, interlamellar pores and microcracks in the as-sprayed ceramic top coat which were clearly recognized in the magnified image (see Fig. 5-4). The qualities of the ceramic coatings could be optimized by spray technologies, spray parameters [14] and feedback particles [16]. However, thermally sprayed coatings are formed by the impact, deformation and solidification of individual liquid droplets so that their structure consists of a series of overlapping lamellae, numerous pores and microcracks because of partially or totally non-molten particles, inadequate flow, and air entrapment [8-11].

Using the two-layer system consisting of 8 wt% yttria-stabilized zirconia (8YSZ) as a top coat and Ni-based alloy as a bond coat, a densified ceramic structure of the solvothermal post-treated ceramic coatings was observed with the help of an EPMA mapping analysis and a better adhesive strength of the ceramic top coat to the bond coat was evaluated. According to the EPMA mapping analysis, the elements oxygen and zirconium were almost homogeneously distributed in the measured region and no connected pores were indicated. It can be proposed that during the solvothermal treatment on the two-layer system the solvothermal gas phase diffused through the open pores and microcracks of the plasma-sprayed ceramic coatings to the top-coat/bond-coat interface, and solvothermal reactions occurred and therefore zirconia was crystallized in the ceramic region.

After the chemical densification post-treatments at 600 °C for 72 hours, there was still a region near the ceramic topcoat surface that was not modified yet (see Fig. 5-6a). This chemical densification process is suggested to be a progressive densification from the top-coat/bond-coat interface towards the ceramic top coat surface. That might be attributed to the treatment duration, and the duration was not long enough. In the densified region remained pores. Due to the microstructure of the plasma-sprayed ceramic coating and the solvothermal process, it can be deduced that these pores were closed as the solvothermal agent did not penetrate and modify them.

In general, the partial pressure of species increases with temperature, hence the partial pressure of solvothermal reactants in the gas phase also increases. This corresponds with the observed rapid densification of YSZ ceramic top coat at a

higher temperature. The whole YSZ top-coat was densified at 800 °C for 24 hours (see Fig. 5-6d). However, the treatment duration has an effect on the microstructure; new microcracks were formed in the ceramic coat after being post-treated at 800 °C for 72 hours (Fig. 5-6c). The X-ray diffraction measurements revealed that the tetragonal phase of YSZ material was stable in the post-treatment conditions (see Fig. 5-7). This might arise from the tensional stress which was caused by the rapid and excessive crystallization of the zirconia in the residual pores. Therefore, at 800 °C a shorter processing time is required

Pores were detected at the top-coat/bond-coat interface of the as-sprayed two-layer system by an EPMA analysis (see Fig. 5-8a). There, pores might arise from the incomplete contact of sprayed lamellae and imply weak adhesive strength of the ceramic coating to the bond coat. It is seen that the elements were randomly distributed in the bond coat and an oxygen content of up to 15% was detected. The alloy is considered to have been partially oxidised during the plasma spraying.

At the YSZ/Ni-based alloy interface of the specimen that was post-treated at 700 °C for 72 hours, a ca. 1 µm new layer without pores was detected. This layer was very thin and uniform. According to the corresponding mapping analysis, we know that this layer consists mainly of chromia and alumina which were formed during the post-treatments and arise from the oxidation of chromium and aluminium from the bond coat. Alumina material is considered to be an oxygen barrier structure, and with regard to some investigations [58, 59], a thin alumina layer by CVD (chemical vapour deposition) process was deposited between the bond coat and zirconia top coat or by atmospheric plasma spray methods as a top coat over YSZ layer to reduce TGO (thermally grown oxide) growth which is formed during the application of thermal barrier coatings at high temperatures and can lead to the failure of the YSZ layer during thermal cycling. This layer at the bond-coat/top-coat interface in this study could prevent the bond coat from further oxidation due to the low oxygen diffusion coefficients of alumina. Therefore, it may increase the oxidation resistance of the coating system when its growth is slow, uniform and defect-free [57, 60].

6.3 Mechanisms of the chemical densification process

Following microchemical analysis of the change of microstructure of the plasma-sprayed YSZ/Ni-based alloy two-layer system after chemical densification post-treatments, the mechanisms of the densification process were proposed. Figure 6-1 illustrates the mechanisms of the chemical densification process for the plasma-sprayed YSZ/Ni-based-alloy coatings. By heating the inorganic solution of zirconia under a nitrogen atmosphere containing 2% HCl partial pressure, the solvothermal gas phase containing zirconium is produced *in-situ* for the chemical densification process. The solvothermal agents transport in the gaseous flux through the open pores of the thermally sprayed ceramic top coat to the top-coat/bond-coat interface. Sulfates react with chromium and aluminium from the bond coat, and then Cr_2O_3 and Al_2O_3 are formed at the top-coat/bond-coat interface. Due to the oxygen ion conducting properties of YSZ, the residual O^{2-} ions can permeate through the YSZ grains to meet zirconium in the gaseous flux, which leads to the crystallization of zirconia in the open pores of the ceramic top coat (densification in the topcoat). This chemical densification is progressive and the whole ceramic top coat can be modified, as shown in Figure 6-1. The other solvents and by-products are released in the gaseous flux as off-gas, which are cleaned up with a basic solution.

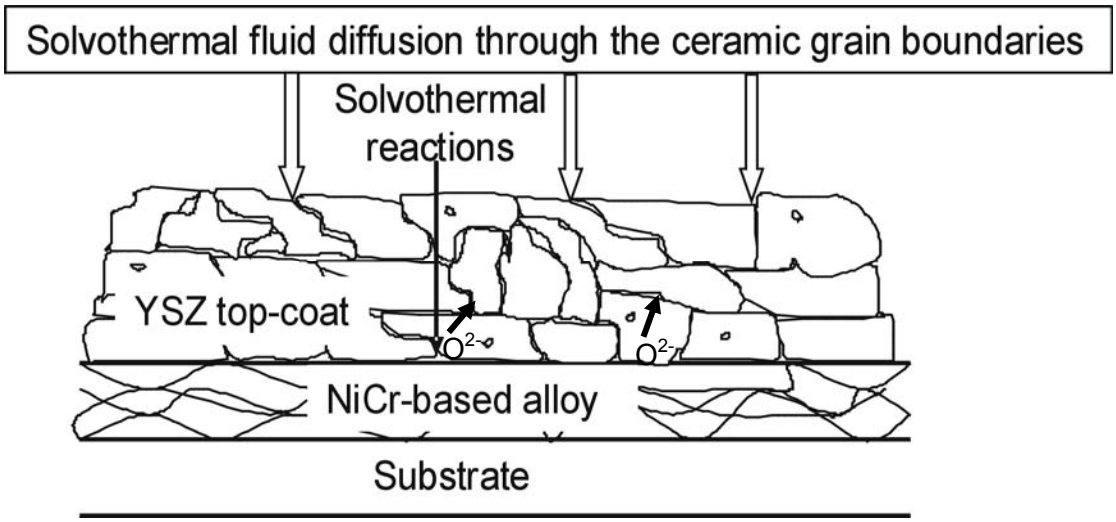

Figure 6-1. *Schematic demonstration of mechanisms of the chemical densification process.*

During the chemical densification process on the two-layer system, the following main solvothermal reactions might take place:

(1) Reactions in the molten sulphate-chloride salts

$ZrO_2 + 4\ H^+ \rightarrow Zr^{4+} + 2\ H_2O$

Zirconium species are produced *in-situ* in the solvothermal gas phase. The solvothermal agents transport through the open pores of the ceramic top coat to the top-coat/bond-coat interface.

(2) Reactions at the bond-coat/YSZ interface

$3\ SO_4^{2-} + 8\ Cr/Al \rightarrow 3\ Cr_2O_3/Al_2O_3 + Cr_2S_3/Al_2S_3 + 3\ O^{2-}$

The residual O^{2-} ions permeate through the YSZ grains.

(3) Reactions on the surface of YSZ grains

$Zr^{4+} + 2\ O^{2-} \rightarrow ZrO_2$

The O^{2-} ions meet zirconium in the gaseous flux, which leads to the crystallization of zirconia on the surface of YSZ grains in the open pores of the ceramic top coat (densification in the topcoat).

These solvothermal reactions lead to the chemical densification of the zirconia/Ni-based alloy two-layer system, starting from the bond-coat/YSZ interface.

6.4 Correlation of tribological behaviours with mechanical properties

A typical microstructure of the as-sprayed YSZ coatings has many pores and microcracks. The pores of a several microns length arising from incomplete contact of the splats were obviously detected by EPMA. These pores indicate weak strength and insufficient functional behaviour of the ceramic coatings. The as-sprayed YSZ coatings in this study had a high average porosity of 7.9%. During the chemical densification treatments, the solvothermal reagent diffused through the open pores and microcracks of the plasma-sprayed ceramic coatings to the top-coat/bond-coat interface, and ZrO_2 was crystallized from the solvothermal gas phase in the residual connected pores. The post-treated coatings presented a denser structure, and the connected pores between the lamellae, in particular, were occupied by the crystallized zirconia. This modification of the splats interface leads to porosity reduction, and hence to the more cohesive structure of the ceramic coatings. The influence of a more cohesive structure on the mechanical and tribological properties of the coating is discussed in the following sections.

He et al. (1997) discovered the relationship between the wear resistance and the porosity of tetragonal zirconia polycrystal (TZP) through the equation: 1/Kw = 1/Kw0 exp (-23P), where 1/Kw0 is the wear resistance of a pore-free TZP material and P is the porosity [12]. Based on this equation we can draw the conclusion that ceramic materials with lower porosity present a higher wear resistance and that, therefore, wear resistance of ceramics could be increased by reducing porosity. This phenomenon has been proven in our work. Specimens with as-sprayed YSZ coatings and post-treated at 700 °C for 72 hours were applied for the scratch tests, Rockwell tests and tribological investigations The application of scratch tests, Rockwell tests and tribological investigations showed that specimens, post-treated at 700 °C for 72 hours, have much better mechanical properties compared to as-sprayed YSZ coatings. During the post treatment the interlamellar pores were occupied by the crystallized ceramics, and hence the porosity of the coating was decreased. Therefore, the post-treated coating presented much higher wear resistance than the as-sprayed one.

Friction force is an important parameter of wear behaviour. Normally, the higher the friction force generated, the lower the wear resistance. The coated and polished specimens were tested regarding their tribological behaviour in the three-ball-on-disc test. The results revealed the friction coefficient of as-sprayed YSZ coatings was not so stable after 850 sliding cycles as it was before, which can be attributed to the worn

surface with hollows due to the removal of materials by grain pull-out. It indicated that after 850 sliding cycles grain pull-out may be the major wear mechanism for the as-sprayed YSZ coatings. The plasma-sprayed YSZ topcoat was densified and the cohesive strength was enhanced by the chemical densification treatment. The denser and more cohesive the structure is, the lower the friction coefficient (see Fig. 5-16).

Based on the typical wear mechanism for thermally sprayed ceramic coatings wear appears to proceed by delaminations, which were induced firstly by plastic deformation and crack initiation between two splats of the same lamella [61]. The scratch tests and Rockwell tests on the solvothermal post-treated YSZ top coats revealed that the interfacial strength of the splats was improved by the crystallized ceramics (see Fig. 5-13 and Fig. 5-14). Therefore, the wear resistance of the plasma sprayed ceramic coatings could be enhanced by the solvothermal post treatments.

The depth profiles of the sliding traces on the as-sprayed specimens after 1350 sliding cycles presented a worn surface with ca. 3 µm wear depth, which indicates a weak cohesion and poor strength in this coating. The as-sprayed YSZ coatings exhibit a higher porosity and a greater number of connected pores, in particular. The connected pores indicate incomplete inter-lamellar bonding and a weak cohesive structure, which could induce the nucleation of microcracks along the splats during the wear tests. Therefore, the nucleation of microcracks along the splats was more likely to occur before the grain pull-out during the wear test. The microcrackings along the splats and then the grain pull-out due to the adhesive wear have been considered to be the serious wear mechanisms of the plasma-sprayed ceramic coatings. This is why the as-sprayed coating was worn so seriously after the sliding test, resulting in increased surface roughness according to the depth profiles of the wear trace and also in the rising friction coefficient. Compared with this, the sliding trace surface of the post-treated coating was still smooth and the wear depth was negligible (see Fig. 5-17). There was no microcracking along the splats, but rather a fatigue surface after extended abrasive wear. After the modification of the interfacial strength between the splats by the post-treatment, a more cohesive and denser structure was obtained and the serious wear mechanisms with microcracking and grain pull-out were prevented. The post-treated ceramic top-coats had a denser structure and a higher level of micro hardness. A structure with a higher hardness can prevent the first wear mechanism step, named plastic deformation. Therefore, on the same wear conditions the post-treated YSZ-coating had higher wear resistance than the as-sprayed one by a factor of 20 (see Fig. 5-18).

6.5 Thermal shock resistance

The efficiency of gas turbines can be increased by higher inlet temperatures, and components such as turbine blades and vanes must have adequate strength and oxidation durability at temperatures above 950 °C [57, 62]. Thermal barrier coatings (TBCs) consisting of a ceramic layer with a low thermal conductivity (usually 8YSZ) and a bond coat (such as MCrAlY-type, where M is Ni, Co, or Ni+Co) have been widely used on the blades and vanes of gas turbines in order to protect these components against high temperatures [57, 63].

Two deposition processes - atmospheric plasma spraying (APS) and electron-beam physical vapor deposition (EB-PVD) - have been applied for the deposition of the TBCs. The YSZ top coat deposited by the EB-PVD is generally relatively denser than the one created by APS [10, 64], but the APS TBCs have lower thermal conductivity and lower processing costs [63, 65]. Therefore, the APS process is attracting the attention of industries and researchers.

The APS TBCs usually have a lamellar structure and possess many pores and micro cracks [66]. During the application of the TBCs, the interlamellar pores arising from incomplete contact of the lamellae, and micro cracks, not only leave the ceramic top coat less strain-tolerant, but also provide channels for gas penetration, especially oxygen diffusion towards the bond coat, and an oxidized scale - the thermally grown oxide (TGO) - could be formed at the ceramic top-coat/bond-coat interface [58, 67, 68]. These TGOs may become thicker and more inhomogeneous during the oxidation process, which causes stress at the interface and ultimately leads to spallation of the ceramic top coat [57, 69].

It is known that the bonding strength retention of the ceramic top coat is key to the durability of TBCs [57, 70]. The shear strength at the rupture between the ceramic coat and the bond coat of the as-sprayed and post-treated specimens revealed that the average adhesive strength of the post-treated top coat was double that of the as-sprayed (see Fig. 5-12). That indicates that the crystallized ZrO_2 in the vicinity of the ceramic coat/bond-coat interface enhanced the bonding between the ceramic top coat and the bond coat during the solvothermal treatment because, it could be assumed, a chemical bond was formed among the crystallized zirconia, the plasma-sprayed top coat and the bond coat. Moreover, the cohesive strength of the splats could also be enhanced by the crystallized zirconia in the connected pores. Here, therefore, the oxidation durability and the thermal cycle properties of these as-sprayed and post-treated TBCs have been investigated and the failure mechanisms of these TBCs discussed.

The YSZ top coat of all three as-sprayed specimens was completely spalled after 2 thermal cycles. The investigation of the backside of the spalled YSZ top coat by EDS revealed a high percentage of Cr, Ni, Al and O along with the Zr and Y (see Fig. 5-28). It can be proposed that oxides, such as Cr_2O_3, Al_2O_3, NiO or others might be formed during the thermal cycle tests and can be called thermally grown oxides (TGOs). The plasma as-sprayed YSZ coatings have a lamellar structure including pores and a network of microcracks. Although these structures might reduce the thermal conductivity, they provide paths for oxygen penetration towards the bond coat, which leads to oxidation of the bond coat and formation of thick TGO layers at the top-coat/bond-coat interface, as well as internal oxidation in the bond coat, during high temperature applications. Large tensile stress was generated in the thick and inhomogeneous TGO layers, which may cause cracks and ultimately the spallation of the ceramic top coat at the interface and TGO layers [71].

These intrinsic detriments of plasma splayed YSZ coatings could be limited by the chemical densification post treatments. For the further investigation of this study, the TBCs were post-treated at 700 °C and 800 °C prior to the thermal shock cycle tests, and all the YSZ top coats were densified to a certain extent (see Table 5-11). After the post treatments, the connection between the open pores was blocked by the crystallized zirconia, effectively limiting the paths of the oxygen penetration. The globular pores, however, remain in the ceramic region, reducing the thermal-conductivity coefficient, and acting as fraction inhibitors, so they are beneficial to the high temperature applications and fracture toughness of the ceramic coatings [9, 72]. The mechanism of the chemical densification process was discussed and proposed in chapter 6.3.

The other examined specimens that were post-treated by the chemical densification process had higher thermal shock resistance and high temperature oxidation resistance. Densification of the ceramic top coat is expected to prevent the oxygen diffusion and control the growth of TGO thickness. However, according to the known primary failure mechanisms in APS TBCs, the key to the durability improvement is the retention of strong bonding between the ceramic top coat and the bond coat [57]. The average adhesive strength of the post-treated top coat was double that of the as-sprayed. However, the thermal cycle lifetime of all the examined specimens was shorter than that of the TBCs investigated by some researchers. That might be due to differences in applied substrates and spraying processes [73]. Nevertheless, the aim of our study is to investigate the influence of the chemical densification process on the thermal cycle behaviors of post-treated TBCs compared with as-sprayed.

The specimen TS3 with lower porosity, post-treated at 800 °C for 72 hours, had a relatively shorter thermal cycle lifetime. This is an interesting point for discussion. The cross-sectional microstructure of the specimen TS3 after 5 thermal cycle tests was investigated (Fig. 5-29). A homogeneous TGO layer existed at the top-coat/bond-coat interface and slight internal oxidation occurred in the bond coat, near the top coat. Compared with the as-sprayed TBCs, the YSZ top coat was still protective and the TGO layer was still stable at this examined position due to the densification of the ceramic top coat and its higher adhesive strength after the post treatment. This homogeneous oxide layer, composed of Cr_2O_3 and Al_2O_3, limited the oxygen penetration towards the bond coat and hence retarded the internal oxidation to some extent [57]. The investigation of the delamination area of this specimen revealed that the spallation did not occur at the top-coat/bond-coat interface, but near the interface and in the ceramic top coat region, which is related to the induced microcracks formed during the post treatment as discussed in chapter 6.2. This specimen was post treated at 800 °C with a higher densification rate and longer treatment duration. Thus, a great stress in the ceramic region had been induced after the post treatment. During the thermal cycle test, the induced tress in the ceramic region was the main culprit for the delamination of the top coat after the thermal cycle test.

Specimen TS4, post-treated at 800 °C for a shorter duration, exhibited the highest thermal shock resistance among the examined specimens, which indicates that the induced stresses in the ceramic top region could be prevented by a shorter post treatment duration. Specimen TS4 was densified by the solvothermal post-treatment and had no induced microcracks (see Fig.5-6d), limiting oxygen penetration towards the bond coat, hence allowing the growth of the TGOs at the high temperature applications to be controlled. Moreover, the top coat adherence was also enhanced during the post-treatment. The two improved properties are considered to be the major factors for the higher protective efficiency of the post-treated YSZ TBCs.

Solvothermal processing was applied in this present study to chemically densify the plasma-sprayed oxide based ceramic coatings. The densified ceramic coatings exhibited lower porosity, increased hardness, and enhanced adhesive strength, which results in better wear, oxidation and thermal shock resistance. Aluminum-casting moulds face more and more severe thermal chemical and mechanical stresses during the production process. Therefore, based on the results of this study, the colleagues of Fraunhofer UMSICHT Sulzbach-Rosenberg studied the thermal shock and corrosion resistance of solvothermal post-treated plasma-sprayed 8YSZ/Ni-based alloy two-layer system against liquid aluminum alloys. During this

study, the coated and post-treated specimens were dipped in liquid aluminum alloys at 800 °C for 4 minutes and air-cooled for 1 minute until the temperature reached 420 °C. The thermocyclic corrosion resistance of the post-treated layer-system in liquid aluminum alloy increased to 1300 cycles [74]. It was observed that the post treated YSZ top-coat using the solvothermal processing exhibited suitable corrosion resistance to liquid aluminum alloys. This could be attributed to the reduced porosity, which, in turn, contributes to the decreased metal infiltration and final spallation during the cooling. In addition, the improved cohesion inside the oxide layer due to the chemical densification as well as the improved adhesion properties to the bond-coat through the presence of chemical bonding provide better resistance to the thermal shocks and mechanical stresses which occur during the solidification of the aluminum alloy at the surface of the oxide layer. These results demonstrate the ability of post-treated plasma-sprayed oxide coatings to be used in aggressive media, and even under thermal and mechanical stresses.

6.6 Chemical densification on YSZ/Al_2O_3 ceramic/alloy two-layer system

Due to the low thermal conductivity of YSZ, frictional heat can cause high temperatures, therefore, inducing stress in the coatings. In order to improve its thermal stability and wear resistance, the addition of a second phase -with higher thermal conductivity and a higher level of hardness- to the zirconia phase, should be effective. Alumina is an attractive material for wear resistance applications, with higher thermal conductivity and hardness. It has been proven that the addition of an alumina phase to the zirconia phase leads to the improved toughness, hardness and wear resistance of the coatings [31, 32].

In this part of the present study, the modified microstructure of post-treated YSZ/Al_2O_3 (70/30) ceramic top-coats was characterized, and their mechanical and tribological properties were also investigated. The “as-sprayed” YSZ/Al_2O_3 ceramic top-coat exhibits a typical lamellar microstructure with a number of pores. In the sample for the EPMA analysis, the epoxy between the top coat and bond coat -which was embedded during the sample preparation- indicated the weak adhesive strength of the as-sprayed ceramic top-coat (see Fig. 5-20a).

The porosity of the zirconia-alumina top-coat, post-treated at 700 °C for 72 hours, was reduced, and the ceramic top-coat did not peel off during the sample preparation for EPMA, which indicated that the post-treated top coat was more adhesive to the bond coat (see Fig. 5-20b). The reduced porosity and enhanced adhesion of the ceramic top coat to the bond coat, suggest that zirconia crystallized in the pores and at the topcoat/bondcoat interface during the solvothermal treatment. However, the pores in the densified region remained, but we suggest that these pores were closed, disallowing the solvothermal agents from penetrating and modifying them. These closed pores can act as crack inhibitors and they are beneficial to the fracture toughness in the tribological applications of the plasma-sprayed ceramic coatings.

As a result of the densification of the oxide layer the hardness was found to be increased by a factor of 50% in the YSZ/Al_2O_3 system, which can be explained by a better cohesion at the local scale. The microhardness evaluation of the zirconia-alumina system indicated that an addition of 30 wt% alumina as a second phase in a zirconia matrix results in the increased hardness of the plasma sprayed ceramic top coat (see Fig. 5-23).

The results of the tribological tests revealed that the wear depth of the as-sprayed YSZ/Al_2O_3 topcoat could be negligible after 1000 sliding cycles, which was not the

same as YSZ system. The wear rate of the as-sprayed YSZ/Al_2O_3 top coat was only slight (see Fig. 5-25). This could be attributed to the higher hardness of the as-sprayed YSZ/Al_2O_3 topcoat. A narrower sliding trace on the post-treated YSZ/Al_2O_3 topcoat was observed, and that might be due to an increased hardness and stronger cohesion and strength in this coating, compared with the untreated topcoat. A positive depth profile for the post-treated YSZ/Al_2O_3 topcoat was created, which indicates that worn materials from the bearing steel ball accumulated on the sliding surface of the ceramic top-coat during testing (see Fig. 5-25).

7 SUMMARY

Plasma spraying is a very efficient deposition technology for ceramic coatings. Plasma-sprayed yttria stabilized zirconia (YSZ) ceramic coatings have been widely used as thermal barrier coatings and wear- and corrosion-resistant coatings in high temperature applications and aggressive environments due to their high hardness, wear resistance, heat and chemical resistance, and low thermal conductivity. However, the highly porous structure and moderate adhesion of the plasma-sprayed YSZ coatings are the most often encountered problems for their high temperature applications involving wear and corrosion. Therefore, the main aim of this work was to reduce the porosity and improve the adhesive strength of the plasma-sprayed YSZ coatings by a novel chemical densification process.

In this study, a two-layer system -consisting of atmospheric plasma-sprayed 8 wt% yttria-stabilized zirconia (8YSZ) as top coat and Ni-based alloy coatings as a bond coat- was used as a model system. In order to conduct the chemical densification post-treatment on the two-layer system at atmospheric pressure, a simple experimental apparatus was created. It contains an oven and a gas system. The temperature may go up to 1100 °C and the concentration of hydrogen chloride in nitrogen gas can be computer-regulated and -controlled.

First of all, the solubility of zirconia in a mixture of molten salts in various gas atmospheres in dependence of temperatures was determined. The maximum solubility of zirconia was achieved in a mixture of equimolar molten salts of KCl, $ZnCl_2$, K_2SO_4 and $ZnSO_4$ in a nitrogen atmosphere containing 2% hydrogen chloride and at temperatures ranging between 600 °C and 800 °C. This was selected as optimal condition for the chemical densification process und used for the post-treatment of the two-layer samples. Investigations of the microstructure of post-treated YSZ coatings showed that the densification of the ceramic coatings could be achieved at 800 °C for a shorter time. During the chemical densification process, solvothermal reactions occurring between the solvent and chromium/aluminium from the bond coat, lead to the crystallization of zirconia at the topcoat/bondcoat interface and in the connected pores of the ceramic layer. The porosity of the densified YSZ top coat was reduced by 50% and the adhesion of the top coat was also improved.

The tribological properties of the plasma-sprayed and post-treated YSZ coatings were investigated by using tribometer in form of the ball-on-disc test and the three-ball-on-disc test under dry conditions. After the sliding tests the worn surfaces were examined. The formation of micro cracks along the splat boundaries are considered

as main wear mechanism, which finally leads to material failure of plasma-sprayed YSZ coatings. The post-treated YSZ coatings presented higher wear resistance and very low friction coefficient after 1350 sliding cycles compared with the as-sprayed coatings. It is caused by the enhanced interfacial strength between the splats of the plasma-sprayed YSZ coatings after the solvothermal treatment. The application of scratch tests and Rockwell tests showed that specimens post-treated at 700 °C for 72 hours have much better mechanical properties compared to as-sprayed YSZ coatings. This observation correlates with the tribological investigation indicating that the tribological properties of the plasma-sprayed ceramic coatings can be improved by the more cohesive structure. A first impression of the wear mechanisms of the coatings was also given.

Thermal shock resistance and high temperature oxidation resistance of the plasma-sprayed YSZ thermal barrier coatings (TBCs) were examined. The post-treated two-layer samples showed increased high-temperature oxidation resistance and thermal shock resistance. Various factors contribute to a durability improvement of the plasma-sprayed YSZ thermal barrier coating. The densification of the YSZ top coat leads to a limitation of oxygen penetration towards the bond coat, which controls the growth of the TGOs at the high temperature applications. Moreover, the inter-lamellar bonding and the ceramic top-coat/bond-coat adherence were also enhanced. The two improved properties are considered to be the major factors for the higher protective efficiency of the post-treated YSZ TBCs. The spalling failure mechanisms for the examined TBCs were discussed.

This innovative process has been successfully used to improve the corrosion resistance of the YSZ coatings against liquid aluminum alloys, where coatings face combined chemical, thermal and mechanical loads. The results showed that the thermocyclic corrosion resistance of the post-treated layer-system in liquid aluminum alloy increased to 1300 cycles. This plasma-sprayed YSZ/Ni-based Alloy layer-system, post-treated by the chemical densification process, could be used as a protective coating for the aluminium casting moulds.

8 ZUSAMMENFASSUNG

Thermisches Spritzen ist eine effiziente Abscheidungstechnologie für keramische Beschichtungen. Plasma-gespritzte Yttriumoxid stabilisiertes Zirkonoxid (YSZ) Beschichtungen werden sehr oft als Wärmedämmschichten und als Verschleiß- und Korrosionsschutzschichten bei hohen Temperaturen Anwendungen und aggressiven Umgebungen verwendet. Allerdings ist der Einsatz plasma-gespritzter YSZ-Beschichtungen gegen Verschleiß und Korrosion bei hohen Temperaturen wegen der hohen Porosität und der schwachen Anhaftung an ihrer Unterfläche problematisch. Deshalb ist Ziel der vorliegenden Arbeit, durch einen neuartigen chemischen Verdichtungsprozess die Porosität der plasma-gespritzten keramischen Beschichtung zu reduzieren und deren Haftungsfestigkeit zu erhöhen.

Bei dieser Arbeit wurde ein Zweibeschichtungssystem gewählt. Eine atmosphärisch plasmagespritzte Ni-Basis-Legierungsbeschichtung wurde mit einer keramischen Beschichtung - bestehend aus mit 8 Gew.-% Yttriumoxid stabilisiertem Zirkonoxid (8YSZ) - überzogen. Für die chemische Nachbehandlung der Zweibeschichtungs-präparate bei atmosphärischem Druck wurde eine einfache experimentelle Anlage aufgebaut, die aus einem Ofen und einer Gasanlage besteht. Die Temperatur reicht bis zu 1100 °C und die Konzentration des HCl-Gases in einer Stickstoff-Atmosphäre kann mit einem Rechner reguliert und kontrolliert werden.

Für den chemischen Verdichtungsprozess wurde Zirkonoxid in einer äquimolaren Salzschmelzemischung aus KCl, $ZnCl_2$, K_2SO_4 und $ZnSO_4$ gelöst und mit einer 2% HCl-Gas enthaltenden Stickstoffatmosphäre in Gleichgewicht gebracht. Die Voruntersuchungen mit dieser Salzschmelzemischung zeigten, dass bei einer Temperatur zwischen von 600 °C und 800 °C die maximale Löslichkeit von Zirkonoxid erreicht wird. Das Zweibeschichtungssystem wurde mit der so entstehenden Gasmischung solvothermal nachbehandelt.

Während des chemischen Verdichtungsprozesses finden entlang der Grenzfläche zwischen der Keramik und der Legierung solvothermale Reaktionen von Chrom aus der Ni-Basis-Legierung mit der Gasphase statt. In den offenen Poren der keramischen Beschichtung erfolgt eine Kristallisation von Zirkonoxid aus der solvothermalen Gasphase. Die Untersuchungen zeigten, dass hierdurch die YSZ-Beschichtung verdichtet und die Porosität um 50% reduziert wird. Die Wirkung der Reaktionsbedingungen auf die Mikrostrukturen der YSZ-Beschichtungen wurde geprüft und die optimierten Parameter für den chemischen Verdichtungsprozess bestimmt.

Die tribologischen Eigenschaften der plasma-gespritzten und nachbehandelten YSZ-Beschichtungen wurden mittels Tribometer in Formen von „ball-on-disc“ und „three-ball-on-disc“ bei trockenen Bedingungen getestet. Im Vergleich mit der „wie-gespritzten“ YSZ-Schicht zeigten die nachbehandelten Beschichtungen nach 1350 Gleitzyklen eine höhere Verschleißbeständigkeit und einen kleinen Reibungskoeffizienten. Dies ist auf die erhöhte Festigkeit zwischen den plasmagespritzten keramischen Körnern und dem abgeschiedenen Zirkonoxid zurückzuführen. Das tribologische Verhalten wurde mit den mechanischen Eigenschaften, die mittels Rockwelltests und Scratchtests ermittelt wurden, korreliert. Die Untersuchung der Verschleißspuren zeigt, dass der wichtigste Verschleißmechanismus für die plasmagespritzten keramischen Beschichtungen durch die Entstehung der Mikrorisse entlang der Körner verursacht wird. Für die Verschleißmechanismen der plasmagespritzten keramischen Beschichtungen wurde in dieser Arbeit ein Modell vorgeschlagen.

Die thermische Schock- und Hochtemperaturbeständigkeit der YSZ Beschichtungen wurde getestet. Verschiedene Faktoren tragen zur Verbesserung der Thermowechselbeständigkeit der plasma-gespritzten YSZ Wärmedämm-Beschichtungen bei. Durch die solvothermale Nachbehandlung wird die Diffusion von Sauerstoff zur Ni-Basis-Legierung begrenzt und das Wachstum von „thermally grown oxides“ (TGO) bei hohen Temperaturen kontrolliert. Zudem wird die Haftungsfestigkeit der oberen keramischen Schicht und auch die Erhöhung des Verbunds zwischen den keramischen Körnern erhöht. Diese beiden verbesserten Eigenschaften gelten als die wichtigsten Faktoren für die höhere Schutzeffizienz der nachbehandelten YSZ-Beschichtungen.

Der innovative Prozess wurde erfolgreich eingesetzt, um die Korrosionsbeständigkeit der YSZ Beschichtungen gegenüber Aluminiumschmelzen zu verbessern. Die beschichten Teststäbe sind bei Kontakt mit Al-Schmelze einer Kombination aus chemischen, thermischen und mechanischen Belastungen ausgesetzt. Die erzielte erhöhte thermozyklische Korrosionsbeständigkeit zeigt, dass durch eine solvothermale Nachbehandlung das plasmagespritzte YSZ/Ni-Basis-Legierung-Beschichtungssystem als Schutzschicht für die Aluminiumabgüsse verwendet werden kann.

9 OUTLOOK

In modern processes, and at the request of a steady efficiency increase, structural materials and production tools or moulds have to face more and more severe thermal, chemical, and mechanical stresses. Therefore, the choice and production of these materials with appropriate properties become a critical criterion along the industrial production process. In addition, the extension of their service life time represents a major economic objective as it enables to decrease the material costs due to replacement, but even more important, it reduces drastically the costs for the regular installation shutdown. And finally, the required quality of the produced components can be maintained and it participates to the global improvement of the industrial productivity and competitiveness.

In industrial areas the criterion for choice of materials is a balance of costs and properties. The use of coating on inexpensive substrates represents an alternative. For high temperature wear and corrosion resistance oxide ceramic coatings are the suitable choice.

The combination of rapid-tooling process and plasma spraying technology is one good idea for efficient production of tools and moulds with wear- and corrosion-resistant oxide ceramic coatings. The coated tools can be further post-treated by chemical densification treatments, in order to achieve the protective work surface.

Figure 9-1 illustrates the process of combination of rapid-tooling and plasma spraying technology. First, a pattern or model normally from wood, composite, plastic or metal has to be made, and then coated with functional materials by plasma spraying. The sprayed shell is then reinforced with steels as required, and finally remove the model and we get the tool with ceramic coatings. This tool can be further post-treated by chemical densification processing and achieve a protective surface.

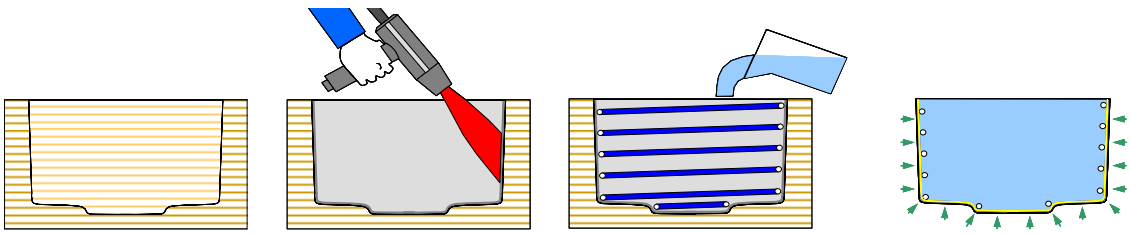

Figure 9-1. *Illustration of combination of rapid-tooling and plasma spraying technology* [75].

10 LITERATURE

[1] Bull, S.J., Davidson, R.I., Fisher, E.H., McCabe, A.R. and Jones, A.M. (2000) A simulation test for the selection of coatings and surface treatments for plastics injection moulding machines, *Surface and Coatings Technology*, **130**(2-3), p. 257-265

[2] Heinze, M. (1998) Wear resistance of hard coatings in plastics processing, *Surface and Coatings Technology*, **105**(1-2), p. 38-44

[3] Cunha, L., Andritschky, M., Pischow, K., Wang, Z., Zarychta, A., Miranda, A. S. and Cunha, A.M. (2002) Performance of chromium nitride and titanium nitride coatings during plastic injection moulding, *Surface and Coatings Technology*, **153**(2-3), p. 160-165

[4] Gurrappa, I. and Rao, A. Sambasiva (2006) Thermal barrier coatings for enhanced efficiency of gas turbine engines, *Surface and Coatings Technology*, **201**(6), p. 3016-3029

[5] Cao, X.Q., Vassen, R. and Stoever, D. (2004) Ceramic materials for thermal barrier coatings, *Journal of the European Ceramic Society*, **24**(1), p. 1-10

[6] Ouyang, J.H. and Sasaki, S. (2002) Microstructure and tribological characteristics of ZrO2-Y2O3 ceramic coatings deposited by laser-assisted plasma hybrid spraying, *Tribology International*, **35**(4), p. 255-264

[7] Mauer, G., Jarligo, M.O., Mack, D.E., Vassen, R. and Stover, D. (2010) Development of plasma spray parameters for ceramic coatings in gas turbines, *International Conference on Surface Modification Technologies 24th*, Dresden Germany

[8] Sobolev, V.V. (1998) Formation of splat morphology during thermal spraying, *Materials Letters*, **36**(1-4), p. 123-127

[9] McPherson, R. (1989) A review of microstructure and properties of plasma sprayed ceramic coatings, *Surface and Coatings Technology*, **39-40**(Part 1), p. 173-181

[10] Stöver, D. and Funke, C. (1999) Directions of the development of thermal barrier coatings in energy applications, *Journal of Materials Processing Technology*, **92-93**, p. 195-202

[11] Ctibor, P., Roussel, O. and Tricoire, A. (2003) Unmelted particles in plasma sprayed coatings, *Journal of the European Ceramic Society*, **23**(16), p. 2993-2999

[12] He, Y., Winnubst, L., Burggraaf, A.J., Verweij, H., Van der Varst, P.G.T. and de With, B. (1997) Influence of Porosity on Friction and Wear of Tetragonal Zirconia Polycrystal, *Journal of the American Ceramic Society*, **80**(2), p. 377-380

[13] Tingaud, O., Bertrand, P. and Bertrand, G. (2010) Microstructure and tribological behavior of suspension plasma sprayed Al2O3 and Al2O3-YSZ composite coatings, *Surface and Coatings Technology*, **205**(4), p. 1004-1008

[14] Brinkiene, K. and Kezelis, R. (2004) Correlations between processing parameters and microstructure for YSZ films produced by plasma spray technique, *Journal of the European Ceramic Society*, **24**(6), p. 1095-1099

[15] Karthikeyan, S., Balasubramanian, V. and Rajendran, R. (2014) Developing empirical relationships to estimate porosity and Young´s modulus of plasma sprayed YSZ coatings, *Applied Surface Science*, **296**, p. 31-46

[16] Chen, H., Zhang, Y. and Ding, C. (2002) Tribological properties of nanostructured zirconia coatings deposited by plasma spraying, *Wear*, **253**(7-8), p. 885-893

[17] Carpio, P., Bannier, E., Salvador, M.D., Borrell, A., Moreno, R. and Sanchez, E. (2015) Effect of particle size distribution of suspension feedstock on the microstructure and mechanical properties of suspension plasma spraying YSZ coatings, *Surface and Coatings Technology*, **268**, p. 293-297

[18] Keyvani, A., Saremi, M., Sohi, M.H. and Valefi, Z. (2012) A comparison on thermomechanical properties of plasma-sprayed conventional and nanostructured YSZ TBC coatings in thermal cycling, *Journal of Alloys and Compounds*, **541**, p. 488-494

[19] Keyvani, A., Saremi, M., Sohi, M.H., Valefi, Z., Yeganeh, M. and Kobayashi, A. (2014) Microstructural stability of nanostructured YSZ-alumina composite TBC compared to conventional YSZ coatings by means of oxidation and hot corrosion tests, *Journal of Alloys and Compounds*, **600**, p. 151-158

[20] Liscano, S., Gil, L. and Staia, M.H. (2005) Correlation between microstructural characteristics and the abrasion wear resistance of sealed thermal-sprayed coatings, *Surface and Coatings Technology*, **200**(5-6), p. 1310-1314

[21] Slamecka, K., Celko, L., Skalka, P., Pokluda, J., Nemec, K., Julis, M., Klakurkova, L. and Svejcar, J. (2015) Bending Fatigue failure of atmospheric-plasma-sprayed CoNiCrAlY+YSZ thermal barrier coatings, *International Journal of Fatigue*, **70**, p. 186-195

[22] Pawlowski, L. (1995) The Science and Engineering of Thermal Spray Coatings, Wiley

[23] Fu, Y., Batchelor, A.W., Xing, H. and Gu, Y. (1997) Wear behaviour of laser-treated plasma-sprayed ZrO2 coatings, *Wear*, **210**(1-2), p. 157-164

[24] Di Girolamo, G., Blasi, C., Schioppa, M. and Tapfer, L. (2010) Structure and thermal properties of heat treated plasma sprayed ceria-yttria co-stabilized zirconia coatings, *Ceramics International*, **36**(3), p. 961-968

[25] Szkaradek, K.K. (2010) Laser melted ZrO2-Y2O3 thermal barrier obtained by plasma spraying method, *Journal of Alloys and Compounds*, **505**(2), p. 516-522

[26] Siebert, B., Funke, C., Vaen, R. and Stöver, D. (1999) Changes in porosity and Young's Modulus due to sintering of plasma sprayed thermal barrier coatings, *Journal of Materials Processing Technology*, **92-93**, p. 217-223

[27] Zhu, C., Li, P., Javed, A., Liang, G.Y. and Xiao, P. (2012) An investigation on the microstructure and oxidation behavior of laser remelted air plasma sprayed thermal barrier coatings, *Surface and Coatings Technology*, **206**(18), p. 3739-3746

[28] Knuuttila, J., Sorsa, P. and Mäntylä, T. (1999) Sealing of thermal spray coatings by impregnation, *Journal of Thermal Spray Technology*, **8**(2), p. 249-257

[29] Vippola, M., Leivo, E., Sorsa, P., Vuoristo, P. and Mäntylä, T. (1997) Wear and Corrosion Properties of Plasma Sprayed Al2O3 and Cr2O3 Coatings Sealed by Aluminum Phosphates, *Journal of Thermal Spray Technology*, **6**(2), p. 205-210

[30] Wielage, B., Steinhäuser, S. and Zimmermann, G. (1998) Improving Wear and Corrosion Resistance of Thermal Sprayed Coatings, *Surface Engineering*, **14**(2), p. 136-138

[31] Esposito, L., Moreno, R., Sànchez Herencia, A.J. and Tucci, A. (1998) Sliding wear response of an alumina-zirconia system, *Journal of the European Ceramic Society*, **18**(1), p. 15-22

[32] Kerkwijk, B., Winnubst, A.J.A., Verweij, H., Mulder, E.J., Metselaar, H.S.C. and Schipper, D.J. (1999) Tribological properties of nanoscale alumina-zirconia composites, *Wear*, **225-229**(Part 2), p. 1293-1302

[33] Davis, J.R. (2001) Surface engineering for corrosion and wear resistance, ASM International

[34] Budinski, K.G. (1988) Wear Modes, Surface Engineering for Wear Resistance, *Prentice Hall*, p. 15-43

[35] Bach, F.-W., Möhwald, K., Laarmann, A. and Wenz, T. (2004) Moderne Beschichtungsverfahren, WILEY-VCH

[36] Archard, J.F. (1953) Contact and Rubbing of Flat Surface, *Journal of Applied Physics*, **24**, p. 981-988

[37] Schmitt, M.P., Rai, A.K., Zhu, D., Dorfman, M.R. and Wolfe, D.E. (2015) Thermal conductivity and erosion durability of composite two-phase air plasma sprayed thermal barrier coatings, *Surface and Coatings Technology,* **279**, p. 44-52

[38] Deb, D., Ramakrishnalyer, S. and Radhakrishnan, V.M. (1996) A comparative study of oxidation and hot corrosion of a cast nickel base superalloy in different corrosive environments, *Materials Letters*, **29**, p. 19-23

[39] Hermanek, F.J. (2001) Thermal Spray Terminology and Company Origins, ASM International

[40] Davis, J.R. (2004) Handbook of thermal spray technology, ASM International

[41] Scott, H.G. (1975) Phase relationships in the zirconia-yttria system, *Journal of Materials Science*, **10**(9), p. 1527-1535

[42] Maier, J. (2005) Nanoionics: ion transport and electrochemical storage in confined systems, *nature materials*, **4**(11), p. 805-815

[43] Courtin, E., Boy, P., Piquero, T., Vulliet, J., Poirot, N. and Laberty-Robert, C. (2012) A conposite sol-gel process to prepare a YSZ electrolyte for Solid Oxide Fuel Cells, *Journal of Power Sources*, **206**, p. 77-83

[44] Hirschenhofer, J.H., Stauffer, D.B., Engelman, R.R. and Klett, M.G. (1998) Fuel cell Handbook, 4th. ed., Dept. of Energy Report No. DOE/FETC-99/1076 Parsons Corp.

[45] Larmine, J. and Andrews, D. (2000) Fuel cell systems explained, John Wiley & Sons Ltd.

[46] Haile, S.M. (2003) Fuel cell materials and components, *Acta Materialia*, **51**, p. 5981-6000

[47] Lima, C.R.C. and Guilemany, J.M. (2007) Adhesion improvements of thermal barrier coatings with HVOF thermally sprayed bond coats, *Surface and Coatings Technology*, **201**, p. 4694-4701

[48] Wielage, B., Steinhäuser, S. and Zimmermann, G. (1998) Improving Wear and Corrosion Resistance of Thermal Sprayed Coatings, *Surface Engineering*, **14**(2), p. 136-138

[49] Ito, H., Nakamura, R. and Shiroyama, M. (1988) Infiltration of Copper into Titanium-Molybdenum Spray Coatings, *Surface Engineering*, **4**(1), p. 35-38

[50] Ohmori, A., Zhoue, Z. and Inoue, K. (1994) Improvement of Plasma-Sprayed Ceramic Coating Properties by Heat-Treatment wiith Liquid Mn, *Thermal Spray Industrial Applications*, Berndt, C.C. and Sampath, S. Ed., ASM International, p. 543-548

[51] Demazeau, G. (1999) Solvothermal processes: a route to the stabilization of new materials, *Journal of Materials Chemistry*, **9**, p. 15-18

[52] Klemme, S. and Meyer, H.-P. (2003) Trace element partitioning between baddeleyite and carbonatite melt at high pressures and high temperatures, *Chemical Geology*, **199**, p. 233-242

[53] Demazeau, G. (2008) Solvothermal Reactions: an original route for the synthesis of novel materials, *Journal of Materials Science*, **43**(7), p. 2104-2114

[54] *Fine ceramics (advanced ceramics, advanced technical ceramics) - Determination of friction and wear characteristics of monolithic ceramics by ball-on-disc method*, Beuth Verlag

[55] Ishitsuka, T. and Nose, K. (2002) Stability of protective oxide films in waste incineration environment--solubility measurement of oxides in molten chlorides, *Corrosion Science*, **44**(2), p. 247-263

[56] Fehr, K.T., Ye, Y. and Wolf, G. (2012) Verfahren zur Herstellung einer keramischen Schicht auf einer aus einer Ni-Basislegierung gebildeten Oberfläche, Patentanmeldung: DE10 2012 200 560.9

[57] Padture, N.P., Gell, M. and Jordan, E.H. (2002) Thermal Barrier Coatings for Gas-Turbine Engine Applications, *Science*, **296**(5566), p. 280-284

[58] Saremi, M., Afrasiabi, A. and Kobayashi, A. (2008) Microstructural analysis of YSZ and YSZ/Al2O3 plasma sprayed thermal barrier coatings after high temperature oxidation, *Surface and Coatings Technology*, **202**(14), p. 3233-3238

[59] Schmitt-Thomas, Kh.G. and Dietl, U. (1994) Thermal barrier coatings with improved oxidation resistance, *Surface and Coatings Technology*, **68/69**, p. 113-115

[60] Limarga, A.M., Widjaja, S., Yip, T.H. and Teh, L.K. (2002) Modeling of the effect of Al2O3 interlayer on residual stress due to oxide scale in thermal barrier coatings, *Surface and Coatings Technology*, **153**(1), p. 16-24

[61] Fervel, V., Normand, B. and Coddet, C. (1999) Tribological behavior of plasma sprayed Al2O3-based cermet coatings, *Wear*, **230**(1), p. 70-77

[62] Miller, R. (1997) Thermal barrier coatings for aircraft engines: history and directions, *Journal of Thermal Spray Technology*, **6**(1), p. 35-42

[63] Helminiak, M.A., Yanar, N.M., Pettit, F.S., Taylor, T.A. and Meier, G.H. (2009) The behavior of high-purity, low-density air plasma sprayed thermal barrier coatings, *Surface and Coatings Technology*, **204**(6-7), p. 793-796

[64] Li, M.H., Zhang, Z.Y., Sun, X.F., Guan, H.R., Hu, W.Y. and Hu, Z.Q. (2002) Oxidation and Degradation of EB-CVD Thermal Barrier Coatings, *Oxidation of Metals*, **58**(5), p. 499-512

[65] Schulz, U., Bernardi, O., Ebach-Stahl, A., Vassen, R. and Sebold, D. (2008) Improvement of EB-PVD thermal barrier coatings by treatments of a vacuum plasma-sprayed bond coat, *Surface and Coatings Technology*, **203**(1-2), p. 160-170

[66] Sobhanverdi, R. and Akbari A. (2015) Porosity and microstructural features of plasma sprayed Yttria stabilized Zirconia thermal barrier coatings, *Ceramics International*, **41**(10), p. 14517-14528

[67] Bennett, A. (1986) *Materials Science and Technology*, **2**, p. 257

[68] Lee, W.Y., Stinton, D.P., Berndt, C.C., Erdogan, F., Lee, Y.-D. and Mutasim, Z. (1996) Concept of Functionally Graded Materials for Advanced Thermal Barrier Coating Applications, *Journal of the American Ceramic Society*, **79**(12), p. 3003-3012

[69] Jin, L., Ni, L., Yu, Q., Rauf, A. and Zhou, C. (2012) Thermal cyclic life and failure mechanism of nanostructured 13 wt%Al2O3 doped YSZ coating prepared by atmospheric plasma spraying, *Ceramics International*, **38**(4), p. 2983-2989

[70] Padture, N.P., Schlichting, K.W., Bhatia, T., Ozturk, A., Cetegen, B., Jordan, E.H., Gell, M., Jiang, S., Xiao, T.D., Strutt, P.R., García, E., Miranzo, P. and Osendi, M.I. (2001) Towards durable thermal barrier coatings with novel microstructures deposited by solution-precursor plasma spray, *Acta Materialia*, **49**(12), p. 2251-2257

[71] Haynes, J.A., Ferber, M.K., Porter, W.D. and Rigney, E.D. (1999) Characterization of Alumina Scales Formed During Isothermal and Cyclic Oxidation of Plasma-Sprayed TBC Systems at 1150 °C, *Oxidation of Metals*, **52**(1), p. 31-76

[72] Stöver, D. and Funke, C. (1999) Directions of the development of thermal barrier coatings in energy applications, *Journal of Materials Processing Technology*, **92-93**, p. 195-202

[73] Tang, F., Ajdelsztajn, L., Kim, G.E., Provenzano, V. and Schoenung, J.M. (2006) Effects of variations in coating materials and process conditions on the thermal cycle properties of NiCrAlY/YSZ thermal barrier coatings, *Materials Science and Engineering: A*, **425**(1-2), p. 94-106

[74] Masset, P.J., Faulstich, M., Fehr, K.T., Weih, C., Wolf, G. and Ye, Y. (2013) Chemical densification of oxide based coatings for high temperature wear and corrosion resistance, *High Temperature Corrosion Materials Chemistry 10* Electrochemical Society ECS, p. 109-116

[75] Fehr, K.T., Ye, Y., Wolf, G., Weih, C. and Faulstich, M. (2012) Ein neues Verfahren zur Optimierung oxidkeramischer Schutzschichten, *Moderne Beschichtungen zum Verschleißschutz von Werkzeugen*, Faulstich, M., Geiger, M., Kukla, H. and Wolf, G. Ed., DORNER PrintConcept

LIST OF ABBREVATIONS

8YSZ	8 wt% Y_2O_3 doped ZrO_2
APS	Atmospheric Plasma Spraying
BSE	Back-Scattered Electron
CVD	Chemical Vapour Deposition
EDS	Energy Dispersive Spectrometer
EPMA	Electron Probe Micro-Analyser
ICPMS	Inductively Coupled Plasma Mass Spectrometer
SCCM	Standard cubic centimetre
PVD	Physical Vapour Deposition
SEM	Scanning Electron Microscopy
TBCs	Thermal Barrier Coatings
TGO	Thermally Grown Oxide
XRD	X-Ray Diffraction

ACKNOWLEDGMENTS

The work presented in this thesis was done at the department of earth and environmental sciences in cooperation with ATZ Entwicklungszentrum (now Fraunhofer-Institut für Umwelt-, Sicherheits- und Energietechnik UMSICHT) within the joint research program ForLayer, financially supported by Bavarian Research Foundation (BFS). I would like to express my gratitude to all people who have contributed to this work.

I warmly thank my supervisor, Prof. Dr. Karl Thomas Fehr for offering me the unique opportunity to work in the department and giving me the chance to be involved in one of the most important and challenging problem in the field of thermal spraying technologies. I am deeply indebted for the support, rich ideas and encouragement that he has provided during my years at the department. I am also very grateful that he let me know much about the interesting Bavarian culture and language.

I would like to give thanks to Prof. Dr. Martin Faulstich for offering me the opportunity to work together with the colleagues within the joint program ForLayer and to learn more about the other coating technologies and characterization methods.

Many thanks to Prof. Soraya Heuss-Aßbichler for her helpful advice and suggests on revising my dissertation. She always gave me a hand, when I needed important documents for scholarship applications, and when I faced problems on supervisor issues.

I acknowledge Dipl.-Ing. Gerhard Wolf for his sincere expression of thermal spraying and allowance of my work at ATZ Entwicklungszentrum (Fraunhofer UMSICHT).

I am grateful that the colleagues within the joint program ForLayer, Dipl.-Wi.-Ing. (FH) Christoph Weih and Dipl.-Wirtsch.-Ing.Tobias Schrader provided Rockwell tests and tribological measurements of my samples.

I also like to thank Prof. Dr. Mario Mocker and Dipl.-Ing. Ingrid Löh for their valuable discussions on the chemistry aspects

My thanks also to Mr. Hilger Lohringer for his EMP sample preparations and his patience.

I am further grateful for the help from Dipl.-Chem. Thomas Dorfner and Mrs. Wimmer in chemistry lab during ordering the chemical reagents and gases.

Dr. Andreas Laumann, Dr. Saskia Bernstein and Dr. Amanda Günther deserve some special thanks, for their scientific discussions, for their rich ideas and encouragement which helped me go forward with this work. I am very grateful that they gave me a family feeling in our office.

I also like to thank the kindly people at the department, in particular, Dr. Yan Lavallée, Dr.Kai-Uwe Hess, Dr. Werner Ertl-Ingrisch and Mrs. Margot Lieske.

Finally, I acknowledge the grand help and support of my family.

ERKLÄRUNG

Hiermit erkläre ich ehrenwörtlich, dass ich die Dissertation “MODIFICATION OF THERMALLY SPRAYED CERAMIC OXIDE COATINGS BY CHEMICAL DENSIFICATION PROCESSING“ selbständig angefertigt und keine anderen als die von mir angegebenen Quellen und Hilfsmittel benutzt habe. Ich erkläre außerdem, dass diese Dissertation weder in gleicher noch in anderer Form bereits in einem anderen Prüfungsvorhaben vorgelegen hat. Ich habe früher außer den mit dem Zulassungsgesuch urkundlich vorgelegten Graden keine weitern akademische Grade erworben oder zu erwerben versucht.

München, den……

Yaping Ye